PHOTOLUMINESCENCE OF ZnSe GROWN BY MOVPE

Submitted by

© Boris Makuc

A thesis submitted to the Faculty of Graduate Studies and Research in partial fulfilment of the requirements for the degree of Master of Science.

Department of Physics

McGill University

3600 Université

Montréal, Québec

H3A 2T8

December 1988

ABSTRACT

Heteroepitaxial ZnSe thin films are grown by conventional metal-organic vapour phase epitaxy (MOVPE) and a novel pulsed technique recently developed at McGill university. An in-depth analysis of photoluminescence spectra recorded at three different temperatures is presented. The epilayer quality and purity are related to the particular growth technique employed and the specific precursors used. Photoluminescence spectra of the best material grown is compared with the existing data on the ZnSe/GaAs system. The material quality in the present case is comparable to that reported in the literature for MOVPE and molecular beam epitaxy (MBE) grown material. The near band edge photoluminescence, recorded at 77 °K, reveals features which have not been reported in the literature on the ZnSe/GaAs system.

RESUME

Des couches minces hétéroépitaxiques de séléniure de zinc ont été obtenues par deux techniques de croissance. La première est l'épitaxie en phase vapeur par composés organo-métalliques (MOVPE). La seconde est une nouvelle technique développée à McGill. Il s'agit d'une procédure dérivée de la première, les gaz étant injectés dans le réacteur de façon pulsée. Une analyse en profondeur des spectres de photoluminescence enregistrés à trois différentes températures est présentée. La qualité et la pureté des couches épitaxiques sont correlées à la technique de croissance et aux composés utilisés. Les résultats de photoluminescence du meilleur matériau obtenu sont comparés avec ceux de la littérature, et indiquent une qualité comparable avec les échantillons obtenus par MOVPE et MBE par d'autres groupes. La photoluminescence correspondant à des transitions voisines de la bande interdite montre des caractéristiques nouvelles à 77 ^{o}K.

ACKNOWLEDGEMENTS

This project was completed with the Semiconductor Research Group of the physics department at McGill University. I am indebted to several people for the assistance I received in preparing the present thesis.

I wish to express my sincere thanks to :

--- Professor D. Walsh for accepting to direct my work, for providing the help and facilities necessary for its completion and for financial assistance through a grant from the Gouvernement du Québec. I would also like to thank Dr. Walsh for the informative discussions about the photoluminescence of semiconductors.

--- Dr. K. Mazuruk for supervising my research, for the design and implementation of a new pulsed growth technique, for the growth of the ZnSe epilayers and for the numerous informative discussions about crystal growth.

--- Dr. M. Benzaquen for technical assistance and friendship.

--- Mr. P. Weissfloch for the design of an automated data acquisition system and for friendship.

Finally, I wish to thank my family, relatives, and friends for their support.

TABLE OF CONTENTS

INTRODUCTION

INTRODUCTION

The recent progress in the physics of III-V compound semiconductors is directly related to major advancements in growth and device technologies. The growth of high purity material by MBE and MOVPE and the ability to fabricate thin multi-layer structures using these techniques has led to a rapid development in the production of electronic and opto-electronic devices based on III-V semiconductors. High speed field effect transistors (FET's) and quantum well lasers have been built using direct gap III-V semiconductors. The advantage of having optical and electronic devices based on a single technology provides the driving force for the replacement of the current Si and Ge based technology by the III-V technology. A thorough understanding of the underlying physics is required for the future improvement and advancement of the III-V growth and device technologies.

A resurgence in the interest in II-VI compound semiconductors is a direct consequence of the current emphasis on III-V semiconductor device technology. The II-VI and III-V systems are compatible in many cases and can be grown using the same technique. ZnSe is a wide direct gap (2.7 eV) II-VI semiconductor and has a close lattice matching to GaAs. It is therefore a suitable candidate for the fabrication of blue light-emitting diodes (LED's), laser diodes (LD's), and electroluminescent

displays [1]. Other potential applications include its use as an insulator in metal-insulator-semiconductor (MIS) structures and GaAs waveguides [2]. High quality ZnSe must be obtained if these applications are to be realized. In addition, both p and n-type material is required in order to fabricate LED's and LD's. The doping of ZnSe is complicated by self-compensation effects and incorporation of undesirable compensating impurities. MOVPE and MBE appear to be the most promising techniques for the growth of high quality ZnSe epilayers. These techniques are regarded as highly non-equilibrium growth processes and are expected to suppress self-compensation effects [3].

The present study is concerned with the growth of ZnSe heteroepitaxial thin films by MOVPE and the characterization of the epilayers by photoluminescence. Thin films were grown using conventional MOVPE and a novel pulsed technique developed here. Material was grown using different precursors. Films were deposited at several temperatures in order to determine the effect of this important growth parameter on epilayer quality.

The photoluminescence technique was utilized to characterize the ZnSe epilayers. Photoluminescence spectra were recorded at temperatures of 300 °K, 77 °K, and 2-16 °K. The spectra provide important information about material purity and quality, the types of impurities and complexes present in the material, and the strain present in the epilayer. The types of luminescent transitions which

occur and the relative importance of the various transitions at different temperatures is deduced from an analysis of the photoluminescence spectra. The analysis includes a detailed comparison with data in the existing literature on the ZnSe/GaAs system.

Chapter 1 is concerned with the MOVPE technique. It includes a summary of the basic concepts involved in the growth process, a description of the setup used in MOVPE, and a general overview of the process. A discussion of the various growth parameters involved, the dependence of material quality on these parameters, and the optimization of the parameters for the growth of ZnSe is also included.

In chapter 2, an outline of the various luminescent transitions is given. A summary of the transitions observed in ZnSe is presented. The temperature dependence of the photoluminescence is also discussed.

An overview of the photoluminescence experimental setup, including a description of the equipment, is presented in chapter 3.

The experimental results and analysis are presented in chapter 4.

Chapter 5 is a summary of the conclusions which can be drawn from this study.

CHAPTER 1

METAL-ORGANIC VAPOUR PHASE EPITAXY (MOVPE)

1.)METAL-ORGANIC VAPOUR PHASE EPITAXY (MOVPE)

In recent years, there has been a rapid development in the production of electronic and opto-electronic devices based on thin single crystal semiconductor films. The growth of such layers on single crystal substrates, with the atoms in the layer duplicating the arrangement of the atoms in the subtrate,is known as epitaxy.

Epitaxial growth techniques are preferrable to bulk growth processes for several reasons. The lower growth temperatures used in epitaxy result in crystals with a higher degree of purity and perfection, essentially because of the decreasing role of entropy at lower temperatures. Slower growth rates allow ultra-thin multi-layer structures to be grown. Finally, alloys having a uniform composition in the growth direction can be formed, something not possible in bulk growth processes.

Epitaxy is divided into three general catogories: liquid phase epitaxy (LPE), vapour phase epitaxy (VPE), and solid phase epitaxy (SPE). Vapour phase epitaxy includes as sub-categories metal-organic vapour phase epitaxy (MOVPE) and molecular beam epitaxy (MBE), among others.

All epitaxial growth techniques are based on the same fundamental principles. A thorough understanding of these principles and their relative importance is necessary for continued improvements and diversification in materials growth technology. The first part of this chapter is a

summary of the basic concepts involved in epitaxial growth processes.

The MOVPE growth technique is emerging as one of the most promising of all the epitaxial growth techniques currently in use. This is primarily due to the versatility of this technique. It is capable of producing a large number of high purity semiconductor materials, including multilayer structures. Advanced digital and optical devices based on thin film structures have been successfully fabricated using this technique. This versatility, combined with the possibility of relatively cheap mass production of thin films by this method, suggests that the MOVPE technique will play an increasingly important role in device fabrication in the future. The second part of this chapter provides a description of the setup used in MOVPE and a general overview of the process.

The various parameters involved in MOVPE must be optimized in order to obtain high quality thin films suitable for device applications. Uniformity of epilayer thickness and material properties over the substrate area is essential. Furthermore, control of material properties via introduction of specific concentrations of the appropriate impurities is necessary. The crystalline quality of the semiconductor thin film is also an important factor. The effects on crystal quality, uniformity, morphology, and other characteristics resulting from the variation of these parameters have been well

studied in the case of GaAs. Results of these studies are presented in the final part of this chapter. Problems encountered in the growth of other III-V compounds are also mentioned. Finally, optimization of the parameters for the growth of ZnSe is discussed. Problems in this case not encountered in the growth of GaAs are mentioned, along with possible solutions.

1.1 Fundamental Principles

All crystal growth processes, including epitaxy, are phase transitions. The thermodynamics of phase transitions is therefore quite useful in an analysis of epitaxy. Furthermore, since epitaxy is a dynamic and not an equilibrium process, an understanding of the kinetics involved, notably, mass transport of the required elements to the growth surface and surface processes, is also necessary for an adequate description of the epitaxial growth process.

A study of the thermodynamics of the epitaxial growth system provides a method for calculating the composition of multicomponent solids. It also determines the conditions required in order for growth to occur and the maximum growth rate possible.

Thermodynamics, when applied to a system in equilibrium at a given temperature and pressure, defines the compositions of the various phases in the system.

Considerations based on the fact that the total Gibbs free energy of the system is a minimum at equilibrium result in the following expression for the equilibrium condition:

$$\mu_i^{\alpha} = \mu_i^{\beta} \tag{1.1}$$

for each component i in the system. μ_i^{α} is the chemical potential of the i^{th} component in phase α. For an ideal gas mixture

$$\mu_i = \mu_i^{\circ} + RT \ln(P_i/P_i^{\circ}) \tag{1.2}$$

where R is the gas constant, T is the temperature, p_i is the partial pressure of the i^{th} component, and the superscript o refers to a standard state, usually chosen as the pure component i. In the case of solid or liquid solutions, which are non-ideal,

$$\mu_i = \mu_i^{\circ} + RT \ln a_i = \mu_i^{\circ} + RT \ln(x_i \gamma_i) \tag{1.3}$$

where x_i is the mole fraction of component i and a_i and γ_i are, respectively, the activity and the non-ideality factor, or activity coefficient, of component i. The activity coefficients are necessary parameters when analyzing liquid-solid multicomponent systems or gas solid systems where the solid is comprised of three or more components. Liquid and solid solutions are described by the

regular solution model. The solid solutions may also be treated using the difference in lattice parameter (DLP) model. In both models, γ_i is expressed in terms of the interaction parameter Ω:

$$\ln \gamma_i = (1-x_i)^2 \Omega / RT \qquad (1.4)$$

The interaction parameters are adjustable in the regular solution model, while in the DLP model they are calculated using the lattice parameters of the various two-component solids making up the multicomponent (3 or more) alloy. It is possible to determine, with the help of the above expressions, the solid alloy composition corresponding to a given temperature and liquid or vapour composition provided thermal equilibrium exists, as is often the case near the growth interface.

The epitaxial growth process is, as mentioned earlier, a non-equilibrium process. When a system is not at equilibrium, a thermodynamic driving force $\Delta\mu$ acts to restore equilibrium. The driving force for epitaxy is precisely this force. In epitaxy, a non-equilibrium situation is deliberately created in the form of a supersaturated gas mixture (VPE) or liquid solution (LPE), where the partial pressures or mole fractions of the crystal constituent elements are in excess of those which would exist in equilibrium with the solid substrate at the growth temperature. The resulting thermodynamic driving

force is responsible for the crystal growth that occurs. The maximum amount of solid that can be produced is determined firstly by the degree of supersaturation, since growth continues until equilibrium is established, and secondly, by the total volume of supersaturated gas passing through the system or the total volume of supersaturated liquid solution present. The maximum growth rate achievable is directly related to the quantity of solid produced and is thus limited by these two basic factors. The actual growth rate is lower than that predicted by thermodynamics because of further rate-limiting associated with the kinetics of the growth process.

A study of epitaxy is incomplete without an analysis of the kinetics involved in the growth process. Kinetics can greatly affect growth rates, composition, morphology, and material properties (impurity incorporation).

The kinetics of epitaxy are quite complex. The growth process consists of several kinetic steps. The reactants must diffuse from the bulk to the surface, where they adsorb onto it at vacant sites. The reactants subsequently desorb, react with other surface species, or simply decompose. The new molecules (or atoms) diffuse along the surface to a low energy site, such as a monatomic step, and then diffuse (if the growth temperature is high enough) along the step to a lower energy site, normally a kink. Incorporation into the lattice ensues, the reaction often resulting in the release of product molecules which then

desorb and diffuse into the bulk. The overall growth rate is limited by the slowest of these steps.

Mass transport, the first of the series of steps listed above, is a complicated process when treated in detail. It involves both fluid flow and diffusion. A detailed study of fluid flow is made difficult because of convection effects arising from temperature and solution concentration gradients present in the system. Models for mass transport that are physically reasonable yet simple have been developed. Such models are generally adequate for a description of mass transport. They are discussed briefly in section 1.2.

Surface kinetics are not nearly as well understood as mass transport. The reactants used in MOVPE decompose or react to form a variety of chemical species. Numerous reaction pathways leading to incorporation of the constituent atoms into the crystal are thus possible. It is difficult to determine which of these pathways are the most important in a given situation (orientation and nature of crystal substrate, precursors being used, growth temperature, carrier gas(es) present, etcetera). Surface catalytic reactions further complicate matters. In-situ infra-red laser spectroscopy is used to identify the various chemical species present and to determine the concentrations of these species both near the growth surface and elsewhere in the system [4]. Raman spectroscopy and mass spectrometry are also used for this purpose [5,6].

Chemical reaction pathways leading to growth are proposed on the basis of the identification of the chemical species present. Surface chemical reactions can significantly alter material properties (eg. GaAs p to n type, as discussed in section 1.3). Such reactions can also affect morphology, if two-dimensional stepwise growth is inhibited by the reaction. The adsorption of atoms or molecules that do not contain the crystal constituents can interfere with the growth process. Surface diffusion of the desired species may be inhibited by the presence of such 'poison' species, resulting in deterioration of crystal quality.

Surface kinetic processes are influenced by the nature of the surface on which growth occurs. Various crystal faces present atomically different surfaces. The surface kinetics, that is, adsorption, diffusion, and surface chemical reactions, will in general depend on the orientation of the substrate. Consequently, materials properties, crystal quality, and morphology may depend on the crystal orientation of the substrate surface. The presence of steps on the surface facilitates two-dimensional stepwise growth. If no steps exist, growth occurs via two dimensional nucleation. Different crystal orientations present surfaces with varying degrees of 'roughness' and thus influence the growth mechanism. Epilayers are often grown on substrates whose surfaces are purposely misoriented from a crystal face by a few degrees, in order to enhance the two-dimensional stepwise growth

process. Other sources of steps include screw dislocations and thermal roughening. Two-dimensional growth generally results in improved morphology and crystallinity.

Surface kinetics are strongly dependent on the growth temperature. Surrface diffusion is facilitated at higher growth temperatures. Low growth temperatures result in slow surface diffusion, and diffusion of the adsorbed species to the lowest energy sites (kinks) prior to incorporation may no longer be possible, energetically speaking. The growth mechanism is apt to be three dimensional when the growth temperature is too low for adequate surface diffusion. Deterioration of morphology and crystallinity ensues. Different surface reactions may dominate at different growth temperatures. Material properties can be altered by changes in surface chemical reactions when impurity incorporation occurs via such reactions. The growth rate is in general limited by surface kinetic processes at low growth temperatures. Low growth rates are necessary in order to obtain single crystal layers when surface diffusion is slow. (NOTE: General reference for section 1.1 is [7]).

1.2)The MOVPE Technique

MOVPE is a deposition technique where metal-organic compounds (metal allyls) and hydrides (or allyls) serve as the sources of the metal and non-metal components,

respectively, of the compound semiconductor to be formed. The desired reaction of these sources is pyrolysis of the compounds near the hot substrate followed by incorporation into the crystal epilayer. A variety of intermediate reactions are, however, unavoidably present. The metal-organics commonly used are high vapour pressure liquids or solids at room temperature, while the hydrides are gases or liquids. A schematic of the MOVPE system is shown in figure 1.1. The stainless steel bubblers containing the metal-organic sources are maintained at constant temperatures, typically in the range 10 to -20 °C, with the help of thermocoolers. The metal-organics are transported to the growth chamber by flowing a carrier gas through the bubblers. Ultra high purity hydrogen was used for this purpose in the present study. The flow rates of the alkyl precursors are determined by the source temperatures and the flow rates of the carrier gas. The flow rates of the hydrides and the carrier gas are set and maintained with the help of electronic mass flow controllers. The transport system is constructed entirely from welded stainless steel gas lines. Connections to the bubblers employ metal to metal seals. Connections to the other gas sources as well as those to the valves use rubber o-rings in the present system. The bypass manifold allows setup of the flow rates of the reactant gases prior to commencing growth. The effluents, consisting of unused reactant gases and various by-products, are pyrolyzed as

figure 1.1 : Schematic of the MOVPE setup (pulsed technique). Gas flow rates are set and regulated using electronic mass flow controllers (MFC). A bypass lines allows initialization of flow rates prior to commencement of growth. Unused reactants and byproducts are pyrolized before being pumped out by the rotary pump. Organo-metallic sources are maintained at the desired temperature with the help of thermal baths. A pressure check valve (PC) prevents flow of a reactant if the pressure in the bubbler is too low. Injection cells are a feature of the pulsed technique. The SiC coated susceptor is radiantly heated. Temperature monitoring and stabilization are done through an electronic temperature control system employing a thermocouple as a sensor.

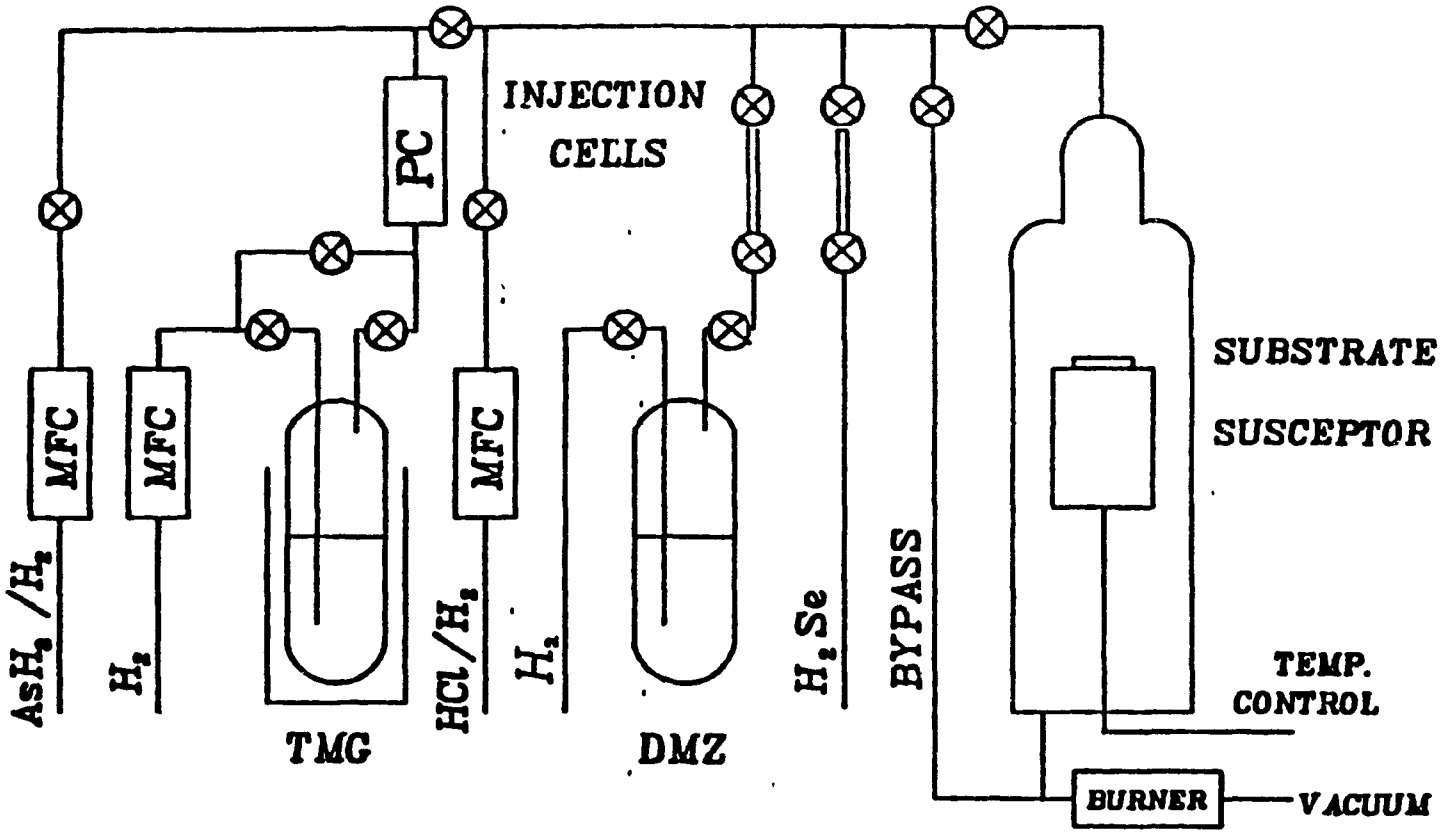

figure 1.1 : schematic of the MOVPE setup (pulsed technique)

they pass through the exhaust line. Low pressure operation is achieved through the use of a mechanical rotary pump in the system used here. The SiC coated graphite susceptor is radiantly heated in this case, with temperature monitoring and stabilization done through an electronic control system employing a thermocouple as a sensor.

Two reactor types were used in this study. A horizontal flow reactor, shown in figure 1.2, was used for conventional growth. A vertical flow reactor constructed of quartz, shown in figure 1.3, was used in a variation of the standard technique. In this second technique, small volumes of the various reactant gases were injected one at a time. A modification in the form of a set of injection cells (see figure 1.1) was necessary. Each consecutive pulse was followed by a time period where the reactant not adsorbed on the growth surface was 'flushed' out of the chamber by a flow of hydrogen gas. Under appropriate conditions growth by atomic layer epitaxy (ALE) was possible.

The MOVPE process consists of several steps: 1)input of reactants, 2)mixing of reactants, 3)diffusion to the substrate (mass transport), and 4)growth at surface and removal of by-products. These steps are discussed in detail below.

1.2.1)Input of Reactants

The source gases containing the metal components of

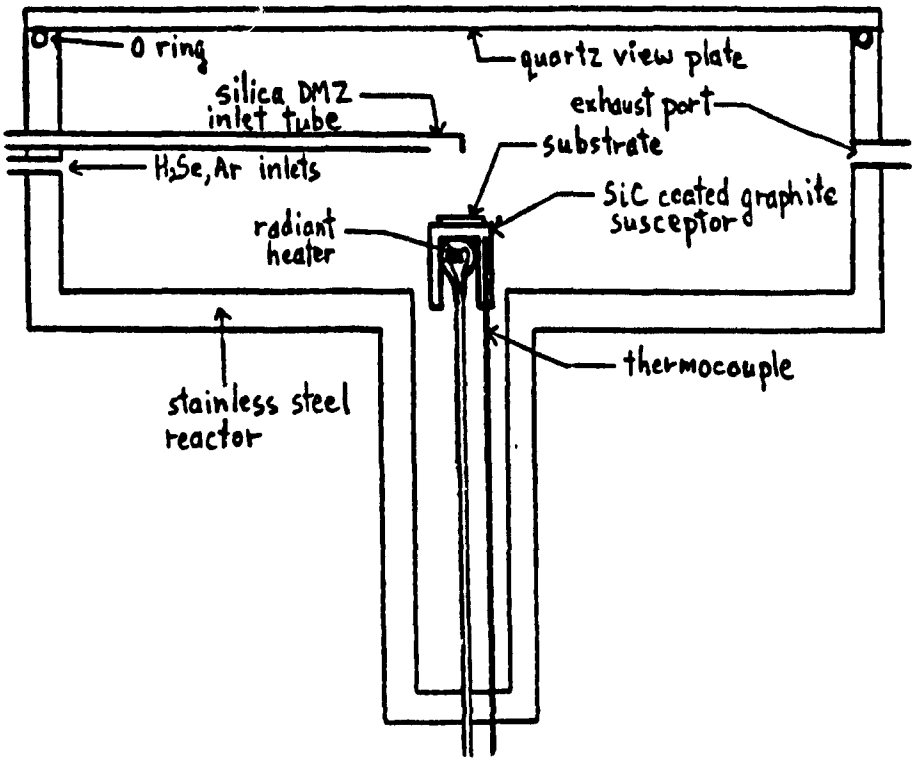

figure 1.2 : conventional MOVPE reactor

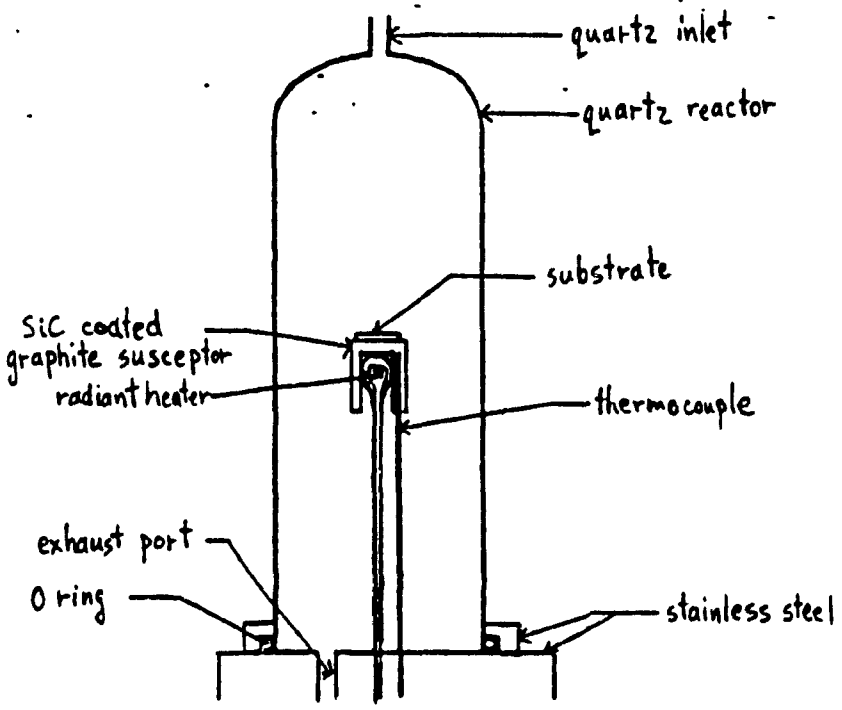

figure 1.3 : pulsed-technique reactor

the compound semiconductor are introduced into the growth chamber through an inlet separate from that through which the non-metal reactant gases pass. The separate introduction of the metal-alkyl and the non-metal hydride is necessary when these precursors undergo premature gas phase reactions. An extended inlet tube which allows introduction of the metal alkyl close to the hot substrate is typically used. Optimization of reactor geometry is then essential in order to obtain uniform (thickness,material properties) epitaxial films. Alternatively, precursors which do not react prematurely can be used in the growth of the compound. Mixing of the reactant gases prior to introduction into the chamber is then possible. Limitations in the number of available precursors (and purity of these) generally make this a difficult proposition.

1.2.2)Mixing of Reactants

Uniform growth over the substrate surface requires that the composition of the gas mixture immediately above the surface be constant. The reactant gases must therefore be well mixed prior to reaching the substrate. A turbulent gas flow region is generally present upstream of the susceptor. Efficent mixing occurs in this region. A proper reactor design ensures that a stable laminar gas flow pattern is established downstream of the turbulent region near the reactor gas inlets. Homogeneous gas phase

reactions may occur following mixing of the reactant gases. One such reaction, adduct formation, occurs in the growth of compound semiconductors containing indium [7,8]. The adduct, R_3III-VR'_3 in the case of III-V compounds, undergoes elimination reactions whereby RF' molecules are released, the end product being RIII-VR'. This highly reactive complex forms polymers $(RIII-VR')_n$ that deposit on the reactor walls upstream from the substrate. Polymer formation results in a low growth efficiency, and thus reduced growth rates. Non-metal alkyls, which are more stable than the corresponding hydrides, may react with the metal alkyl to form adducts that do not undergo elimination reactions. These adducts can then serve as the transport agents, provided that dissociation of the adduct and pyrolysis of the non-metal alkyl and, of course, the metal alkyl, occurs at the elevated temperature found near the substrate. Premature gas phase reactions can lead to homogeneous nucleation of the compound (dust particles). Precursors having low pyrolysis temperatures may partially pyrolyze upstream of the substrate and subsequently react with other chemical species present to produce various complexes. Complete pyrolysis of the reactants leading to deposition of component elements on the reactor surface is also possible. Heterogeneous reactions between the precursors with the reactor surface acting as a catalyst are possible, as is the surface catalyzed pyrolysis of the precursors. The specific reactions occurring in the growth

of a given compound and the extent of these reactions is greatly dependent upon the choice of precursors. Growth efficiency can be high if the proper precursors are selected.

1.2.3)Diffusion to the Substrate (Mass Transport)

Mass transport involves two processes, gas flow and diffusion. The thermal gradients present in the reactor produce convection, thus the gas and thermal systems are coupled, introducing further complications to the already complex mass transport problem.

Gas flow is treated assuming no temperature gradients for simplicity. The gas flow pattern is determined for flow through a tube. A stable laminar flow having a parabolic velocity profile is established after a certain distance down the tube, assuming uniform gas velocity across the tube at the entrance. The introduction of a plate (susceptor) in the presence of a uniform velocity profile results in the formation of a laminar boundary layer of width

$$d \propto (Dx/U)^{1/2} \qquad (1.5)$$

where D is the diffusion coefficient, x is the position along the plate, and U is an average velocity [7]. The velocity is zero at the surface and gradually increases

with increasing distance from the plate.

Mass transport occurs via diffusion as well as forced and thermal convection. If convection effects are absent, mass transport is essentially by diffusion through the boundary layer formed at the surface. A simple model assumes a stagnant boundary layer [7]. The flux of the metal alkyls and non-metal hydrides (or alkyls) diffusing from the homogeneous bulk region through the boundary layer to the interface is given by

$$J = D(p-p_o)/RTd \qquad (1.6)$$

where p is the partial pressure of the element in the bulk, p_o is the equilibrium partial pressure at the interface, and D is the diffusion coefficient of the element (proportional to T^2). Assuming the growth temperature is sufficiently high, so that surface reactions are rapid, the growth rate is determined by diffusion. In general, III-V (II-VI) compounds are grown with a high ratio of V to III partial pressures in the input gas stream. Under these two conditions, the growth rate is limited by the flux of the group III element. Diffusion limited growth is characterized by a growth temperature and substrate orientation independent growth rate. (A more sophisticated model assumes a well mixed bulk gas phase with diffusion transport to the surface through a boundary layer formed in the presence of a parabolic velocity

profile [7]. The growth rate was determined assuming a temperature gradient in the boundary layer which increased linearly with height. Comparison of results from this analysis with experimental data obtained in the growth of Si by VPE showed good agreement). The presence of turbulent gas flow in the vicinity of the growth surface gives rise to local variations in the growth ambient above the substrate, resulting in non-uniform material properties, growth rate, and alloy composition, and is thus to be avoided.

1.2.4)Growth at the Surface (Surface Kinetics) and Removal of By-products

The presence of several chemical species leads to a variety of possible surface reactions. As mentioned in section 1.1, surface chemical reactions can greatly alter material properties, morphology, and crystallinity. The information available on these reactions is sparse if not non-existent, primarily because of the difficulties involved in probing the surface non-intrusively, and also because the reactions occurring depend upon the particular precursors being used.

The by-products formed during incorporation must diffuse out through the boundary layer if they are to be removed from the system. Turbulence and thermal convection may result in gas recirculation, preventing the rapid

removal of the by-products. These effects can also lead to difficulties in the formation of abrupt interfaces. (NOTE: General references for section 1.2 are [7,8]).

1.3)Optimization of the Growth Parameters

The effects of growth variables such as growth temperature, reactor pressure, substrate crystallographic orientation, gas phase composition, and precursors used on deposition rates and material properties have been studied in detail for GaAs. Results of these studies and those on other III-V compounds are now discussed.

The choice of precursors can affect both growth efficiency and material properties. As pointed out earlier, growth efficiency is greatly reduced when the precursors react prematurely to form unstable adducts (leading to polymer formation), tiny crystallites (dust particles), or other unwanted complexes, or when the precursors decompose (pyrolyze) prematurely resulting in elemental deposition on the reactor walls. The problem of polymer formation encountered in the growth of InP using TMIn and PH_3 was circumvented with the replacement of the hydride by the more stable alkyl $P(C_2H_5)_3$ (or $P(CH_3)_3$) [9]. The adduct formed in this case does not undergo the elimination reaction and readily dissociates at the growth temperature normally used. The P alkyl does not easily decompose, however, thus PH_3 must also be added to the system.

Tri-methyl group III alkyls are generally favoured over the less stable ethyl alkyls, since the latter will prereact to a greater extent, thus reducing growth efficiency. The low growth rates observed in the growth of GaAs when TEG are explained by polymer formation resulting from the creation of unstable adducts from this less stable metal alkyl [10]. The hydride AsH_3 is generally used in the growth of GaAs. The pyrolysis of AsH_3 is catalyzed by a GaAs surface [8]. This process facilitates growth at lower temperatures where a lower degree of impurity incorporation is expected [8]. Increased growth efficiency also results. Growth surface assisted catalytic pyrolysis is precursor dependent.

Precursors affect material properties via impurity incorporation. The purity of the precursors being used in the growth of a compound is of vital importance in this respect, since contaminants present in the precursors can be incorporated into the solid. Common contaminants present in TMG include Zn, Sn, and Ge allyls and methyl silanes [8]. O_2 and/or H_2O may be found in AsH_3 and H_2, while alkoxides can originate in Al alkyl sources [8]. GaAlAs grown using the above compounds contains O, an unwanted impurity that acts as a deep non-radiative acceptor. Purification of the reactants as concerns oxygen generally involves the use of TMA as a getterer. Precursors, being chemical compounds, are inherently a source of impurities, specifically, carbon. Carbon is present as an impurity in GaAs grown using TMG. Experimental evidence links carbon

incorporation to a surface reaction involving methyl radicals $CH_{x<=3}$ and $GaCH_{x<=3}$ and $AsH_{x<=3}$. The formation of methane via a transfer of a H atom from the $AsH_{x<=3}$ species to the methyl radicals (in the gas phase as well as on the surface) removes the source of carbon [8]. A low concentration of arsine (and therefore $AsH_{x<=3}$) results in increased carbon incorporation. The material undergoes a p to n type transition as the V/III ratio is increased, as expected, if the above reaction mechanism determines the degree to which C is incorporated. The use of TEG in the growth of GaAs results in material that is free of C [8]. It is proposed that the formation of stable reaction products C_2H_4 and C_2H_6 readily occurs, thereby lowering the concentration of ethyl radicals that may contribute to C incorporation [8]. The availability of new precursors of high purity is essential if purer materials are to be grown.

Kinetic processes are strongly temperature dependent, hence growth temperature is an important parameter in MOVPE. The growth rate of GaAs as a function of temperature, in the standard case where TMG and AsH_3 are used as reactants and the V/III ratio is large, is characterized by three temperature regimes. The growth rate increases with increasing growth temperature at temperatures below about 550 °C. This temperature dependence is ascribed to the reduced rate of surface decomposition (pyrolysis) of AsH_3. The rate limiting step

is thus a surface kinetic reaction [8,10]. At temperatures above 750 °C, the growth rate decreases with increasing temperature. The possible mechanisms responsible for this behavior include desorption of As and/or Ga species, homogeneous nucleation in the gas phase (depletion of reactants), or the increased equilibrium vapour pressure of Ga at higher temperatures [8,10] (thermodynamic limitation also possible [10]). The growth rate is weakly temperature dependent in the range 550 to 750 °C. Diffusion limited growth occurs in this temperature regime. The growth rate is independent of the V/III ratio, provided it is much greater than unity. It is also independent of the substrate orientation, since surface kinetics are rapid at these temperatures. The growth rate is directly proportional to the flow rate of TMG. The above observations are consistent with those expected for diffusion limited growth. GaAs is generally grown in the diffusion limited growth regime. The use of low temperatures within this regime results in a decreased incorporation of impurities when the sources of these are contaminants present in the precursors.

The nature of the growth surface is different for the various crystallographic orientations of the substrate. The nature and number of surface sites present are unique to the specific orientation chosen. Surface kinetic processes such as adsorption of the various chemical species present and surface reactions of these species are sensitive to the type of surface sites found on the surface, hence substrate

orientation can affect growth rates, morphology, and material properties. The growth rate for GaAs is dependent on the substrate orientation when the rate limiting step is a surface kinetic process [8]. Two-dimensional stepwise growth may be inhibited by the bonding of hydrocarbon radicals to certain surface sites, thus explaining the rough surface morphology observed in the growth of GaAs [8]. Impurity incorporation can depend on substrate orientation, since the adsorption of a particular chemical species may occur with greater probability at specific surface sites. The extent of C incorporation in GaAs grown using TMG is substrate orientation dependent. The <111>As surface has a strong affinity for radicals containing C, that is, $Ga(CH_3)_{x<=3}$ and $(CH_3)_{x<=3}$. The increase in the relative number of these species compared to As bearing species is expected to result in an increased C concentration on the basis of a model presented above. Experimental evidence is in agreement with this conclusion [8].

Gas phase composition (V/III ratio) can have an effect on material properties. The high vapour pressure of As, as compared to that of Ga, necessitates the use of V/III ratios that are greater than unity . The proper sttoichiometry of the epilayers is then maintained. In the case of GaAs grown using TMG and AsH_3, an increase in the V/III ratio results in a decreased C concentration [8]. The number of methyl radicals present is reduced by the

increased hydrogen transfer from the greater number of AsH_3 species to the radicals to form methane. The methyl radicals are the source of C, hence less C is available for incorporation. The increase in flow of a reactant, keeping the flow of the other reactant constant, will result in increased impurity concentration if contaminants are present in this reactant, since a greater quantity of these contaminants are then introduced to the system.

A change in reactor pressure while keeping flow rates constant alters the gas velocities. A lowering of the pressure increases the velocities of the reactants, thus reducing their transit times. This can be beneficial when using precursors which have low pyrolysis temperatures or undergo premature reactions, since interaction of the chemical species is then reduced. Low pressure growth of GaAs using TMG requires an increased V/III ratio if the concentration of C is to be kept low. This may be due to the reduced interaction of the C and As bearing species [8]. Increasing the reactor pressure by flowing an inert gas results in dilution of the gas mixture. This may also prevent premature gas phase reactions from occurring. Increased growth efficiency is expected when the extent of prereaction is reduced.

1.3.1) MOVPE of ZnSe

The crystal quality, morphology, and material

properties of ZnSe epitaxial layers grown by MOVPE are dependent on the choice of growth variables. Optimization of the growth parameters is necessary for the growth of high quality ZnSe thin films.

The specific reaction pathways which lead to growth are precursor dependent, hence precursors must be chosen which allow the purest, highest quality material to be grown. Several precursors, including $(C_2H_5)_2Zn$ [3], $(CH_3)_2Zn$, H_2Se [11], $(C_2H_5)_2Se$, $(CH_3)_2Se$ [12], and the heterocyclic compound C_4H_4Se [13] have been used in the growth of ZnSe. The precursors in standard use, DMZ and H_2Se, have a low degree of stability [14]. DMZ decomposes at temperatures above 150 °C [15], although the pyrolysis temperatures of the reactants will differ in the growth environment. Premature decomposition of the reactants is thus expected to occur at the typical growth temperature of 300 °C. Premature pyrolysis is of minor importance. The serious problem when using H_2Se and DMZ (or DEZ) as reactants is that these precursors undergo homogeneous gas phase reactions. The reactions proceed at room temperature [3,14,16]. It is proposed that adduct formation occurs and the adduct rapidly undergoes elimination reactions to form ZnSe as the end product [15]. Crystallites (dust particles) present in the gas phase upstream from the susceptor result from the homogeneous nucleation of the ZnSe molecules. Heterogeneous deposition on the reactor walls also occurs [16]. The suppression of the unwanted premature reactions

requires the separate introduction of the reactant gases. DMZ is introduced into the reactor through a silica inlet tube terminating approximately 2 cm from the substrate [17]. This arrangement does, however, make it difficult to produce uniform layers. It is preferrable to use DMZ as opposed to DEZ, since the former is chemically more stable [14]. The problem of premature reactions can be eliminated through the use of alternate precursors. Prereaction is negligible when the precursors used are DMZ and C_4H_4Se [13], although higher growth temperatures (approximately 500 °C) must be used in this case. A stable double adduct formed from DMZ and DESe (or DMSe) which dissociates at the growth temperature could perhaps block the premature reaction of DMZ and H_2Se, however, it appears that such adducts cannot be formed [18]. The extent of premature reaction can be greatly reduced through the use of Zn and Se allyls as the precursors [12]. High growth temperatures (400-600 °C) are necessary when using the more stable Se allyl, however, photo-MOVPE allows layers to be grown at lower temperatures, with a corresponding improvement in photoluminescence spectra [19]. Surface reactions are possibly enhanced by irradiation with short wavelength light (200-400 nm). The premature reaction of DMZ and H_2Se is avoided when growing epilayers by a variation of the standard MOVPE technique (ALE--as previously described). Layer thickness variations of 10% or better over an area of 1 cm^2 are possible using this technique. (Little

information is available concerning the reaction mechanisms involved in the MOVPE growth of ZnSe using the various precursors mentioned above, however, see [20]). The precursors used in this study were DEZ or DMZ and 100 % H_2Se. DEDSe was used in place of H_2Se in one case.

Reactor pressure is an important parameter in the growth of ZnSe when the standard precursors, namely, DMZ (or DEZ) and H_2Se, are used. The premature gas phase reactions associated with these precursors are suppressed when a low pressure technique is employed [21]. Low pressures result in higher flow velocities and hence decreased transit times, thus the probability of interaction of the reactants prior to reaching the growth surface is reduced. Low pressures are achieved through the use of low reactant flow rates and a high capacity pumping system. A change in pressure does not alter the flow pattern in the reactor.

Low reactant flow rates were used in this study, however, limitations in the pumping capacity of the present system prevented the attainment of reactor pressures lower than 1-5 torr (compared to .15 torr in [21]). In a detailed study of low pressure (.3-1 torr) MOVPE growth of ZnSe and ZnS using the precursors DMZ, H_2Se, and H_2S, an increase in the growth rate with increasing pressure (flow rates constant, pumping capacity altered by adjusting exhaust valve) was observed [20]. An increase in reactor pressure, which increases the probability of adduct formation, would

lead to an increased growth rate if the adduct formation mechanism dominates the growth rate. In another experiment, the growth rate was found to increase when the pressure was increased by flowing a greater amount of buffer gas (He) (reactant flow rates constant,exhaust valve wide open). The probability of adduct formation decreases with increasing pressure in this case and the growth rate should decrease accordingly if the adduct formation mechanism dominates the growth rate. A mechanism consistent with the experimental observations is a pressure dependent sticking coefficient of DMZ or its complexes. An increase in pressure suppresses the desorption of these species, thus the sticking coefficient increases and the growth rate is higher. The species are prevented from desorbing by collisions with other molecules in the gas ambient. Surface kinetics are important if this interpretation of the data is correct. A different approach to the problem of premature reactions involves the use of a high pressure technique. A large quantity of a buffer gas such as H_2 or argon is flowed into the reactor. The dilution of the reactant gas mixture is thus increased, and correspondingly, a decrease in the extent of premature reaction occurs [3,22,23]. Argon and pentane were used as dilutants in this study, however, only small quantities of these gases were injected (pressure approximately 10-20 torr).

The single most important parameter in the growth of ZnSe is the growth temperature. Material properties and

crystal quality are strongly dependent on the growth temperature, as revealed by comparison of the photoluminescence spectra and X-ray rocking curves of samples grown at different temperatures [22,24]. Transport measurements also indicate changes in carrier concentration, mobility, and resistivity as the growth temperature is varied [25,26].

The temperature dependence of the growth rate has been studied for both low pressure (0.1-1 torr) [20,24] and high pressure (80 torr) [22] growth of ZnSe using the standard precursors DMZ (or DEZ) and H_2Se and VI/II ratios greater than one. In the high pressure case, the growth rate was found to be independent of temperature in the range 250-500 °C, and decreased at higher temperatures. The growth rate also increased linearly with the DEZ flow rate. These two observations led to the conclusion that growth in the temperature range 250-500 °C corresponds to the diffusion limited growth regime. Premature reactions are eliminated in their setup, so that the growth rate is determined by the diffusion of DEZ. In the case of low pressure growth, the growth rate exhibits a maximum at a growth temperature of about 300 °C. The decreased growth rate at lower temperatures is indicative of limitations imposed by surface reactions. The reduced growth rate at higher temperatures is attributed to a decrease in the sticking coefficient of DMZ or its complexes. Another possible explanation, namely, an increase in the extent of

homogeneous nucleation in the gas phase, which effectively depletes the amount of nutrients available for growth, is ruled out, since it is inconsistent with the observation that the growth rate increases with increasing pressure. The possibility of homogeneous nucleation is greater at higher pressures, hence decreased growth rates are expected if this is the case [20].

Surface kinetics are slow at the low growth temperatures used in the MOVPE growth of ZnSe (typically 250-350 °C), hence low growth rates are necessary to ensure good crystallization.

The low growth temperature characteristic of the MOVPE technique (and MBE) is a desired feature. A lower degree of contamination and a reduced concentration of stoichoimetric defects are expected as the growth temperature is decreased, hence these techniques should produce pure material with minimal compensation by complexes such as the A-center (zinc vacancy-donor complex). ZnSe epilayers were grown at temperatures ranging from 200-400 °C in the present study.

The gas phase composition (VI/II ratio) is another variable which can affect the material properties of ZnSe thin films. An investigation of the transport properties and photoluminescence of ZnSe epilayers grown at VI/II ratios varying from 5 to 75 (pressure 1 torr, T=300 °C, thickness=1 micron, reactants are DMZ and H_2Se) has been carried out [27]. An increase in the ratio resulted in

decreased carrier concentrations and increased resistivities and mobilities (room temperature). The ratio of near band edge luminescence to luminescence associated with deep centers (at 77 °K) also increased with increasing VI/II ratio. The growth of stoichiometric material requires the use of high VI/II ratios because Se has a high vapour pressure. Material grown using low values of this ratio may contain a larger number of Se vacancies. The observed changes are possibly related to changes in the number of Se vacancies and associated complexes. Se vacancies create deep donor levels in ZnSe [28]. In both low pressure [14,20] and high pressure [22] growth, the growth rate is found to depend solely on the flow rate of the minority reactant (DMZ or DEZ, for the standard case where VI/II > 1) over a large range of the VI/II ratio. Flow rates must be kept low, since the surface reactions are slow at the low growth temperatures generally used and low growth rates are therefore required to ensure proper crystallization of the material.

The growth of high quality ZnSe epitaxial layers requires the use of a lattice matched substrate. Furthermore, the substrate should have a thermal expansion coefficient close in value to that of ZnSe. In this respect, the ideal substrate crystal is ZnSe, however, high quality stoichiometric ZnSe single crystal substrates are difficult to obtain (Such crystals have good crystalline quality but are non-stoichiometric, as revealed by

luminescence-SA emission due to Zn vacancy related complex is present-these vacancies diffuse into epilayer) [1]. GaAs has been used extensively as a substrate because the lattice mismatch between these two materials is only 0.27%. There is, however, a difference of 33% in the thermal expansion coefficients of the two materials. The epilayers in the ZnSe/GaAs system are unavoidably subject to strain effects arising from these mismatches. These effects are reflected in the differences in PL spectra of bulk versus heteroepitaxial ZnSe , as discussed later in this report. Lattice mismatch will also result in degradation of crystal quality through the introduction of low angle grain boundaries. Lattice mismatch can be eliminated through the use of lattice matched substrate materials such as $In_xGa_{(1-x)}As$ [29], or alternatively, by growing a lattice matched ternary epilayer $ZnS_xSe_{(1-x)}$ [17] on GaAs, however, residual strain due to the mismatch in the thermal expansion coefficients of the epilayer and the substrate is not eliminated.

The crystallographic orientation of the substrate has a pronounced effect on the crystal quality, morphology, and material properties of the ZnSe epilayer. Layers grown on (100) and (111)B GaAs substrates are epitaxial, however, polycrystalline layers are formed when growing on (111)A GaAs [16]. Morphology of the epilayers also depends on the substrate orientation. A hillock structure, the hillocks lying parallel to the (0,-1,-1) plane, is found on layers

grown on (100) GaAs. This structure is absent on layers grown on (111)B GaAs [17]. The growth mechanism is thought to be responsible for the observed morphology [17]. Optimization of growth parameters, including the use of different precursors, is necessary if specular surfaces are to be obtained [14,23]. Photoluminescence spectra indicate that the optoelectronic quality of ZnSe epilayers grown on (100) GaAs is superior to that of layers grown on (111)B GaAs [17,30]. The observed variations in the PL spectra are possibly due to differences in defect densities generated by the growth mechanism operative in each of the two cases, which would result in materials which have different types and concentrations of impurities (and complexes).

(100) GaAs substrates, both semi-insulating and n-type, were used in the present study. ZnSe layers were grown directly on the substrate in most cases. ZnSe layers were also deposited on GaAs epilayers deposited in-situ on the GaAs substrate prior to the ZnSe growth. The growth of epitaxial layers with reproducible properties requires that the substrate surface be free of any contaminants [14]. A clean surface was prepared in the following manner: Residues were first removed by scrubbing the surface with a detergent solution. The substrate was then rinsed in de-ionized water and placed in electronic grade H_2SO_4 for approximately one minute. Surface damage was then removed through a chemical etch of duration 2 minutes in an $H_2SO_4:H_2O_2:H_2O$ 5:1:1 solution at 40 °C. This was followed

by a rinse in de-ionized water and then a rinse in propanol. The substrate was blown dry using N_2 gas. The substrate was placed on the susceptor and the system pumped down. The surface was then thermally etched to remove oxides by heating the susceptor to 650 °C and flowing H_2 (or HCl) through the reactor for a duration of 5 minutes. The substrate was cooled down to the growth temperature immediately after the thermal etch, and the growth run was then begun.

A list of the samples grown in the present study is given in table 1.1. Information concerning the choice of precursors, as well as the growth temperature and reactant flow rates (VI/II ratio) used in each case is also provided. All the samples, with the exception of samples 40 and 41, were grown by conventional MOVPE on (100) GaAs substrates. Samples 40 and 41 were grown by the pulsed technique (ALE), following the in-situ deposition of a GaAs buffer layer (thickness 0.5 microns) on the (100) GaAs substrate.

Samples 8, 9, and 10 were grown at temperatures of 200, 250, and 300 °C, respectively, with all remaining parameters kept fixed. This enabled a study of the effect of the growth temperature on the optoelectronic quality of the material to be carried out.

The use of different sets of precursors in the growth of samples 32, 29, and 50 allowed information about precursor-related effects on material quality to be

obtained.

Changes associated with the use of the pulsed growth technique as opposed to the conventional MOVPE technique were investigated by comparing the photoluminescence spectra of samples 39 and 40.

Samples 40 and 41, which were grown under identical conditions, were used to study the thickness dependence of material quality.

TABLES

Table 1.1 : Growth Parameters

Sample	Precursors sccm's/minute			VI/II Ratio	Growth Temperature °C	Growth Rate microns/hour	Epilayer Thickness microns
	Ar	H_2Se	DEZ1-H_2				
8	50	20	6 (10 °C)	48	200	6	1
9	50	20	6 (10 °C)	48	250	6	1
10	50	20	6 (10 C)	48	300	6	1
	--	H_2Se	DEZ2-H_2				
32		20	10 (-10 °C)	110	300	6	2
	--	H_2Se	DMZ - H_2				
29		8.5	10 (-20 °C)	4	300	3	1.5
40		n.a.	n.a.	n.a	300	n.a.	0.8
41		n.a.	n.a.	n.a.	300	n.a.	0.4
	--	DEDSe	DMZ - H_2				
50		unknown		unknown	400	unknown	unknown

CHAPTER 2

PHOTOLUMINESCENCE

2.)PHOTOLUMINESCENCE

Luminescence refers to all de-excitation processes whereby a crystal initially in an excited state undergoes a radiative transition to a lower energy state. The excited state involves either the presence of electron-hole pairs or the occupation (by electrons (or holes)) of internal excited states of defects. A variety of light emitting transitions are possible in semiconductors. Intrinsic radiative recombination processes involve electron-hole pairs and include band to band recombination, the radiative decay of excitons (and excitonic complexes - exciton molecules), and intraband transitions. The presence of defects such as impurities, vacancies and complexes formed from these two introduces the possibility of extrinsic radiative transitions. In the case of transitions involving electron-hole pairs, the defects act as recombination centers. A free hole may recombine with an electron bound to a defect. A free electron may recombine with a hole bound to a defect. An electron-hole pair bound to a defect can recombine (radiative decay of a bound exciton). Finally, a hole bound to one defect may recombine with an electron bound to another defect. In certain cases, defects (eg. transition metals) may interact with crystal fields. The energy levels of the center may be split by this interaction. Internal electronic transitions between two such levels can be accompanied by light emission. The

radiative transitions can occur with the simultaneous emission or absorption of phonons. Line broadening and structure in emission bands can provide indications of the relative importance of phonon assisted transitions.

Recombination can alternatively occur through non-radiative channels. The energy released in the transition may be transferred to another electron (Auger process). It may be given up to the lattice phonons (multi-phonon emission process). A continuum of energy states across the bandgap would also lead to non-radiative recombination. Surfaces and precipitates in the crystal may generate this continuum of states [31]. The lifetime of the excited state is shortened in the presence of non-radiative de-excitation channels. The quantum efficiency of luminescent processes is reduced as well (the quantum efficiency is 1 in the complete absence of non-radiative mechanisms).

In photoluminescence, the necessary excited state, in the form of electron-hole pairs, is usually created by excitation of electrons from the valence band to the conduction band via absorption of photons having energies greater than the minimum band gap energy. The absorption process involves the interaction of the electron and the electromagnetic radiation. This interaction is treated as a perturbation to the electronic Hamiltonian. The interaction is expressed as [32]

$$H' = A*p + A^2 \qquad (2.1)$$

where A is the vector potential operator and p is the electron momentum operator. The second term in this expression is neglected here. An analysis of the perturbation problem leads to the following expressions for the conservation of wavevector and energy:

$$k_f = k_i + k_{photon} \;,\; E_f(k_f) = E_i(k_i) + \hbar w_{photon} \qquad (2.2)$$

k_{photon} is, in general, much smaller in value than k_f and k_i, hence the above expressions are replaced, to good approximation, by the expressions

$$k_f = k_i = k \quad , \quad E_f(k) = E_i(k) + \hbar w_{photon} \qquad (2.3)$$

Electronic transitions involving only photon absorption (or emission) are known as direct transitions, since the electron wavevector remains unchanged in going from the initial state to the final state. Transitions in which photon absorption (or emission) is accompanied by the simultaneous absorption (or emission) of a phonon of wavevector q are known as indirect transitions. Indirect transitions are second order processes and therefore have a lower probability of occurring than direct transitions.

The magnitude of the absorption coefficient for photons having energies greater than the band gap energy

depends on the nature of the band gap (direct or indirect). The absorption coefficient is much larger in the case of direct gap semiconductors. The absorption strength also depends on whether the transition (valence to conduction band) is allowed or not. Electric dipole transitions, if allowed, result in stronger absorption. ZnSe, as a zincblende type crystal, has a direct gap. The band structure in the vicinity of the energy gap is shown below.

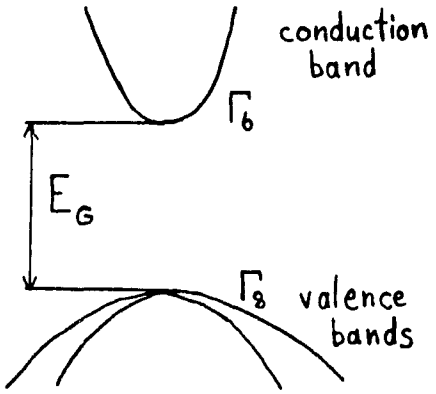

$E_G = 2.822$ eV at 4°K [33]
$m_e = 0.16m$ [33]
$m_h = 0.6m$ [34]
m is the electron mass

figure 2.1 : band structure of ZnSe near the Γ point ($\vec{k}=(0,0,0)$)

The valence band wavefunctions are p-like and the conduction band wavefunctions are s-like in ZnSe, hence the electric dipole transition is allowed. Creation of electron-hole pairs via absorption of above band gap light is thus very efficient in this material. Excitation is followed by rapid thermalization of the electrons and holes. The electrons (holes) quickly lose excess kinetic energy through collisions with other electrons (holes) and the emission of acoustic and optical phonons. A quasi-equilibrium distribution of electrons and holes among the existent energy levels is set up under continuous excitation. Excitation is balanced by luminescent and

non-radiative recombination processes.

Van Roosebroeck and Shockley (see discussion in [31]) derived a theoretical expression relating the radiative recombination rate to the absorption coefficient by applying the principle of detailed balance and assuming unit quantum efficiency. Absorption and emission spectra are thus intimately related. Structure associated with a particular transition (eg. free excitons) may be more pronounced in absorption spectra. Transition energies determined from an analysis of absorption spectra can facilitate the identification of structures observed in photoluminescence spectra.

In the next few pages, the various radiative transitions are explained in detail. The temperature dependence of the photoluminescence spectra of ZnSe is also discussed.

2.1)Excitons

Free excitons are mobile electron-hole pairs. The important exciton transition in direct gap materials such as ZnSe is a direct transition involving the creation or destruction of excitons with wavevector k=0. The exciton energy levels form a hydrogenic spectrum ($E = E_g - const/n^2 + \hbar^2k^2/2m_{exciton}$) if spherical conduction and valence bands are assumed. The transition probability associated with the excited states of the exciton decreases as $1/n^3$ relative to

the ground state exciton transition probability [35]. Exciton transitions involving direct transitions with the simultaneous absorption or emission of q=0 LO phonons are also possible. The transition probability is lower in this case.

The free exciton transition in ZnSe has been observed in several studies. Absorption spectra obtained from transmission and reflectance measurements on bulk ZnSe crystals contain structure which is associated with the formation of K=0 excitons, that is, the creation of bound electron-hole pairs via direct ($k_1=k_2$, $K=k_2-k_1=0$) allowed electronic transitions, at the gamma point (band gap--k=0) [34]. Reflectance [36] and magnetoreflectance [37] spectra of bulk ZnSe crystals also reveal structure attributable to free excitons. An analysis of free exciton related structure appearing in photoluminescence excitation spectra of ZnSe [33] yielded a value of 19.0 ± 0.5 meV for the free exciton binding energy (transverse exciton - E_{ex}^{T}). Luminescence peaks due to free exciton recombination have been observed in photoluminescence spectra of both bulk ZnSe crystals [38,39,40,41,42] and epitaxial ZnSe layers grown by LPE [33] (ZnSe substrates), MBE [43,44,45,46] (GaAs substrates), and MOVPE [11,47,48] (GaAs substrates). Luminescence peaks arising from the recombination of free excitons with the simultaneous emission of optical phonons have been observed in some cases (LO replica - [33,40,47]; LO,2LO,TO,TO-LO replicas - [42]). Emission due to the

radiative recombination of free excitons in the excited state (n=2) has also been observed [42,45]. Results of a study of luminescence reabsorption in ZnSe [40] indicate that polariton effects are important in ZnSe. Polaritons are quasi-particles which include the effect of exciton-photon coupling. Two distinct branches (upper and lower polariton branches) having different energy-wavevector dispersion relationships are formed when the exciton-photon interaction is taken into account. Two emission peaks, corresponding to UPB (higher energy of the two) and LPB emission, have been observed in the photoluminescence spectra of GaAs [49]. Double-peaked structures present in the excitonic energy region in photoluminescence spectra of ZnSe have been similarly ascribed to polariton emission [41,42,43,44].

Free exciton recombination is the dominant luminescent transition at low temperatures only in intrinsic or extremely pure semiconductors. Ionized impurities present in less pure materials create local fields which act to 'tear' apart the excitons. The free exciton transition is important only if the temperature is sufficiently low such that $kT_{\perp}$ exciton binding energy. Excitons are broken up when the thermal energy exceeds the free exciton binding energy thus at higher temperatures, the electron-hole pairs remain as 'free' carriers in the conduction and valence bands. Luminescence resulting from the recombination of the interacting unbound electron-hole pairs, that is, the band

to band transition, is then dominant. Since free excitons are mobile and therefore have kinetic energy, the radiative decay of free excitons results in a luminescence band. In ZnSe, the free exciton emission peak has a linewidth (FWHM) of about 1-2 meV at 4 °K [33,42].

Relatively pure semiconductors containing low concentrations of impurities are characterized by a low temperature photoluminescence spectrum in which the dominant luminescent transitions are those involving the radiative decay of excitons localized at donor or acceptor impurities. Emission lines arising from the decay of bound excitons are downshifted in energy relative to the free exciton emission peak by amounts equal to the binding (or localization) energies of the exciton to the particular impurities in question. The linewidths (FWHM) of bound exciton luminescence peaks are substantially reduced from that observed for the free exciton emission peak, since localization implies that the exciton has essentially no kinetic energy. The limiting linewidth (FWHM) associated with a bound exciton transition in ZnSe is approximately 0.2 meV [33]. Impurity broadening effects present at higher impurity concentrations effectively increase this linewidth. Random fluctuations in residual strain present in the crystal also act to increase the linewidth. In the heteroepitaxial growth of ZnSe on GaAs substrates, strain effects arising from lattice mismatch and difference in thermal expansion coefficients act to greatly increase the

bound exciton emission linewidth.

The transition energies of the various donor bound exciton (DBE) components (ground and excited states of the complexes) were determined through a detailed analysis of photoluminescence spectra of bulk ZnSe crystals grown from the vapour phase [39]. Comparison of photoluminescnce spectra of both undoped and lightly doped crystals made possible the identification of the spectral features associated with the individual donors. The spectral lines (transition energies) identified for each donor included the ground and excited state neutral donor bound exciton transitions (D^0,X), labelled I_{2o}, I_{2a}, I_{2b}, etcetera, the two-electron satellites (TES) associated with each of these, and the emission line due to the radiative decay of excitons bound to an ionized donor (D^+,X). Two-electron transitions refer to bound exciton transitions which leave the neutral donor in an excited state. These transitions can occur with the bound exciton complex initially in its ground state or in any one of its excited states. The emission peak corresponding to a two-electron transition in which the neutral donor is left in the 2p state is downshifted in energy relative to the transition where the neutral donor remains in the ground state following the bound exciton transition by precisely the 1s-2p donor excitation energy. The 1s state is subject to chemical shifts due to central-cell effects, thus, the 1s-2p energy difference, and therefore the position of the two-electron

satellite relative to the 'main' peak, is dependent on the chemical nature of the donor. The 1s-2p energy differences can be determined for the individual donors provided the relevant luminescence peaks have been identified. An estimate of the donor binding energies can then be obtained using the formula [39]

$$E_D = E_{2p} - E_{1s} + 0.25E_o \qquad (2.4)$$

where E_o is the effective-mass binding energy (the 2p effective-mass energy is 1/4 of E_o). The 'theoretical' binding energy, E_o, is given by [39]

$$E_o = (m/m_e \epsilon_s^2) E_H \qquad (2.5)$$

where E_H is the hydrogenic binding energy, m is the mass of the electron, and m_e and ϵ_s are experimentally determined values of the electron effective mass and static dielectric constant, respectively. m_e can be determined from a measurement of the Zeeman splitting of the 2p two-electron satellites in the presence of a magnetic field. Donor binding energies were calculated as outlined above. The dielectric constant was determined in an independent study.

A more recent study of DBE transitions in ZnSe samples grown by LPE involved the use of selective photoluminescence (SPL) and photoluminescence excitation

(PLE) techniques [33]. A tunable dye laser is required in these experiments. In the first technique, photoluminescence spectra are obtained for different excitation frequencies. Resonant excitation of certain transitions is possible with the proper choice of incident photon energy. Separation of the enhanced transitions from a background of overlapping luminescence peaks is facilitated. Another advantage of this technique is that contributions to spectral linewidths arising from inhomogeneous broadening processes, including broadening due to inter-impurity interactions and broadening related to strain effects, can be reduced considerably in relatively pure crystals, hence line narrowing of the enhanced transitions occurs. The linewidth is limited ultimately by the laser linewidth. The technique is of limited value in the study of doped material due to the intersite hopping of excitons following resonant excitation into a specific DBE state ($n<10^{17}$ is necessary to observe resonantly excited TES in MOVPE ZnSe/GaAs [50]). An analysis of resonantly excited TES yielded values for the 1s-2s,2p donor excitation energies which were in excellent agreement with the values determined earlier by Merz et al [39]. TES associated with DBE transitions where the donor remains in the 3s or 3p excited state following the transition were also observed. The 2p and 3p donor energy levels are not subject to shifts due to central-cell effects, hence the experimentally determined 2p-3p binding

energy difference can be used to obtain the 'theoretical' effective-mass donor binding energy E_o. A more accurate value of E_o=26.06 ± 0.15 meV was obtained by this method. The revised value of E_o was used to determine the donor binding energies (as previously outlined).

In the PLE technique, the intensity of an emission line is monitored as the incident photon energy is varied. The plot of the detected line intensity versus the excitation energy contains maxima and minima corresponding to excitation channels and absorption processes associated with the monitored transition (eg. I_{2a} TES transition for In donor monitored - PLE spectrum contained peaks at I_{2c}, I_{2b}, I_{2a} and minima at transverse free exciton n=1,2,3 states). The binding energy of the free exciton was determined by the analysis of PLE spectra, as previously mentioned. The DBE transition energies, the donor excitation energies, and the calculated donor binding energies obtained by Dean et al [33] are listed in tables 2.1, 2.2, and 2.3.

The identification of donors present in heteroepitaxial ZnSe/GaAs epilayers via comparison of DBE transition energies with those obtained from the study of unstrained, pure crystals is not possible. The total energy range spanned by the principle DBE transitions for the known donors is 0.75 meV, whereas the DBE linewidth is 1 meV or greater in heteroepitaxial layers. Emphasis is thus placed on TES as a means of identifying donors. The energy

spread of the TES luminescence resulting from DBE transitions in which the donor is left in the 2p excited state is about 3.2 meV. The resolution of the TES is poor in standard photoluminescence spectra obtained using above band gap exciting light, however, the TES associated with different donors can be resolved with the use of the SPL technique. This technique is therefore an important tool in the study of heteroepitaxial ZnSe thin films.

Little information concerning excitons bound to neutral acceptors (labelled I_1 or (A^o,X)) is available, due to the difficulties encountered in attempts to incorporate impurities which form shallow acceptor energy levels. Incorporation of these impurities is invariably accompanied by the introduction of compensating centers. It is extremely difficult to obtain p-type ZnSe. Information concerning shallow acceptor states is generally obtained through the analysis of donor-acceptor pair (DAP) luminescence bands present in low temperature photoluminescence spectra of n-type ZnSe containing shallow acceptor impurities. In a study of luminescence associated with shallow acceptors in vapour grown ZnSe crystals [51], it was proposed that an emission line observed in the bound exciton luminescence region resulted from the radiative decay of excitons bound to neutral Li acceptors. Evidence supporting this assignment for the emission line included a correlation between the strength of this line and that of DAP emission associated with Li acceptors, the explanation

of the triplet structure of the line by a model which describes the excited states of neutral acceptor bound exciton complexes, and an exciton localization energy consistent with that expected for the binding energy of this acceptor (Haynes' rule $E_{BX}/E_A=0.1$ [52]). Another emission line appearing at a slightly higher energy was tentatively identified as the emission due to radiative decay of excitons bound to neutral Na acceptors. Identical assignments for the two lines have been made in other research papers [33,53,54]. An emission line due to the radiative decay of excitons bound to neutral N acceptors has been identified in photoluminescence studies of N doped ZnSe grown by LPE [55] (ZnSe substrates) and MOVPE [52,55] (GaAs substrates). The correlation in the intensity of this emission line (and a DAP band) with the introduction of N into the system supports this identification. Two-hole satellites of the bound exciton luminescence peaks, involving 2S and 3S acceptor excited states, have been observed in the case of N and Li acceptors using the SPL technique [55]. The difference in the 1S-2S excitation energies for the two acceptors indicates that the binding energy of the N acceptor is 2.1 $\pm$ 0.7 meV less than that of Li. No conclusive evidence regarding bound exciton luminescence associated with shallow P or As acceptor states exists, although DAP emission involving P and As-related shallow acceptors has been observed [56] (ZnSe/GaAs MBE growth). An emission line characterized by a

transition energy which is lower than that for the decay of excitons bound to the shallow acceptors discussed above may be due to the the recombination of excitons bound to a neutral acceptor [39,57]. The emission line is associated with Cu, possibly along with Li and Na [58], or the acceptor Cu_{Zn} [57]. The acceptor bound exciton transition energies and acceptor binding energies are listed in tables 2.4 and 2.5.

DBE or ABE transitions involving the simultaneous emission of one or more q=0 LO phonons are also possible, albeit with progressively lower transition probabilities. Since the coupling to phonons is stronger for deeper levels, in this case, the acceptors, the LO phonon replicas are more prominant in the case of ABE transitions.

The observation of DBE and ABE transitions requires that the temperature be sufficiently low to allow the capture of excitons by the donors or acceptors (ie. kT $\leq$ exciton localization energy).

A luminescence band having a zero phonon peak energy of approximately 2.60 eV at 4 °K is sometimes observed in ZnSe grown by MOVPE. The band is known as the Y band. The characteristics of this band, namely, the weak coupling to phonons and a large linewidth (FWHM = 4 meV or more), are explained with the help of a model proposed by Dean [59]. The model assumes that the emission is due to the localized recombination of excitons at an extended defect, possibly a small dislocation loop.

A luminescence band whose peak energy is downshifted from the free exciton energy by an amount equal to the 1s-2s,2p shallow donor excitation energy has been attributed to the radiative recombination of free excitons which scatter inelastically at neutral donors [47].

2.2)Donor-Acceptor Pair (DAP) Transitions

Low temperature photoluminescence spectra of semiconductors containing both donor and acceptor impurities (or complexes which form donor and acceptor levels) include luminescence bands associated with electronic transitions between the excited and ground states of donor-acceptor pair systems. The DAP transitions become increasingly important and eventually dominate over the excitonic transitions as the impurity concentration in the material is increased.

An analysis of the DAP system was carried out with the assumption of simple coulomb interactions (reduced in strength by the dielectric constant) between the various particles in the system (ie. electron, hole, donor and acceptor ion cores). It was also assumed that the electron and hole masses are given by their effective masses [60]. A Heitler-London approach, in which the two-particle wavefunction describing the electron and hole is approximated by a product of donor and acceptor wavefunctions, was used in calculating the energy of the

system. A transition from an excited state of the system (electron in one of the donor states, hole in one of the acceptor states) to the ground state (electron tunnels to acceptor site and recombines with the hole, leaving a positively charged donor ion core and a negatively charged acceptor ion core), results in the emission of a photon of energy

$$\hbar w = E_g - E_{Di} - E_{Aj} + e^2/\epsilon * R_{DA} + J \qquad (2.6)$$

where E_g is the band gap energy, E_{Di} is the binding energy of an electron in the i^{th} excited state of the donor, E_{Aj} is the binding energy of a hole in the j^{th} excited state of the acceptor, e is the electronic charge, R_{DA} is the separation between the donor and acceptor, ϵ is the dielectric constant, and J is a coulomb integral representing the cohesive energy of the excited state of the pair system. The pairing in effect modifies the binding energies of the donors and acceptors. The donor and acceptor levels are shifted towards the respective band edges. The inclusion of the second order Van-der Waals interaction in the above analysis introduces another energy term in the above expression (-e*adjustable constant/$\epsilon * P^6$ [61]). This term is not appreciable and is generally neglected. The use of the static dielectric constant is valid provided that the period of the orbital electronic motion is greater than the period of the polar lattice

modes [60]. In general, the coulomb integral J is assumed to be negligable in order to simplify the analysis of DAP spectra.

The emission intensity of a DAP transition for a given pair separation R_{DA} is determined both by the number of pairs $N(R_{DA})$ and the transition probability $W(R_{DA})$. A random distribution of impurities is assumed in order to simplify the problem of determining $N(R_{DA})$. $N(R_{DA})$ depends on the crystal geometry and, in the case of compound semiconductors, on the lattice sites which the donors and acceptors occupy. In a type I configuration, the donors and the acceptors occupy equivalent substitutional sites, that is, the sites corresponding to either those of the cation or those of the anion crystal constituent (eg. donor Al_{Zn} and acceptor Li_{Zn}). In a type II configuration, the donors and acceptors occupy opposite lattice sites (eg. donor Al_{Zn} and acceptor N_{Se}). $N(R_{DA})$ has been calculated for type I and type II configurations in cubic binary crystals [62]. The probability $W(R_{DA})$ for an electron initially bound to a donor, in a state approximately described by the wavefunction $\phi_D(\vec{r}) = u_{c0}(\vec{r}) F_b(\vec{r})$, to undergo a photon-assisted quantum-mechanical tunneling to a final state where it is bound to an acceptor a distance R_{DA} away, in a state described by the wavefunction $\phi_A(\vec{r}-\vec{R}) = u_{v0}(\vec{r}-\vec{R}) F_A(\vec{r}-\vec{R})$, is proportional to the square of the dipole matrix element $\langle i|H|f\rangle$ linking the initial and final states [60]. $u(\vec{r})$ is the periodic part of the Bloch wavefunction (band theory). $F(\vec{r})$

is the envelope function (effective-mass theory of shallow impurities). The matrix element can be written as the product of two terms, one of which is the overlap integral of the envelope functions [60]. If R_{DA} is much greater than the Bohr radii of the donor and acceptor states, the overlap is significant only in the region of the exponentially decreasing tails of the envelope functions. The transition probability is then given by

$$W(R_{DA})=A*\exp(-R_{DA}/C) \qquad (2.7)$$

where A and C are constants [63]. The transition probability increases with decreasing pair separation. The number of possible pairs, on the other hand, decreases as R_{DA} decreases. The R_{DA} dependence of these two factors ensures that the DAP emission band exhibits a maximum in intensity as a function of emission energy.

In standard photoluminescence, DAP transitions generally involve the recombination of donor electrons and acceptor holes which are in their respective ground states (this is true at low temperatures, where thermalization to the ground state is rapid), thus only the ground state binding energies are used in the expression for the DAP transition eneergy given above. Since R_{DA} tales on discrete values, a series of discrete lines is generated. The energy spacing between adjacent lines increases as the pair separation decreases. Discrete pair lines have been

observed in photoluminescence studies of ZnSe crystals [38,51]. Pair lines corresponding to smaller R_{DA} values are more easily resolved, since the energy separation between the lines is greater, however, the emission associated with close pairs is relatively weak because of the reduced number of pairs ($N(R_{DA})$ decreases with decreasing R_{DA}). High excitation densities are therefore required for the observation of discrete pair lines. The excited pair state may be split, as a result of strain associated with the pair or spin-spin interactions between the electron and hole, into closely spaced levels [61] which are thermally populated at higher temperatures. Spectra must be obtained at low temperatures (1.6 °K in study by Merz et al. [51]) if fine structure in the pair lines resulting from transitions from these levels is to be eliminated. The samples must be relatively pure, so that the donors and acceptors form discrete levels rather than impurity bands. Finally, the samples must be strain free, since fluctuations in the band gap introduce broadening effects.

The study of DAP emission bands, as well as their identification as such, is facilitated by two other characteristic properties. The radiative lifetime of DAP transitions is inversely proportional to the transition probability, hence the lifetime of pairs increases with increasing pair separation R_{DA}. Consequently, time resolved DAP spectra are characterized by a shift of the DAP peak intensity towards lower energies as the time elapsed

following an excitation 'flash' increases [54]. The pair distance dependence of the lifetime also accounts for the observed shift of the DAP peak towards higher energy and broadening of the band as the excitation density is increased [38]. Saturation of distant DAP transitions, which have a longer lifetime than close pairs, is responsible for this behavior.

DAP recombination can occur with the simultaneous emission of phonons. The coupling of electrons to LO phonons is particularly strong in compound semiconductors, hence a series of progressively less intense LO phonon replicas of the main DAP emission band is present in photoluminescence spectra. DAP emission associated with deep donor and/or deep acceptor levels is characteristically observed as a broad, featureless emission band. This is a consequence of the strong electron-phonon coupling associated with deep levels.

The DAP emission bands observed in photoluminescence spectra of ZnSe have been the subject of numerous studies. The investigations have centered around the identification of the donors and acceptors involved in each case and the determination of their binding energies.

Several shallow acceptor levels have been identified in photoluminescence studies of DAP emission in ZnSe. A detailed investigation of DAP luminescence in vapour grown ZnSe crystals doped with the shallow donors Al_{Zn}, Ga_{Zn}, and In_{Zn}, and the acceptor Li provided conclusive proof that

Li_{Zn} is indeed a shallow acceptor [51]. Discrete pair lines were resolved in photoluminescence spectra of these doped crystals. Analysis of the pair lines involves the assignment of different pair separations R_{DA} to the lines observed. The task is made possible by noting that since the transition probability varies slowly with R_{DA}, the relative intensities of adjacent lines depend only on the number of pairs $N(R_{DA})$. The assumption of a type I configuration was necessary in order to obtain a respectable fit to the data. This indicated that the acceptor occupied Zn sites. Energy shifts in the pair lines occurred upon doping with an isotope of Li, thus proving that Li acceptors were involved. Extrapolation of the fits to the DAP emission energy versus pair separation data to R_{DA}--infinity for the Al, Ga, and In doped samples yielded values for E_A+E_D. Since E_D was known, E_A for Li_{Zn} could be determined. DAP emission bands due to electronic transitions between shallow donors substituting for Zn and the shallow acceptor Li_{Zn} are known as the D bands (zero phonon peak energy - 2.692 eV [38]). Discrete pair lines have been observed only for this band. Time resolved spectra of DAP emission in ZnSe crystals grown by VPE and LPE were obtained in another study [54]. The acceptor associated with a DAP band, labelled the F band, was identified. Time resolved spectra provided a means of both isolating the D and F DAP luminescence bands observed and separating the DAP bands from the associated 'free to

bound' emission bands present at higher temperatures. The DAP bands become progressively narrower as the time elapsed following excitation increases. The DAP peals shift to lower energy with increasing time elapsed. No such shift occurs in the case of the free electron to bound hole transition. The presence of two 'free to bound' bands eliminated the possibility that the Q and P DAP bands were due to the same acceptor (and different donors). A correlation in the intensities of the I_1 Na bound exciton emission line and a DAP emission band labelled the P band indicated that Na (Na_{Zn}) was the shallow acceptor associated with this band. The binding energy of the Na acceptor was obtained by comparison of the peak positions of the P (zero phonon peak energy - 2.680 eV [54]) and Q bands. The SPL and PLE techniques have been used to measure excited impurity levels (acceptors and donors) and thus confirm the identity of the acceptors involved in the P and Q DAP emission bands [53]. A measurement of the excited acceptor and donor states for another DAP band, the P band (zero phonon peak energy - 2.708 eV [38]), indicated that the acceptor was Li_{Zn} and also that the donor involved had a binding energy close to that of the standard donors. The concept of preferential pairing was suggested to explain the higher peak energy of this band relative to that of the Q band. A Li associated donor, possibly Li_{int}, could account for the observed characteristics of the P band [54]. DAP emission bands associated with the shallow

acceptor N_{Se} have been observed in N doped ZnSe [55] (zero phonon peak energy - 2.698 eV [55]). SPL measurements were used to obtain the 1S-2S excitation energy. Comparison of this energy with that for Li_{Zn} yielded the binding energy for the N acceptor. A DAP luminescence band associated with a shallow acceptor level is present in P doped ZnSe crystals (zero phonon peak energy - 2.728 eV [64]) grown by LPE [54,65] and MBE [56]. The binding energy of the acceptor level is estimated to be approximately 85 meV [64]. Resonant excitation of the DAP luminescence in the P doped LPE ZnSe confirms the presence of a new shallow acceptor [57]. Low temperature Raman spectra obtained for a ZnSe epilayer grown on GaAs by MOVPE contain peaks associated with the 1S-2S hole excitation in a shallow acceptor [66]. Comparison with theoretical excitation energy values indicates that the acceptor is P. It is unknown whether the shallow acceptor level is associated with substitutional P at a tetragonal site (P_{Se} - T_d symmetry) or a P-related complex. The intensity of a DAP band (zero phonon peak energy - 2.705 eV [64]) correlated with the As doping level in As doped ZnSe grown by LPE [64], indicating the presence of a shallow acceptor level associated with As. It is unknown whether the level is due to As_{Se} or an As - related complex.

Studies of DAP emission bands associated with deep acceptor levels have led to the identification of the impurities or complexes that form these deep levels.

Estimates of their binding energies have also been obtained. An emission band peaking at an energy of 1.91 eV at 2 °K has been observed in P doped ZnSe crystals grown from the melt [67]. Optically detected magnetic resonance (ODMR) studies of the band indicated that it was due to a DAP transition involving shallow donors and a deep acceptor level. The deep level, which has a binding energy of 0.6-0.7 eV, corresponds to the center P_{Se}. The symmetry of the center, C_{3v}, indicates a Jahn-Teller distortion of the surrounding lattice. Electron spin resonance measurements [68] show that a similarly distorted center As_{Se}, which also forms a deep acceptor level, is present in As doped samples, however, the identification of a luminescence band associated with this level has not been possible [69]. A broad luminescence band appearing in photoluminescence spectra of Cu doped ZnSe is a DAP transition involving shallow donors and the deep acceptor Cu_{Zn} [57]. The peak intensity of the band occurs at an energy of about 1.95 eV at a temperature of 5 °K. The binding energy of this acceptor is estimated to be about 0.65 eV. The ODMR technique was used to determine the origin of a green emission band which sometimes appears in photoluminescence spectra of ZnSe [70]. The results of the study showed that the band, which peaks at an energy of about 2.34 eV at 2 °K, was the result of DAP recombination involving shallow donors and a Cu complex center which acts as a deep acceptor. The results suggested that the complex is

Cu_{Zn}-Cu_{int}. A broad luminescence band observed in photoluminescence spectra of ZnSe has been the subject of several studies. The band peaks at an energy of about 2.0 eV at 2 °K. Time-resolved photoluminescence spectra indicate that the band results from a DAP transition involving shallow donors and an acceptor having a binding energy of 0.35 eV [71]. ODMR studies show that the acceptor is the A-center, a complex which consists of a zinc vacancy and an adjacent donor impurity [72]. The emission band is known as the self-activated emission. ODMR studies of another band, which peaks at an energy of 1.7 eV at 2 °K, show that it is due to a DAP transition between shallow donors and a zinc vacancy, V_{Zn}^{-}, which acts as a deep acceptor [72]. Deep levels are strongly coupled to the lattice, hence transitions involving deep acceptor levels lead to characteristically broad, featureless luminescence bands. The S band, which peaks at an energy of aprroximately 2.52 eV at 4 °K, is sometimes observed in material grown by MOVPE [59]. LO phonon replicas of this band are resolvable in some cases. The general shape of the band suggests that it is due to a DAP transition involving an unidentified acceptor having a binding energy E_A=275 meV [59].

2.3)Free to Bound Transitions

Radiative recombination processes whereby a free

electron in the conduction band recombines with a hole bound to an acceptor (transition denoted by the symbol (e,A°)) or a free hole in the valence band recombines with an electron bound to a donor (transition denoted by the symbol (D°,h)) are referred to as 'free to bound' transitions. The transition rate associated with these processes has been calculated for direct energy gap materials containing shallow, non-overlapping impurity states [73]. The transition probability is k-dependent and is found to rapidly decrease as k (and therefore the kinetic energy of the free particle) increases. The decrease occurs at energies of the order of $E_{vk}=(m_c/m_v)E_D$ and $E_{ck}=(m_v/m_c)E_A$ for the donor to valence band and conduction band to acceptor transitions, respectively. In ZnSe, the transition probability is significant for a greater energy range in the case of transitions involving the recombination of free electrons and bound holes (deeper levels more localized in real space and therefore more spread out in k space). The transition energies are

$$\hbar w=E_g-E_A \qquad (2.8)$$ and

$$\hbar w=E_g-E_D \qquad (2.9)$$

for the (e,A°) and (D°,h) transitions, respectively [31]. The thermal kinetic energy of the free particle has been neglected. The free to bound luminescence peaks, unlike the DAP emission bands, do not shift in energy as

the excitation density is varied. Free to bound transitions may also occur with the simultaneous emission of q=0 LO phonons.

Luminescence bands associated with the free to bound transitions have been observed in ZnSe crystals. Transitions involving the recombination of free electrons and holes bound to shallow acceptors are important in the temperature range where significant donor ionization occurs and acceptors remain neutral. New bands associated with transitions to different acceptors appear on the high energy side of the corresponding DAP luminescence peaks. Evidence of these transitions exists in the case of the Q band [38], the P band [54], and the band involving N acceptors [52]. The contribution of the free to bound transition to the luminescence is not discernable in the case of transitions involving deep acceptors due to the characteristic broadness of these bands and the small energy shift associated with the change from DAP to free electron to bound hole luminescence. The results of a study of the temperature dependence of luminescence bands apppearing in the photoluminescence spectra of solution grown ZnSe crystals indicate that the transition involving the recombination of free holes with electrons bound to shallow donors makes a substantial contribution to the luminescence at higher temperatures [41]. A correlation in the intensity of a near band edge luminescence peak,

present in room temperature photoluminescence spectra, with the concentration of Cl, a shallow donor, incorporated into ZnSe crystals grown by MBE, together with observations of the energy position of the peak, has led to the conclusion that the emission is due to the recombination of free holes and electrons bound to the shallow donor Cl_{Se} [46]. A similar correlation in the intensity of the room temperature near band edge photoluminescence with the Cl doping level has been observed for epitaxial ZnSe layers grown by MOVPE [48]. This lends further credence to the above interpretation of the origin of the near band edge emission present at room temperature.

2.4) Temperature Dependence of the Photoluminescence Spectra of ZnSe Crystals

The contributions of the various transitions outlined above to the photoluminescence spectrum of ZnSe crystals depend on the sample temperature. Studies of the electroluminescence spectra of metal-insulator-semiconductor (MIS) ZnSe diodes over the temperature range 20-290 °K [74] and photoluminescence spectra of bulk ZnSe crystals over the temperature range 4-290 °K [41] indicate the temperature ranges over which specific transitions may be observed. Quenching of certain emission bands and the appearance of new bands was observed as the sample temperature was increased. The conclusions of

these two studies are presented below.

The electroluminescence spectra [74] contain a DAP emission band associated with transitions involving shallow donors and acceptors. The band is observed up to a temperature of about 55 °K. The corresponding free electron to bound hole, or (e-A°), luminescence band is present at 20 °K and gradually increases in intensity relative to the DAP band. The free to bound emission (e-A°) is completely quenched at temperatures above 110 °K. A similar behavior for these two bands was reported in the photoluminescence study [41]. The emission resulting from the radiative decay of excitons bound to neutral donors was found to contribute to the electroluminescence up to a temperature of about 70 °K [74]. The same emission was resolved up to a temperature of about 90 °K in the photoluminescence spectra [41] before it merged with a lower energy band labelled A'. The free exciton emission was resolved in electroluminescence spectra up to a temperature of 85 °K before it merged with a lower energy band, labelled E_{LP}, which appears at a temperature of 80 °K [74]. The lower polariton emission was resolved in photoluminescence spectra up to a temperature of 90 °K [41]. This emission merged with the A' band above this temperature. The upper polariton emission was resolved up to a temperature of about 130 °K. It subsequently merged with the A' band [41]. The A' and E_{LP} bands persist up to room temperature. Two separate interpretations for the origin of this band are presented. The response of the room

temperature E_{ex} band to changes in excitation density led to the conclusion that the band is associated with the recombination of free excitons after interaction with free electrons [74]. The observed position of the A' emission band relative to the experimentally determined free exciton energy is consistent with the interpretation that the emission results from the radiative recombination of free holes and electrons bound to shallow donors [41]. Correlations in the intensity of the near band edge emission present in room temperature spectra with the donor concentration support the latter interpretation [46]. It is possible that both transitions contribute to the observed emission.

TABLES

TABLE 2.1 : (D^0,X) TRANSITION AND LOCALIZATION ENERGIES

DONOR	I_{2o} TRANSITION ENERGY (eV)	LOCALIZATION ENERGY (meV)	
Al	2.7978	4.9	[33]
Cl	2.7977	5.0	[33]
Ga	2.7975	5.2	[33]
In	2.7972	5.5	[33]
F	2.7971	5.6	[33]

TABLE 2.2 : (D^+,X) TRANSITION AND LOCALIZATION ENERGIES

DONOR	I_3 TRANSITION ENERGY (eV)	LOCALIZATION ENERGY (meV)	
Cl	2.7966	6.1	[33]
	2.7964	6.3	[33]
	2.7960	6.7	[33]
In	2.7945	8.2	[33]
	2.7941	8.6	[33]

TABLE 2.3 : DONOR EXCITATION AND IONIZATION ENERGIES

DONOR	EXCITATION ENERGIES 1s-2s (meV)	1s-2p (meV)	IONIZATION ENERGY E_D (meV)	
Al	18.8	19.1	25.6	[33]
Cl	19.4	19.7	26.2	[33]
Ga	20.2	20.7	27.2	[33]
In	20.9	21.7	28.2	[33]
F	--	22.3	28.8	[33]

TABLE 2.4 : (A^0,X) TRANSITION AND LOCALIZATION ENERGIES

ACCEPTOR	I_1 TRANSITION ENERGY (eV)	LOCALIZATION ENERGY (meV)
Na	2.7931	9.6 [33]
Li	2.7922	10.5 [33]
N	2.7918	10.9 [55]
unknown	2.7830	19.7 [33]

TABLE 2.5 : ACCEPTOR EXCITATION AND IONIZATION ENERGIES

ACCEPTOR	EXCITATION ENERGIES 1S-2S (meV)	1S-2P (meV)	IONIZATION ENERGY E_A (meV)
Na	97.6	83.1	128 [53]
Li	82.6	72.9	114 [53]
N	--	--	111 [55]
P	--	--	85 [64]
As	--	--	110 [64]

CHAPTER 3

PHOTOLUMINESCENCE - EXPERIMENTAL SETUP

3.)PHOTOLUMINESCENCE-EXPERIMENTAL SETUP

A brief description of the experimental setup used for the photoluminescence measurements is presented below. A schematic of the setup is shown in figure 3.1.

The photoluminescence excitation source is a Spectra Physics 171 krypton ion laser. The continuous wave output in the ultraviolet consists of several lines in the wavelength range 337.4-356.4 nanometers. The intensity of the 100 mW output is attenuated through ultraviolet neutral density filters. The laser beam is directed through a quartz focussing lens by a beam steering instrument and a mirror held in an adjustable optical mount. The aluminum coated mirrors are highly reflecting in the ultraviolet (approximately 90% reflectence). The orientation of the mirrors is controlled by micrometer adjustments. The laser beam is focussed onto the sample surface. The photoluminescence is collected by an astigmatic lens with a low F number and focussed on the spectrometer entrance slit with an F/8 optical lens matched to the F number of the spectrometer. The photoluminescence is spectrally analyzed using a Jobin-Yvon HG 25 double monochromator equipped with holographic gratings of 1 meter focal length. Optimum efficiency of the spectrometer is achieved in the range 22720-12500 cm^{-1}. The four electronically controlled slits in the spectrometer are independently adjustable. The resolution obtained using a 200 micron slit width is 2 cm^{-1}. The exit slit is coupled to a cooled GaAs Hamamatsu R666S

figure 3.1 : Photoluminescence setup. The laser beam is directed through a quartz lens (QL) by a beam steering instrument (BS) and a mirror M_1. Neutral density filters (ND) attenuate the beam intensity. The photoluminescence passes through a collecting lens (CL) and is directed through an F/8 lens onto the spectrometer slit S_1 by a dielectric coated mirror (DM). The light is diffracted by the holographic gratings (HG). The photomultiplier (PM) signal passes through a preamplifier (P) and a discriminator (D). The electronic pulses are sent to a data conversion unit interfaced to a PC compatible computer.

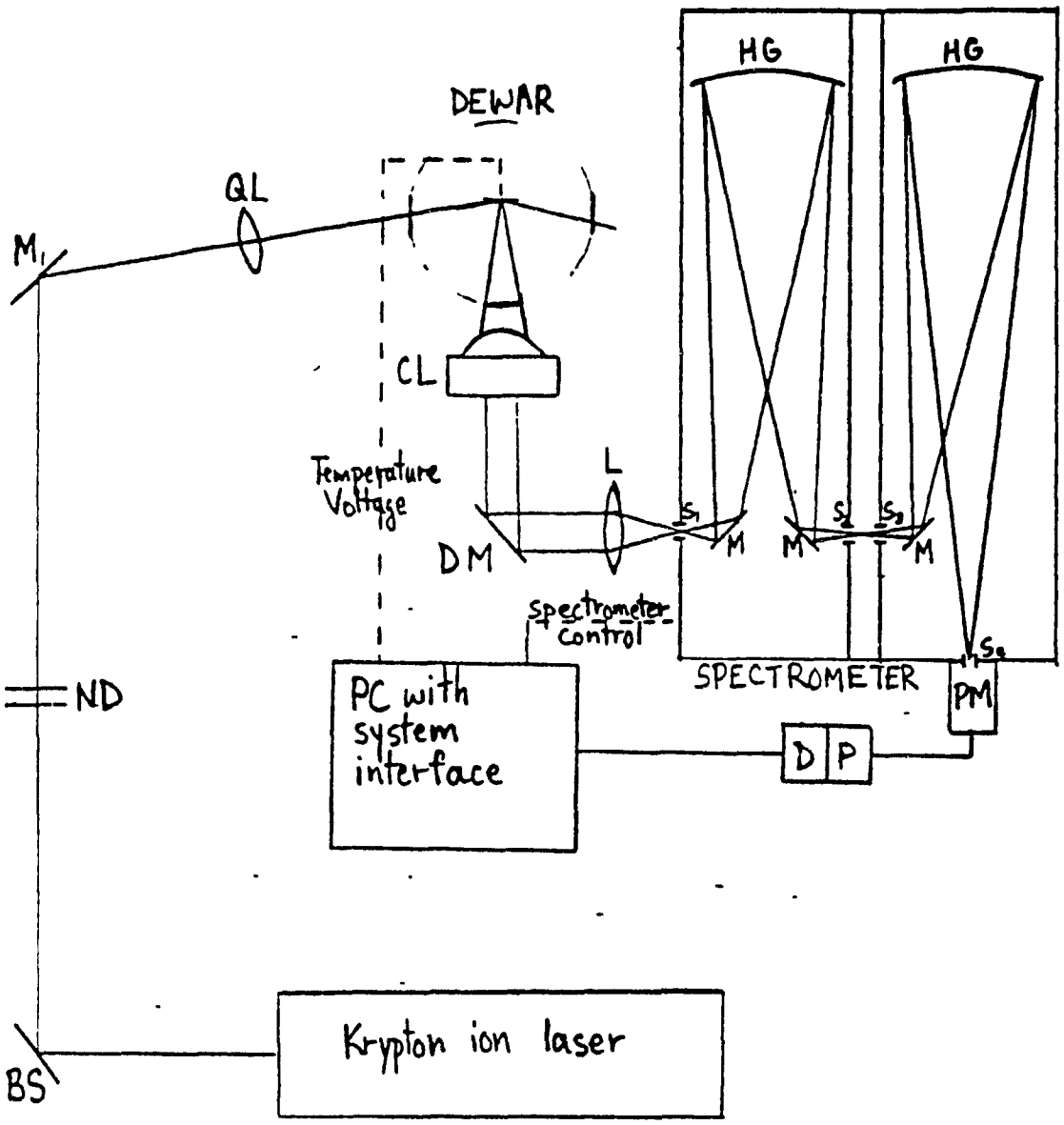

figure 3.1 : photoluminescence setup

photomultiplier tube. The electrical pulses generated by the detector pass through a preamplifier-discriminator unit. The discriminator selects only those pulses which are of sufficient amplitude. The rate at which pulses are generated is directly proportional to the intensity of the light incident on the detector. The pulses are sent to a data conversion unit interfaced to a PC compatible computer. The computer records the sample temperature, the detector signal intensity, and the spectrometer position on a hard disk. The computer also controls the spectrometer position. The user inputs the desired values of the sample time, scanning resolution, and scanning range.

The sample is mounted on a copper holder with the aid of a small quantity of varnish deposited on the reverse side of the sample, near an edge of the GaAs substrate. Photoluminescence is excited away from this edge in order to minimize the effects of strain. The sample is placed in a Janis 8 DT variable temperature optical dewar. The sample is cooled by flowing cold helium gas (or nitrogen gas) through the sample space. A sample temperature lower than 4 °K is achieved by flooding the sample zone with liquid helium and pumping on the sample space with the liquid below the lambda point. The temperature sensor is a DT-500-HL silicon diode mounted on the copper sample holder. A constant current passes through the diode. The voltage drop across the diode varies with temperature. The voltage is monitored by the computer and converted to a temperature value.

CHAPTER 4

RESULTS AND ANALYSIS

4.)RESULTS AND ANALYSIS

Photoluminescence spectra of thin epitaxial ZnSe films deposited on GaAs substrates provide valuable information about the optoelectronic quality of the material grown, the types of impurities and complexes present, the concentrations of these impurities and complexes, and the strain present in the epilayer as a result of the inherent mismatches in the lattice constants and the thermal expansion coefficients of the substrate and epilayer materials.

Photoluminescence spectra have been obtained at temperatures of 300 °K, 77 °K, and 2-16 °K for several ZnSe epilayers grown by MOVPE or ALE. The spectra are used to characterize the thin films.

The growth temperature, T_g, is an important parameter in MOVPE. A comparison of the 300 °K photoluminescence spectra of a series of ZnSe thin films grown at different T_g's, with all remaining parameters kept constant, reveals an important dependence of optoelectronic quality on this growth parameter.

The photoluminescence spectra of thin films grown using different precursors, specifically, DEZ as opposed to DMZ, and H_2Se as opposed to DESe, differ significantly. These differences indicate that precursor purity is an important factor in the growth of high purity ZnSe epitaxial layers. Contaminants present in a precursor may

be incorporated into the material. The presence of specific impurities or impurity-related complexes induces radical changes in photoluminescence spectra.

Variations in the photoluminescence spectra of ZnSe films of different thicknesses reveal strain-related changes in the band gap which are consistent with the conclusions drawn in previous studies. Comparison of photoluminescence spectra of two samples grown by ALE reveals a thickness dependence of crystal quality and purity.

Differences in the photoluminescence spectra of ZnSe thin films grown on GaAs substrates (by MOVPE) and GaAs epilayers (by ALE) indicate an improved epilayer quality and purity in the latter case.

The 77 °K near band edge (NBE) photoluminescence of a pure, relatively strain-free ZnSe epilayer is shown to result from contributions of several luminescent transitions.

The presentation and analysis of the photoluminescence data is divided into four sections. The 300 °K spectra form the subject of section 4.1. The 77 °K data is presented, along with a discussion, in section 4.2. An analysis of the low temperature (2-16 °K) data is presented in section 4.3. Several high resolution spectra of the near band edge emission, obtained at about 77 °K, are presented and analyzed in section 4.4. Table 4.1 serves to summarize important photoluminescence results and facilitates a

comparison of the features of the various spectra.

4.1)300 °K Photoluminescence Spectra

An important criterion in determining the optoelectronic quality of ZnSe crystals is the value of the ratio R between the near band edge (NBE) and deep level-related luminescence intensities of the room temperature photoluminescence. The NBE emission is less favoured on the basis of the thermal stability of the electronic states associated with these two emission bands [59]. The ratio R is a measure of the degree of compensation of donors by deep centers. High R values are indicative of superior (doped or undoped) material. The intensity of the NBE emission, which, at room temperature, is due to the radiative recombination of free holes with electrons bound to donors [41,46,48] depends on the concentration of donor impurities and the degree of compensation. The peak energy of the room temperature NBE emission is approximately 2.69 eV for all room temperature spectra recorded in this study. The broadness of the band is attributable to the hole kinetic energy, phonon broadening, and the Stark effect due to ionized impurities [41]. The deep center-related luminescence bands result from the recombination of free electrons and holes bound to deep acceptors, specifically, A-centers. An increase in both the NBE and deep emission, for a fixed value of P,

implies an increase in the concentrations of donors and deep acceptors. The ratio R and the intensity of the NBE and deep emission bands thus provide information concerning the extent of compensation and the purity of the ZnSe crystals under investigation.

The growth temperature is an important parameter in MOVPE. In order to investigate the effect of T_G on the optoelectronic quality of ZnSe epilayers, 300 °K photoluminescence spectra were recorded for three epilayers grown at different temperatures under otherwise equivalent growth conditions. Table 1.1 indicates the growth parameters used in the growth of samples 8 (T_G=200°C), 9 (T_G=250°C), and 10 (T_G=300°C).

The spectra of samples 8, 9, and 10 are shown in figures 4.1, 4.2, and 4.3, respectively. The incident power density used in all three cases was approximately 2.5 W/cm^2. Additional information, including incident power, sampling information, and spectrometer slit width is listed in the figure captions. Direct comparison of emission intensities for the three spectra is possible. The ratio R between the peak intensities of the NBE and deep emission bands increases as the growth temperature is increased. The R values are 0.5, 6.2, and 11.2 for material grown at temperatures of 200, 250, and 300 °C, respectively. The peak intensity of the deep luminescence progressively decreases as T_G increases. Relatively high growth rates, coupled with slow surface diffusion at low T_G's, are

expected to result in higher densities of dislocations and hence higher concentrations of vacancies and vacancy-related complexes (such as A-centers) in material grown at low temperatures. A decrease in the concentration of A-centers may account for the reduction in the peak intensity of deep luminescence as T_s is increased from 200 to 250 °C. The simultaneous enhancement in the NBE emission is explained by an increase in the number of neutral donors due to a reduction in the number of compensating A-centers. The reduction in both the NBE and deep emission peak intensities for sample 10 relative to sample 9 (see figures 4.2 and 4.3) suggests that sample 10 contains fewer donors and A-centers than sample 9 and is therefore of higher purity. The R value is also higher for sample 10 and indicates a lower degree of compensation by deep A-centers.

Room temperature photoluminescence spectra have been obtained for a number of ZnSe epilayers grown at a temperature of 300 °C. The precursors used in the growth of these thin films included a DEZ source different from the one used in the growth of samples 8, 9, and 10, or alternatively, a DMZ source. The non-metal source, H_2Se, was identical to the one used previously in the growth of samples 8, 9, and 10. The incident power density used to record these spectra was 2.5 W/cm^2, unless stated otherwise. Comparison of the intensities of emission bands for the spectra presented below is valid. Comparison of luminescence intensities with those of figures 4.1, 4.2,

and 4.3 is not possible, however, since the incident power used and spectrometer slit widths differed from those used in recording these three spectra.

The 300 °K photoluminescence spectrum of sample 32, which was grown using a DEZ source (see table 1.1), is shown in figure 4.4. The R value is 9.0, hence the degree of compensation is slightly higher relative to that of sample 10. The NBE and deep emission (peak energy 2.12 eV) bands are quite intense. The NBE emission was observed when an excitation power density as low as 250 mW/cm^2 was used, however, the ratio R decreased to a value of 4.8 at this power density (High power densities result in an enhanced NBE emission intensity, hence a more rigorous test of optoelectronic quality, as determined by the ratio R, requires the use of low power densities [75]). Sample 32 was the only sample having a luminescence intensity sufficiently high to permit the recording of a 300 °K photoluminescence spectrum using an incident power density of only 250 mW/cm^2. The high luminescence intensity suggests that sample 32 has a high concentration of donor impurities and A-centers. Low temperature spectra provide further evidence that the concentration of donors is high in this sample (large I_2 linewidth - see table 4.1). High concentrations of donor impurities could lead to a higher concentration of A-centers (these centers are comprised, in part, of donor impurities), and subsequently, an increased deep emission band intensity.

The 300 °K photoluminescence spectrum of an epilayer grown using the precursor DMZ (see table 1.1), sample 29, is shown in figure 4.5. The ratio R is about 6.0, hence the degree of compensation is higher for this sample than for samples 32 and 10. The NBE and deep emission (peak energy 2.18 eV) bands are much less intense than those of sample 32. This suggests that sample 29 contains far fewer donors and A-centers than sample 32, however, spectra recorded at 77 °K reveal that, unlike sample 32, sample 29 contains an additional, shallower compensating center which is optically inactive at room temperature. The nature of this acceptor center is discussed later. The degree of compensation is consequently greater than that implied by the room temperature photoluminescence, and thus the donor concentration is higher than that expected on the basis of the intensity of the NBE emission at 300 °K. Further evidence that this is indeed the case is provided by the low temperature (4 °K) photoluminescence.

The 300 °K photoluminescence of a ZnSe epilayer grown by a novel technique in which the DMZ and H_2Se sources are introduced at separate times, so that the growth is essentially by ALE, is shown in figure 4.6 (sample 40). Prior to the growth of the ZnSe thin film, a thin GaAs epilayer was deposited in-situ by conventional MOVPE, using the precursors TMG and AsH_3. The value of R is 5.3. The degree of compensation by deep acceptors is thus greater for this sample than for samples 32 and 10. The deep

emission is very weak in comparison to that observed for sample 32, as is the NBE emission. This suggests that sample 40 has a low concentration of donors and A-centers. An increase in the power excitation density (and the incident power) led to an enhancement in the NBE emission peak intensity, as expected [75], however the intensity of the deep emission remained essentially unchanged (see figure 4.6a). The virtual absence of deep emission, which indicates a low concentration of A-centers, may be due to an improvement in crystal quality resulting from the use of low growth rates. Two-dimensional stepwise growth is favoured when growing on a GaAs epilayer and may also account for the improved crystal quality. Low temperature spectra provide conclusive evidence that the donor concentration is indeed much lower for sample 40 than for sample 32. A photoluminescence spectrum of sample 40, recorded at 77 °K, reveals the presence of an additional shallower compensating center identical to the one found in sample 29. The origin of this center is discussed later.

Figure 4.7 shows the 300 °K photoluminescence spectrum of sample 41. This sample was grown in the same fashion as sample 40. The sample thickness is 0.4 microns (see table 1.1). The ratio P is 1.2, thus the degree of compensation is higher than for samples 32, 29, 10, and 40. Comparison of the peak intensities of the NBE and deep emission (peak energy 2.14 eV) bands with those observed for sample 32 suggests that sample 41 has substantially lower

concentrations of donors and deep A-centers, however, such a comparison may not be appropriate, since the samples are of different thicknesses. X-ray diffraction measurements indicate that heteroepitaxial ZnSe thin films (thickness less than 0.15 microns) are coherently strained as a result of the two-dimensional compressive stress present due to the 0.27% lattice mismatch (at room temperature) between ZnSe and GaAs [45,76,77]. Relaxation of this strain via the formation of lattice imperfections, specifically, misfit dislocations, occurs for thicknesses greater than 0.15 microns. The lattice strain is fully relaxed when the film thickness reaches approximately 1 micron. Epilayers thicker than 1 micron are under a two-dimensional tensile (dilatative) stress due to the larger thermal expansion coefficient of ZnSe compared to that of GaAs. The magnitude of this stress depends on the growth temperature used. The thermal strain is smaller in magnitude compared to the strain associated with the lattice mismatch [2]. The dislocations act as sinks for various defects such as impurities and vacancies, among others. Samples thinner than 1 micron thus have a higher density of dislocations than samples thicker than 1 micron. The difference in dislocation densities implies differences in the concentrations of impurities, vacancies and related centers, and other defects. Photoluminescence spectra are sensitive to changes in the concentrations and types of defects present, and will therefore differ in the two

cases. The concentration of non-radiative recombination centers is expected to be higher in material having a high density of dislocations. The photoluminescence intensity depends on the number of non-radiative recombination centers present. Low temperature spectra presented later on show that the donor concentration in sample 41 may be comparable to that in sample 32, hence the large reduction in room temperature luminescence intensity for sample 41 relative to sample 32 may be due to a increased concentration of non-radiative recombination centers in the former.

It must be pointed out that the discussion and conclusions reached in this section, although consistent with the results of low temperature data, involve the assumption that non-radiative recombination is, in general, negligable in the case of thick (greater than 0.8 micron) samples. This assumption is implicitly made in many photoluminescence studies of ZnSe. The extent to which non-radiative recombination affects the photoluminescence efficiency in the samples studied here is unknown, hence the statements made in this section do not necessarily accurately describe the actual situation. Non-radiative recombination effects may in some (or all) cases account for the observed differences in the photoluminescence spectra of the various samples. A literature search to uncover experimental studies done on non-radiative recombination in ZnSe was unsuccessful. In any case, the

techniques used to study non-radiative recombination require experimental equipment which was not accessible.

4.2 77 °K Photoluminescence Spectra

A lowering of the sample temperature leads to an enhancement of transitions involving relatively shallow levels and exciton-related emission. New emission bands may appear, while the intensities of others may be substantially increased. Spectral features present in low temperature photoluminescence spectra provide information about impurities and complexes which are optically inactive at room temperature. 77 °K photoluminescence spectra were recorded for samples 10, 32, 29, 40, 41, and 50. The features of these spectra are discussed below. High resolution scans of the NBE emission were also obtained. These spectra are presented and analyzed later in this chapter.

Comparison of the 77 °K photoluminescence spectra of the above mentioned samples reveals important differences in the types of compensating centers present and the degree of compensation in each case. The presence of a particular center correlates with the type of precursor used thus the appearance of a new emission band is directly linked to the presence of a contaminant in the precursor. Comparison of absolute intensities is valid in some cases (incident power and power densities must be the same). A NBE emission peak

centered at an energy of about 2.79 eV was observed in all spectra. Several transitions contribute to this luminescence, as discussed later.

The 75 °K photoluminescence of sample 10 is shown in figure 4.8. The excitation power density used was identical to that used in obtaining the 300 °K spectrum. The ratio R at 75 °K is 60.5. The large increase over the room temperature R value of 11.2 is essentially due to a sharp increase in the NBE emission intensity, as expected [75]. The low intensity of the deep emission (it saturates at high power densities) indicates a low concentration of A-centers in this sample.

Figure 4.9 shows the 72 °K photoluminescence of sample 32. The spectrum was recorded using an excitation power density of approximately 250 mW/cm². The broad emission band peaking at an energy of about 2.13 eV is due to the recombination of free electrons with holes bound to A-centers. The ratio R is 6.3. The use of an excitation power density similar to the one used in recording the room temperature spectrum of sample 32 yielded a spectrum with an R value of about 130.

The 73 °K photoluminescence spectrum of sample 29 is shown in figure 4.10. The excitation power density used was 250 mW/cm². An intense, broad luminescence band peaking at an energy of approximately 2.31 eV is the dominant emission band at this temperature. The peak energy of the band compares favourably with that of a green emission band

previously studied using the ODMR technique (see chapter 2 - section 2.2), hence the emission is attributed to the radiative recombination of free electrons with holes found at neutral Cu-complex (Cu_{Zn}-Cu_{int}) acceptors. The peak energy for a similar transition involving A-centers, observed as a luminescence band peaking at an energy of 2.18 eV at room temperature (see figure 4.5), decreases as the temperature is lowered [71] therefore this transition is excluded as a possible source of this emission band. The shoulder present on the low energy side of the Cu-green emission band is due to the emission associated with the A-center. The Cu-complex center acts as an additional compensating center. Its presence accounts for the weak NBE emission observed at room temperature, as previously mentioned.

The absence of the Cu-green emission in the 77 °K spectra of samples grown using DEZ sources (samples 10 and 32) and the fact that the same H_2Se source was used in the growth of samples 10, 32, 39, 40, and 41, imply that Cu is present as a contaminant in the DMZ source. The reaction to form DMZ involves the use of a Zn/Cu couple, therefore the DMZ source is likely to contain Cu as a contaminant [78].

Figure 4.11 is the 79 °K photoluminescence of sample 40 obtained using an excitation power density of 250 mW/cm^2. The broad emission band peaking at an energy of about 2.26 eV, completely absent at room temperature (see figure 4.6a), is also attributed to the transition

involving the Cu-complex acceptor center. DMZ was used in the growth of this thin film. The R value at 77 °K is substantially higher for this sample than for sample 29, hence the degree of compensation is lower for sample 40. Furthermore, the peak intensities of both the NBE and Cu-green emission bands are substantially lower for sample 40. The weak intensities are indicative of low impurity concentrations. Low temperature spectra presented later support this conclusion. As pointed out earlier, slow growth rates and growth on epilayers of GaAs are expected to result in improved crystal quality and purer material. The change in R value reflects a change in the incorporation rate of various impurities. The reaction mechanisms leading to crystal growth may differ when growing by ALE as opposed to standard MOVPE. A change in reaction mechanism could affect incorporation rates of the different types of impurities and may explain the change in R (incorporation rates of donors and Cu vary depending on the growth technique used).

The 83 °K photoluminescence spectrum of sample 41 is shown in figure 4.12. The incident power density used was 250 mW/cm^2. In addition to the NBE emission, a broad luminescence band peaking at an energy of 2.09 eV is observed. The deep emission peal is downshifted relative to its position at room temperature (see figure 4.7). As mentioned previously, this behavior is characteristic of the emission associated with A-centers, hence the emission

is attributed to radiative transitions involving A-centers. Emission on the high energy side of the deep emission band is due to the free to bound transition involving the Cu-complex acceptor level mentioned above. Sample 41 is expected to have a higher density of dislocations than sample 40 since the strain relaxation process is incomplete when the sample thickness is less than approximately 1 micron. The tendency to form a particular complex may depend on the dislocation density and is a plausible explanation for the observed differences in the relative intensities of the deep and Cu-complex emission bands when comparing the spectra of samples 40 and 41. The overall reduction in luminescence intensities of sample 41 relative to those of samples 32 and 29 is presumably due to an increase in the number of non-radiative centers in this first sample, which has a higher density of dislocations (the strain is not yet fully relieved).

Figure 4.13 shows the 73 °K photoluminescence of sample 50, grown by the conventional MOVPE technique using DEZ and DEDSe as reactants. An excitation power density of 1.25 W/cm^2 was used in recording the spectrum. In addition to the NBE emission, four other luminescence bands are observed. The dominant emission band peaking at an energy of 2.24 eV is presumably the Cu-green band, judging from its position. A tail on the low energy side of this band is due to luminescence associated with A-centers. A luminescence band centered at an energy of 2.49 eV has been

observed in material grown by MOVPE using DMZ and DMSe [19] and the standard precursors [22,59], and in material grown by MBE [79]. This band, known as the S band, is believed to be due to a free to bound transition (DAP transition at low temperatures) involving an unidentified acceptor [59]. The luminescence band peaking at an energy of about 2.59 eV is identified as the Y band. The Y band, thought to arise from the recombination of excitons at an extended defect, perhaps a dislocation loop [59], is frequently observed in material grown by MOVPE [19,22,29,50]. The origin of the emission lying between the NBE emission and the Y band is discussed later in this chapter.

4.3)Low Temperature (2-16 °K) Photoluminescence Spectra

Photoluminescence spectra recorded at low temperatures exhibit luminescence peaks associated with exciton-related transitions and DAP transitions. The relative intensities of the bound and free exciton luminescence peaks provide an indication of the purity of the material. The types of bound exciton peaks present (I_2, I_1) reveal what types of impurities (donor, acceptor) the material contains. Shallow acceptor impurities, if present, can be identified through an analysis of the DAP emission bands. Linewidths of the bound exciton peaks provide information about crystal quality (inhomogeneous strain broadening associated with

dislocations) and impurity concentration (inhomogeneous Stark effect broadening). Low temperature spectra have been obtained for samples 29, 32, 40, and 41. An analysis of the various spectral features appearing in the spectra is presented below.

The excitonic photoluminescence of sample 40, recorded at a temperature of 7 °K, is shown in figure 4.14. The excitation power density used was approximately 250 mW/cm^2. The dominant luminescence peak positioned at an energy of 2.7980 ± 0.0002 eV is the (D^o,X), or I_2, transition. The peak at 2.8027 ± 0.0002 eV is the free exciton emission. The energy difference between these two peaks, 4.7 ± 0.4 meV, is the localization energy. Comparison with the localization energies listed in table 2.1 suggests that the dominant donor impurity is Al. If the uncertainty in the measured value is taken into account, however, it is seen that Cl and/or Ga donors may also contribute to the I_2 emission. The SPL technique must be employed in order to determine unambiguously which donors contribute to the I_2 emission. The precursors are probably the sources of these impurities. The linewidth (FWHM) of the I_2 peak is approximately 1.9 meV. This width is comparable to that observed for material grown by MOVPE [25,59] and MBE [80,81]. It should be noted that the linewidth depends on the epilayer thickness [2,82], since the dislocation density, and hence the strain-related and impurity-related broadening, changes with changing thickness. The intense

free exciton emission is an indication that the material is of high purity. The relatively narrow linewidth of the I_2 peak is also characteristic of high purity material containing a low number of dislocations. The tail appearing on the low energy side of the I_2 peak is due to I_{D^*}, or (D^*,X), and I_1, or (A^o,X), emission (see tables 2.2 and 2.4). Luminescence in the range 2.77-2.79 eV is due to TES transitions associated with the I_2 transition and the radiative decay of free excitons with the simultaneous emission of an LO phonon.

Of particular interest is the fact that a shoulder appears on the high energy side of the free exciton peak. Reflectance [45] and photoluminescence [2,83] measurements of heteroepitaxial ZnSe films of different thicknesses reveal important changes associated with the presence of two-dimensional stress. In epilayers suffering two-dimensional stress, the fourfold degenerate $J_{3/2}$ valence band is split into two doubly degenerate bands, the heavy hole [hh] band - $m_J = \pm 3/2$, and the light hole [lh] band - $m_J = \pm 1/2$. The two bands are shifted in energy relative to the conduction band by amounts which depend on the magnitude and nature (compressive or tensile) of the stress, which in turn depends on the epilayer thickness. In epilayers suffering compressive stress (thickness less than 1 micron), the hh band lies closest to the conduction band. The effective bandgap energy (conduction band to hh band) is greater than that of unstrained material. In epilayers

under tensile stress (thickness greater than 1 micron), the lh band lies closest to the conduction band. The effective energy gap (conduction band to lh band) is less than that of unstrained material. The free exciton emission in stressed layers consists of two components corresponding to the light hole and heavy hole exciton transitions. The high energy component is less intense than the low energy component since occupation of the lower energy hole levels is favoured at low temperatures. Likewise, the I_2 emission is split into two components. The absence of an additional higher energy I_2 component in the photoluminescence spectrum of sample 40 rules out the possibility that the high energy shoulder on the free exciton peak is the higher energy stress-split free exciton transition. The free exciton and I_2 peak energies are identical to those observed in strain-free ZnSe (table 2.1 lists I_2 transition energies ; E_{ex}^T = 2.8027 eV in strain-free ZnSe [33]), hence the residual strain in the epilayer is negligable and the energy gap is precisely the bulk value (conduction band to fourfold degenerate valence band). X-ray diffraction measurements [84] show that epilayers are strain-free at a thickness of approximately 0.9 microns. Sample 40 is 0.8 microns thick and is therefore expected to be strain-free. It is concluded, on the basis of the above observations, that the high energy shoulder at 2.8040 $\pm$ 0.0002 eV is the upper polariton branch (UPB) emission. The peak at 2.8027 eV is the lower polariton branch (LPB) emission and occurs

at the transverse free exciton energy (E_{ex}^{T}) [49].

Figure 4.15 shows the 7 °K photoluminescence of sample 40 in the DAP (shallow acceptor) region. The excitation power density used in recording the spectrum was 8 W/cm². No DAP emission bands are observed, hence the concentration of shallow acceptor impurities is very low. The observed luminescence is the high energy tail of the DAP emission associated with the Cu-complex acceptor center (Cu-green band).

The 16 °K photoluminescence of sample 32, recorded using an excitation power density of 2.5 W/cm², is shown in figures 4.16, 4.17 and 4.18. The first of these three figures shows the emission associated with excitonic, as well as DAP (shallow acceptor), transitions. The dominant peak at 2.7957 ± 0.0006 eV is the (D^{o},X), or I_2, transition. Since the epilayer thickness is 2 microns, the layer is under two-dimensional tensile stress. The effective bandgap is lower than that of strain-free material, therefore the I_2 transition is downshifted in energy relative to the I_2 transition energy in strain-free material. The I_2 transition is due to the radiative decay of light hole excitons bound to neutral donors (I_2^{lh}). DAP emission is completely absent, hence the material contains very few shallow acceptor impurities. The structure appearing on the low energy side of I_2 is exciton-related emission. A high resolution scan of the excitonic emission is shown in figure 4.17. The shoulder on the high energy

side of the I_2 peak is due to the radiative decay of heavy hole excitons bound to neutral donors (I_2^{hh}). This transition increases in intensity relative to the I_2^{lh} transition as the temperature increases [83]. The splitting between the two I_2 transitions is about 1.5 meV, in agreement with the splitting observed for a 2 micron thick epilayer [83].

The recombination of free excitons also contributes to the shoulder. Free exciton emission is relatively strong at this temperature, since the (D^o,X) emission is gradually quenched as the temperature increases.

The SA emission, shown in figure 4.18, peaks at an energy of 2.06 eV. At this temperature, the emission corresponds to a DAP transition involving the A-center. The emission is extremely weak in comparison to the I_2 emission. The R value is approximately 232.

Figure 4.19 shows the 6°K exciton-related emission. The spectrum was recorded using an excitation power density of about 120 mW/cm^2. The linewidth (FWHM) of the I_2 peak, centered at 2.7950 ± 0.0002 eV, is approximately 3.5 meV. Similar linewidths have been observed in material grown by MOVPE [11,30,82]. The large linewidth is due in part to the inhomogeneous Stark effect broadening associated with high concentrations of donor impurities. Inhomogeneous strain broadening associated with dislocations also contributes to this linewidth. The I_2^{hh} transition is not resolved, partly because of the large linewidth, but also because the

transition is less favoured at low temperatures. The large I_2 linewidth prevents the resolution of the free exciton emission. I_1 emission is quite weak, as expected (no DAP emission observed). The I_3 transitions may contribute to the luminescence.

The intense NBE emission at room temperature (see figure 4.4) is characteristic of material containing a high concentration of donor impurities [46,48]. The I_2 linewidth is therefore thought to result in large part from the inhomogeneous Stark effect broadening, since this is consistent with the strong NBE emission observed at 300 °K.

The exciton-related photoluminescence, recorded at a temperature of 2 °K, is shown in figure 4.20. The incident power density used was 120 mW/cm^2 in the range 22700-22500 cm^{-1} and 3.8 W/cm^2 in the range 22500-21750 cm^{-1}. The peak at 2.7759 ± 0.0002 eV is downshifted in energy with respect to the I_2^{1h} peak centered at 2.7950 ± 0.0002 eV by an amount equal to 19.1 ± 0.4 meV. This energy displacement compares favourably with the 1s-2p donor excitation energy for Al (see table 2.3), hence the emission at 2.7759 eV is due to TES (two-electron satellite) transitions associated with the principal I_2 luminescence. Shoulders appearing on the high and low energy sides of the TES peak correspond to donor excitation energies of 18.6 ± 0.4 meV (Al : 1s-2s) and 19.8 ± 0.4 meV (Cl : 1s-2p), respectively. If the uncertainty in these displacement energies is taken into account, it is seen that three donors, namely Al, Cl, and

Ga, may contribute to the I_2 luminescence and the associated TES emission. The DEZ precursor is presumably the source of these impurities. The SPL technique must be employed in order to resolve the individual TES transitions. The I_2^{hh} transition, the associated TES transitions, and the heavy hole free exciton transition are expected to be quite weak in intensity at this low temperature. It is assumed in the analysis which follows that the dominant donor is Al. The results are unchanged if it is assumed that Cl or Ga is the dominant impurity because of the uncertainties in the measured peak energies. In strain-free ZnSe, the I_2^{A1} transition energy is 2.79776 $\pm$ 0.00010 eV (see table 2.1). The I_2^{A1} transition in sample 32 is downshifted with respect to the strain-free transition energy by an amount 2.8 $\pm$ 0.3 meV as a consequence of the reduction in the effective band gap due to the presence of two-dimensional tensile stress. The strain-shifted E_{ex}^{T} (or FE) peak energy is thus

$$E_{ex}^{T}(\text{sample 32}) = E_{ex}^{T}(\text{strain-free}) - 0.0028 \text{ eV}$$

$$= 2.8027 - 0.0028 \text{ eV}$$

$$= 2.7999 \pm 0.0004 \text{ eV}.$$

The 1 LO phonon replica of the free exciton emission peak occurs at an energy of

$$E_{ex}^{T-1\ LO} = E_{ex}^{T}(\text{sample 32}) - E_{LO\ phonon(k=0)}$$

$$= 2.7999 - 0.0316\ [66]\ \text{eV}$$

$$= 2.7683 \pm 0.0006\ \text{eV}.$$

The peak centered at an energy of 2.7688 ± 0.0002 eV is therefore due to the radiative decay of free excitons with the simultaneous emission of an LO phonon (FE_{1-LO}). The origin of the peak at 2.7836 ± 0.0002 eV is uncertain. The I_1^{deep} transition energy (see table 2.4 : I_1^{deep} acceptor is unknown), taking into account the strain induced downshift, is approximately 2.7802 eV. The radiative decay of free excitons which scatter inelastically at neutral donors, leaving them in an excited state, corresponds to an emission energy ranging from 2.7811 eV (Al 1s-2s) to 2.7792 eV (Ga 1s-2p) (see table 2.3). Free exciton recombination following inelastic scattering at other free excitons corresponds to a transition energy of 2.7857 eV (FE 1s-2s excitation energy is 14.2 meV [33]. Some or all of these transitions contribute to this luminescence peak.

Figure 4.21 again shows the 2 °K exciton-related photoluminescence. The excitation power density used was 80 mW/cm² in the range 22700-22500 cm⁻¹, 2.5 W/cm² in the range 22500-22300 cm⁻¹, and 8 W/cm² in the range

22300-21750 cm^{-1}. In addition to the luminescence peaks previously identified, a peak at 2.7365 ± 0.0002 eV is observed. The 2 LO phonon replica of the free exciton emission peak occurs at an energy of

$$E_{ex^T-2\ LO} = E_{ex^T}(\text{sample 32}) - 2E_{LO\ phonon(k=0)}$$

$$= 2.7999 - 0.0632\ eV$$

$$= 2.7367 \pm 0.0008\ eV.$$

This peak is therefore due to the radiative decay of free excitons with the simultaneous emission of two LO phonons (FE_{2-LO}). The 2 °K photoluminescence in the DAP (shallow acceptor) emission region is shown in figure 4.22. No DAP emission is observed even at this low temperature and high excitation density (about 8 W/cm^2). It is evident that the material contains virtually no shallow acceptor impurities.

The photoluminescence of sample 29, recorded at a temperature of 7 °K, is shown in figures 4.23 and 4.24. An incident power density of 250 mW/cm^2 was used in obtaining the spectra. The dominant peak in the exciton emission region (figure 4.23) occurs at an energy of 2.7957 ± 0.0004 eV. It corresponds to the I_2^{1n} transition, since the epilayer is 1.5 microns thick and is therefore under two-dimensional tensile stress. A shoulder appearing on the

high energy side of this peak is due to the free exciton transition. The I_2^{hh} transition may also contribute to the shoulder. The linewidth (FWHM) of the I_2 peak is approximately 4.3 meV. The linewidth results from strain and impurity-related inhomogeneous broadening. This crystal therefore contains many dislocations and a high concentration of impurities. Two poorly resolved peaks at 2.770 and 2.777 eV are due to the recombination of free excitons with the simultaneous emission of an LO phonon (FE_{1-LO}) and TES emission, respectively. The I_1 and I_a transitions may contribute to the luminescence on the low energy side of the I_2 peak.

The photoluminescence in the DAP (shallow acceptor) emission region is shown in figure 4.24. Luminescence in the low energy part of the scan is the high energy tail of the Cu-green luminescence band. The peak at 2.741 eV is presumably DAP emission (see chapter 2 - section 2.2). The acceptor involved is probably P, since Raman spectra of material grown using the same precursors indicate the presence of this acceptor [66]. An LO phonon replica of the principal peak is also observed. Another peak occurring at an energy of 2.685 eV is the DAP emission associated with the impurity Na, judging from its position (see chapter 2 - section 2.2). The intensity of these bands is extremely low, hence few acceptors are present.

The poor crystal quality and purity of this sample, which was grown using the same precursors as those used in

the growth of sample 40, is an indication that slow growth rates and growth on a GaAs epilayer as opposed to a GaAs substrate are required in order to obtain crystalline thin films having a high degree of perfection.

The exciton-related photoluminescence of sample 41 is shown in figure 4.25. The spectrum was recorded at a temperature of 6 °K using an excitation power density of 250 mW/cm². The peak situated at 2.7983 ± 0.0002 eV is the I_2^{hh} transition. The transition energy is slightly higher than the strain-free value (see table 2.1), since for the epilayer thickness of 0.4 microns, the strain relaxation process is not fully completed and the layer is under a two-dimensional compressive stress [45,76,84]. The higher energy I_2^{lh} transition is expected to lie quite close in energy to the dominant I_2^{hh} transition and is not resolved due to the large I_2 linewidth. Its contribution to the luminescence is presumably small at this low temperature. A partially resolved peak positioned at an energy of 2.8030 ± 0.0002 eV is caused by the recombination of free excitons (FE). The I_2 localization energy is 4.7 ± 0.4 meV. This value is in reasonable agreement with the localization energies listed in table 2.1 and confirms the assignment given to the peaks. The partially resolved peak at 2.7938 ± 0.0002 eV corresponds to a localization energy of 9.2 ± 0.4 meV. Comparison with the localization energies listed in table 2.4 indicates that this emission is due to the I_1 transition at Na acceptors. The precursors are possible

sources of this impurity. The linewidth (FWHM) of the I_2 peak is about 3.7 meV. The linewidth results from strain broadening associated with dislocations and Stark effect broadening. The extent to which either of these two effects dominates over the other is uncertain. The strain relaxation process which occurs at this thickness results in the generation of dislocations. The dislocations, in turn, act as impurity sinks. The large linewidth is consistent with the high density of dislocations and high impurity concentration expected for samples of this thickness [82].

4.4)77 °K Near Band Edge Emission

The NBE photoluminescence spectra have been obtained for several samples. It is found that the emission is due to several transitions. The transitions involved are identified through an analysis of the spectra.

The NBE photoluminescence of sample 40, recorded at temperatures of 82 °K and 73 °K, is shown in figures 4.26 and 4.27, respectively. The excitation power densities used were 8 W/cm² (figure 4.26) and 1.25 W/cm² (figure 4.27). The spectral features appearing in the two spectra are essentially identical. The peaks in figure 4.26 are downshifted in energy relative to the peak positions in figure 4.27 because of the decrease in the energy gap with increasing temperature. The analysis which follows refers

to peak positions in figure 4.26, since the uncertainty in the peak positions is smaller for this spectrum. The peak situated at 2.7933 ± 0.0002 eV is the free exciton emission (FE). The energy separation between the peak appearing at an energy of 2.7878 ± 0.0002 eV and the free exciton peak is 5.5 ± 0.4 meV. The separation energy is approximately equal to the localization energy for excitons bound to neutral donors (see table 2.1), hence the peak at 2.7878 eV is due to the I_2 transition. A second peak positioned at an energy of 2.7859 ± 0.0002 eV corresponds to the radiative recombination of free holes with electrons bound to donor impurities. The donor binding energy is obtained using the expression (equation 2.9 in chapter 2)

$$(D^o,h) = E_g - E_D$$

$$(D^o,h) = E_{gx^T} + FE_{binding\ energy} - E_D$$

$$2.7859 = 2.7933 + 0.0190 - E_D \text{ eV}$$

$$E_D = 26.4 \pm 0.9 \text{ meV}.$$

The calculated value is in close agreement with the values listed in table 2.3, and provides confirmation that the above assignment is indeed correct. The donor may be Al, Cl, or Ga. The broad luminescence peak appearing on the low energy side of the dominant luminescence bands is

presumably due to TES transitions, free exciton recombination with the simultaneous emission of an LO phonon, and possibly the I_1^{deep} transition, although this last transition was not present in the 7 °K photoluminescence.

In reported studies of photoluminescence of ZnSe films grown on GaAs, the 77 °K NBE emission is attributed to either the (D^o,h) or a free exciton-related (FE-electron inelastic scattering) transition. The emission is observed as a single-peaked luminescence band [17,21,22,23]. The data shown in figures 4.26 and 4.27 indicates that three transitions contribute to the NBE emission at this temperature. A similar conclusion was reached in a photoluminescence study of bulk ZnSe (see section 2.4) [41]. No such conclusion has been presented in the literature for heteroepitaxial ZnSe thin films.

Figure 4.28 shows the 75 °K NBE photoluminescence of sample 10. The spectrum was recorded using an excitation power density of 2.5 W/cm². The dominant peak positioned at an energy of 2.786 eV is attributed to the I_2 and (D^o,h) transitions. The shoulder on the high energy side of the peak is the free exciton emission. The emission is poorly resolved due to the relatively large linewidth of the dominant emission band.

The NBE emission of samples 32, 29, and 41 consists of a single broad luminescence band. The large linewidth prevents the resolution of the individual transitions

observed in the case of sample 40.

The NBE photoluminescence of sample 50, recorded at 72 °K, is shown in figure 4.29. The incident power density used was 4 W/cm². In addition to the NBE emission at 2.788 eV, other luminescence bands are observed. The peak appearing at 2.5945 ± 0.0006 eV is the Y band. A series of progressively weaker peaks, the first of which is located at an energy of 2.7022 ± 0.0006 eV, is due to the radiative recombination of free electrons and holes bound to shallow acceptors with the simultaneous emission of 0, 1, and 2 LO phonons. If the free exciton emission energy (FE = E_{ex}^{T}) is taken to be 2.7960 ± 0.0002 eV (see figure 4.27), the acceptor binding energy is obtained using the expression (equation 2.8 in chapter 2)

$$(e,A^{o}) = E_{ex}^{T} + FE_{binding\ energy} - E_{A}$$

$$2.7022 = 2.7960 + 0.0190 - E_{A}\ eV$$

$$E_{A} = 112.8 \pm 1.3\ meV.$$

The calculated acceptor binding energy is in reasonable agreement with the Li acceptor binding energy listed in table 2.5. The energy separation between the principal transition and the 1 LO phonon replica situated at 2.6696 ± 0.0006 eV is 32.6 ± 1.2 meV, while the separation between the 1 LO phonon replica and the 2 LO

phonon replica positioned at an energy of 2.6388 ± 0.0006 eV is 30.8 ± 1.2 meV. The calculated LO phonon energies are in reasonable agreement with the LO phonon energy of 31.4 meV at 90 °K [85].

TABLES

Table 4.1 : Summary of the Features of the Photoluminescence Spectra of Heteroepitaxial ZnSe Thin Films

Sample	7 °K Photoluminescence					77 °K Photoluminescence						300 °K Photoluminescence		
	DAP	Free Exciton	(A^o,X) or I_1	(D^o,X) or I_2	FWHM of I_2 Peak	Deep Emission Bands	(e,A^o)	Near Band Edge (NBE)			Ratio R	Deep Emission Bands	NBE	Ratio R
								Free Exciton	(D^o,X) or I_2	(D^o,h)				
	eV	eV	eV	eV	meV	eV	eV	eV	eV	eV		eV	eV	
8	not obtained					not obtained						1.90	2.69	0.5
9	not obtained					not obtained						2.09	2.69	6.2
10	not obtained					none	none	FE partly resolved, main peak at 2.79 eV			60.5	2.13	2.69	11.2
32	none	not resolved	none	2.7950	3.5	2.13	none	not resolved, one peak at 2.79 eV			6.3	2.12	2.69	9.0
29	2.741 2.685	not resolved	not resolved	2.7957	4.3	2.31 2.18	none	not resolved, one peak at 2.79 eV			0.8	2.18	2.69	6.0
40	none	2.8027	very weak	2.7980	1.9	2.26	none	2.7960	2.7911	2.7892	3.1	very weak	2.69	5.3
41	no scan	2.8030	2.7938	2.7983	3.7	2.09	very weak	not resolved, one peak at 2.79 eV			1.7	2.14	2.69	1.2
50	not obtained					2.24 2.49 2.59	2.7022	not resolved, one peak at 2.79 eV			1.0	not obtained		

R values at 300°K were obtained using an incident power density of 2.5 W/cm².
R values at 77°K were obtained using the following incident power densities : sample 10 - 2.5 W/cm², samples 32,29,40,41 - 250 mW/cm², sample 50 - 1.25 W/cm².

The photoluminescence spectra are uncorrected for photomultiplier response. The sensitivity is reduced by approximately 20 % at 650 nm relative to that at 450 nm.

FIGURES

FIGURES (CONTINUED)

figure 4.1 :

incident power - 25 mW

power density - 2.5 W/cm^2

scan range - 22400-15000 cm^{-1}

energy sampling - 5 cm^{-1}

sample time - 1 sec

slit width - 100 microns

Emission Bands :

NBE -- The near band edge emission peaks at an energy of approximately 2.69 eV.

A -- The emission band centered at 1.90 eV corresponds to a free to bound transition involving the A-center (deep acceptor).

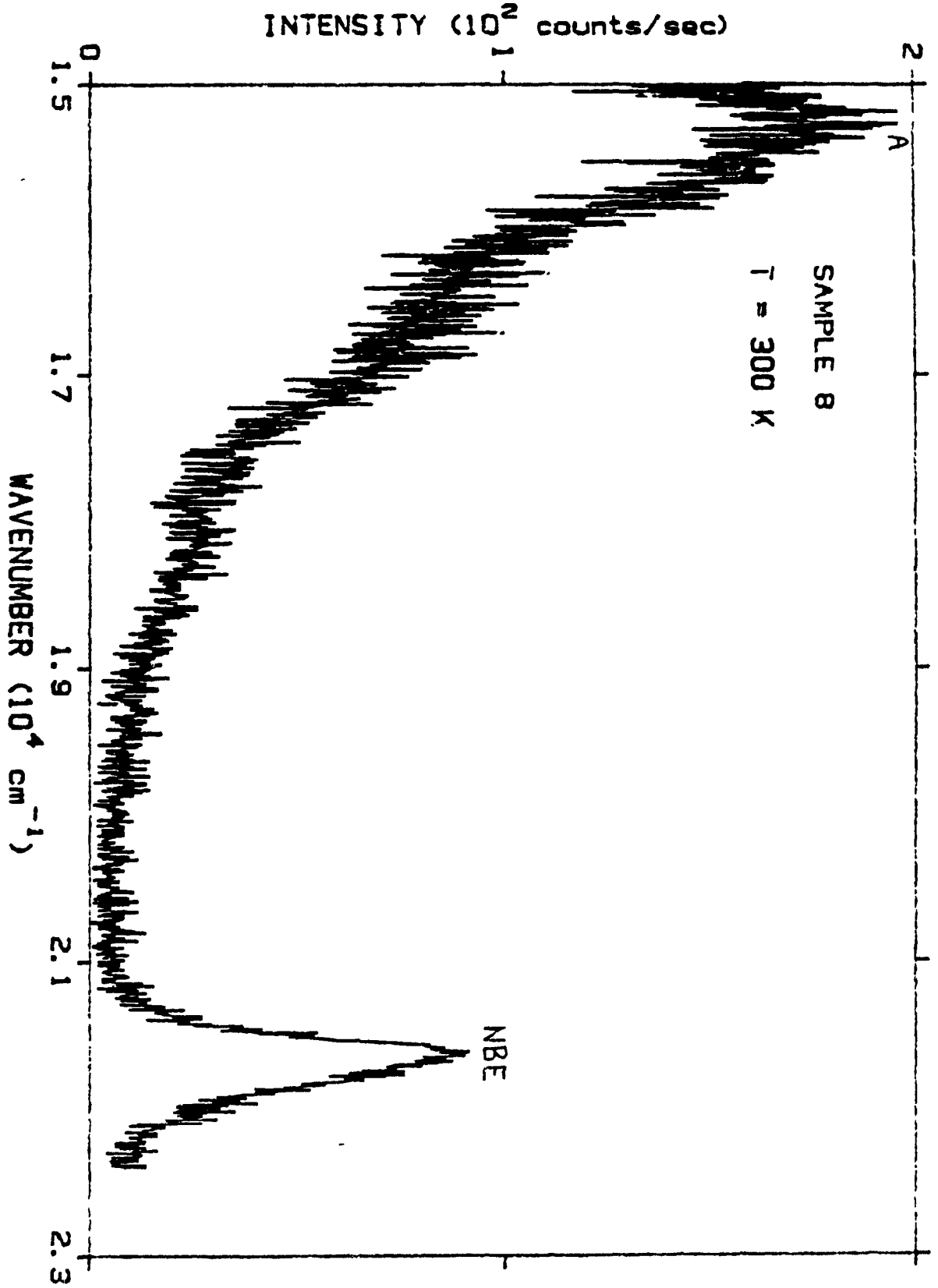
INTENSITY (10^2 counts/sec)
0
1
2
1.5
1.7
1.9
2.1
2.3
WAVENUMBER (10^4 cm^{-1})
A
NBE
SAMPLE 8
T = 300 K

figure 4.1

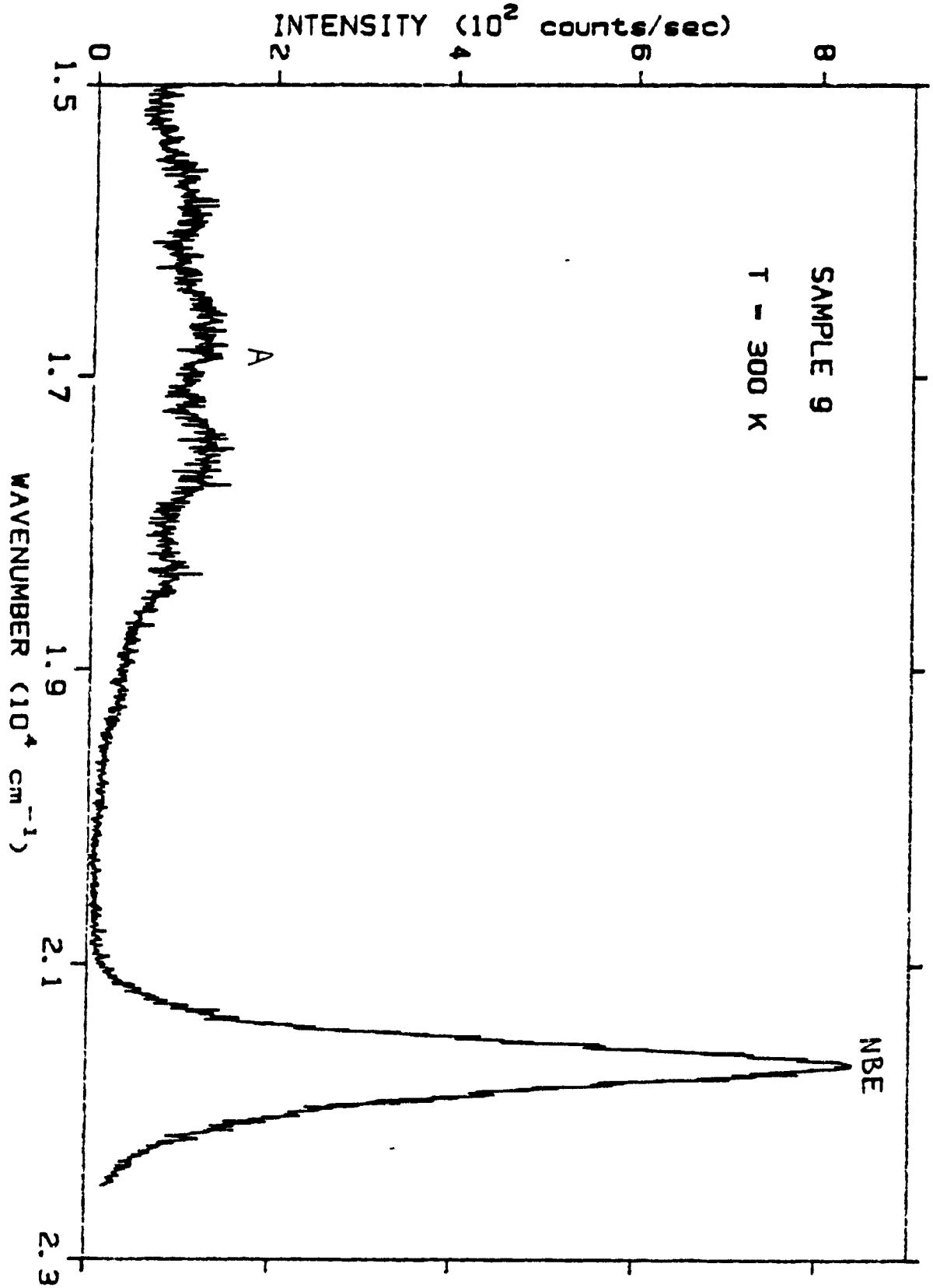
INTENSITY (10^2 counts/sec)
0
2
4
6
8
1.5
1.7
1.9
2.1
2.3
WAVENUMBER (10^4 cm^{-1})
SAMPLE 9
T - 300 K
A
NBE

figure 4.2

figure 4.3 :

incident power - 25 mW

power density - 2.5 W/cm^2

scan range - 22500-15000 cm^{-1}

energy sampling - 5 cm^{-1}

sample time - 1 sec

slit width - 100 microns

Emission Bands :

NBE -- The near band edge emission peaks at an energy of 2.69 eV.

A -- The emission band centered at 2.13 eV corresponds to a free to bound transition involving the A-center (deep acceptor).

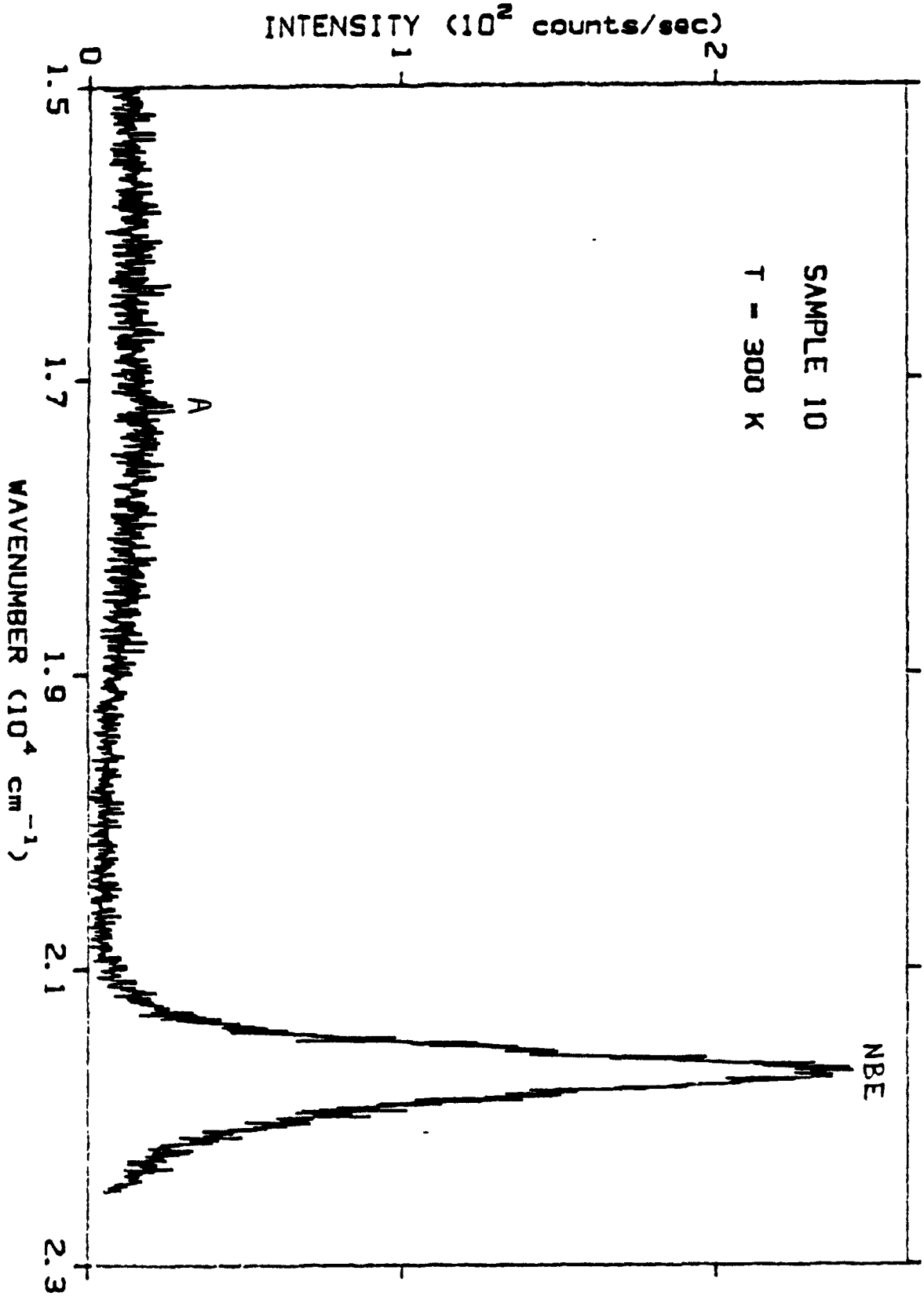
INTENSITY (10^2 counts/sec)
0
1
2
SAMPLE 10
T = 300 K
A
NBE
WAVENUMBER (10^4 cm^{-1})
1.5
1.7
1.9
2.1
2.3

figure 4.3

figure 4.4 :

incident power - 12.5 mW

power density - 2.5 W/cm^2

scan range - 23000-14000 cm^{-1}

energy sampling - 25 cm^{-1}

sample time - 1 sec

slit width - 200 microns

Emission Bands :

NBE — The near band edge emission peaks at an energy of 2.69 eV.

A — The emission band centered at 2.12 eV corresponds to a free to bound transition involving the A-center (deep acceptor).

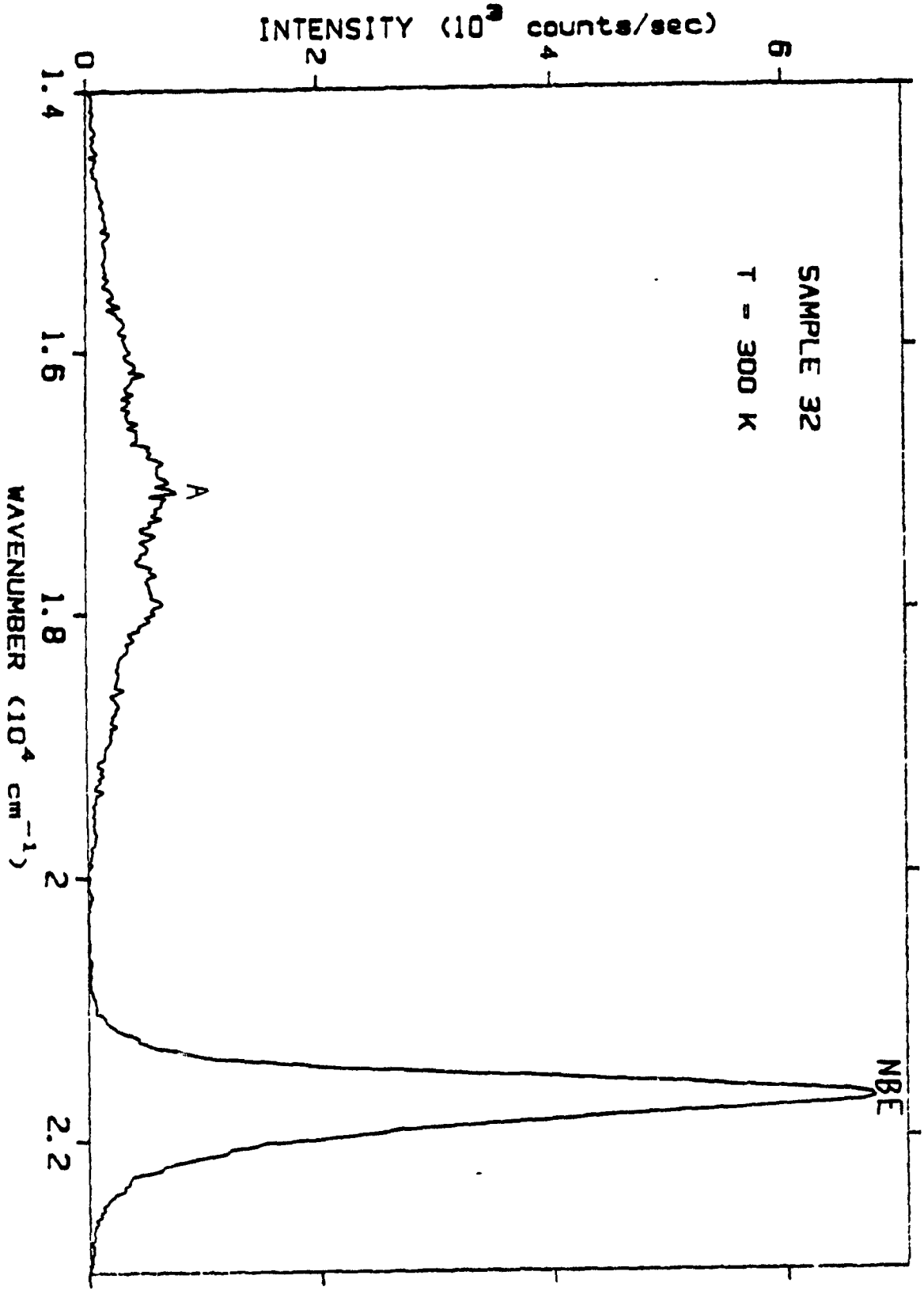
INTENSITY (10³ counts/sec)
0
2
4
6
1.4
1.6
1.8
2
2.2
WAVENUMBER (10⁴ cm⁻¹)
SAMPLE 32
T = 300 K
A
NBE

figure 4.4

figure 4.5 :

incident power - 12.5 mW

power density - 2.5 W/cm^2

scan range - 23000-14000 cm^{-1}

energy sampling - 25 cm^{-1}

sample time - 3 sec

slit width - 200 microns

Emission Bands :

NBE -- The near band edge emission peaks at an energy of 2.69 eV.

A -- The emission band centered at 2.18 eV corresponds to a free to bound transition involving the A-center (deep acceptor).

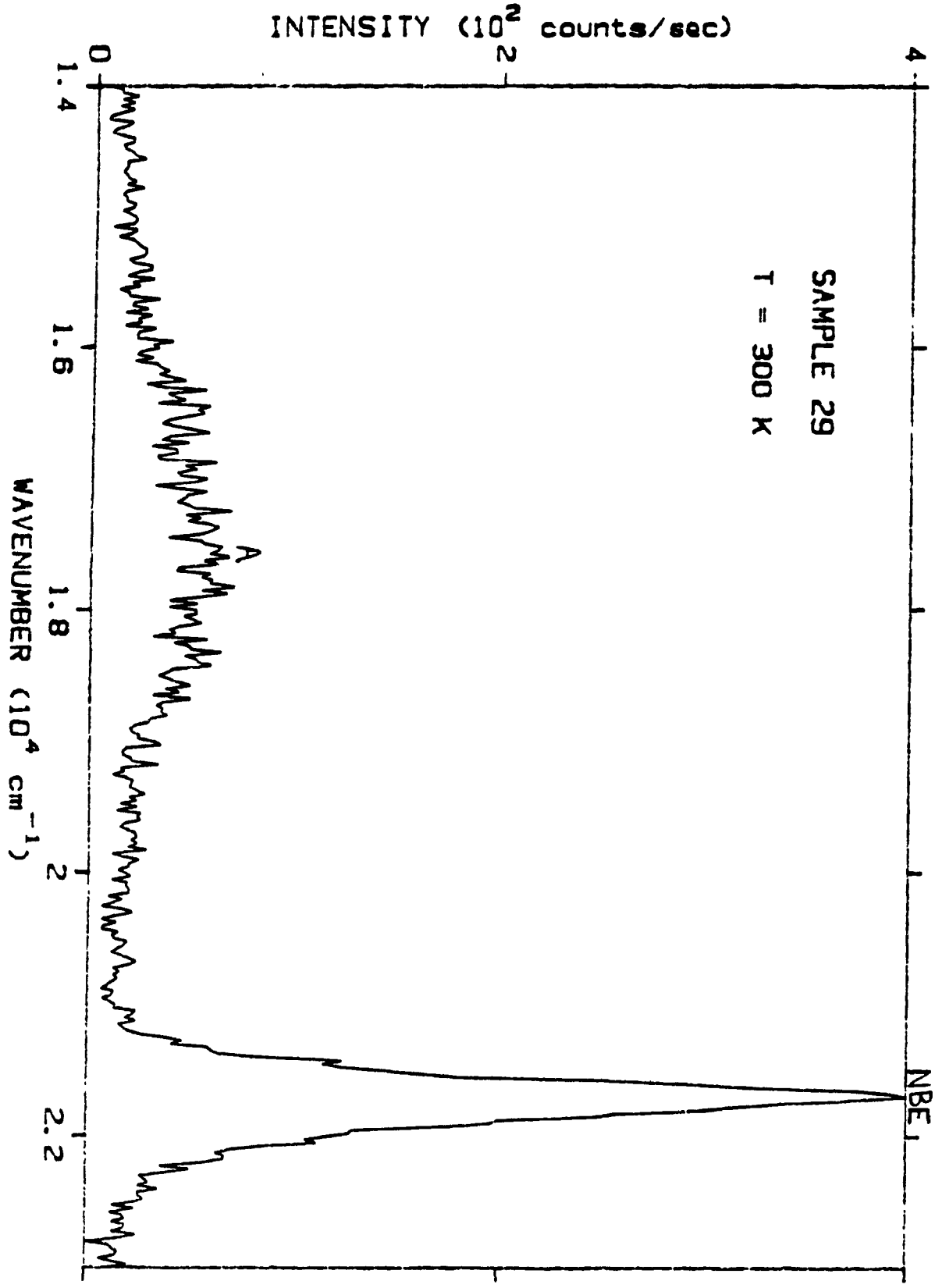
INTENSITY (10^2 counts/sec)
0
2
4
1.4
1.6
1.8
2
2.2
WAVENUMBER (10^4 cm^{-1})
SAMPLE 29
T = 300 K
A
NBE

Figure 4.5

figure 4.6 :

incident power - 12.5 mW

power density - 2.5 W/cm^2

scan range - 23000-14000 cm^{-1}

energy sampling - 25 cm^{-1}

sample time - 3 sec

slit width - 200 microns

Emission Bands :

NBE -- The near band edge emission peaks at an energy of 2.69 eV.

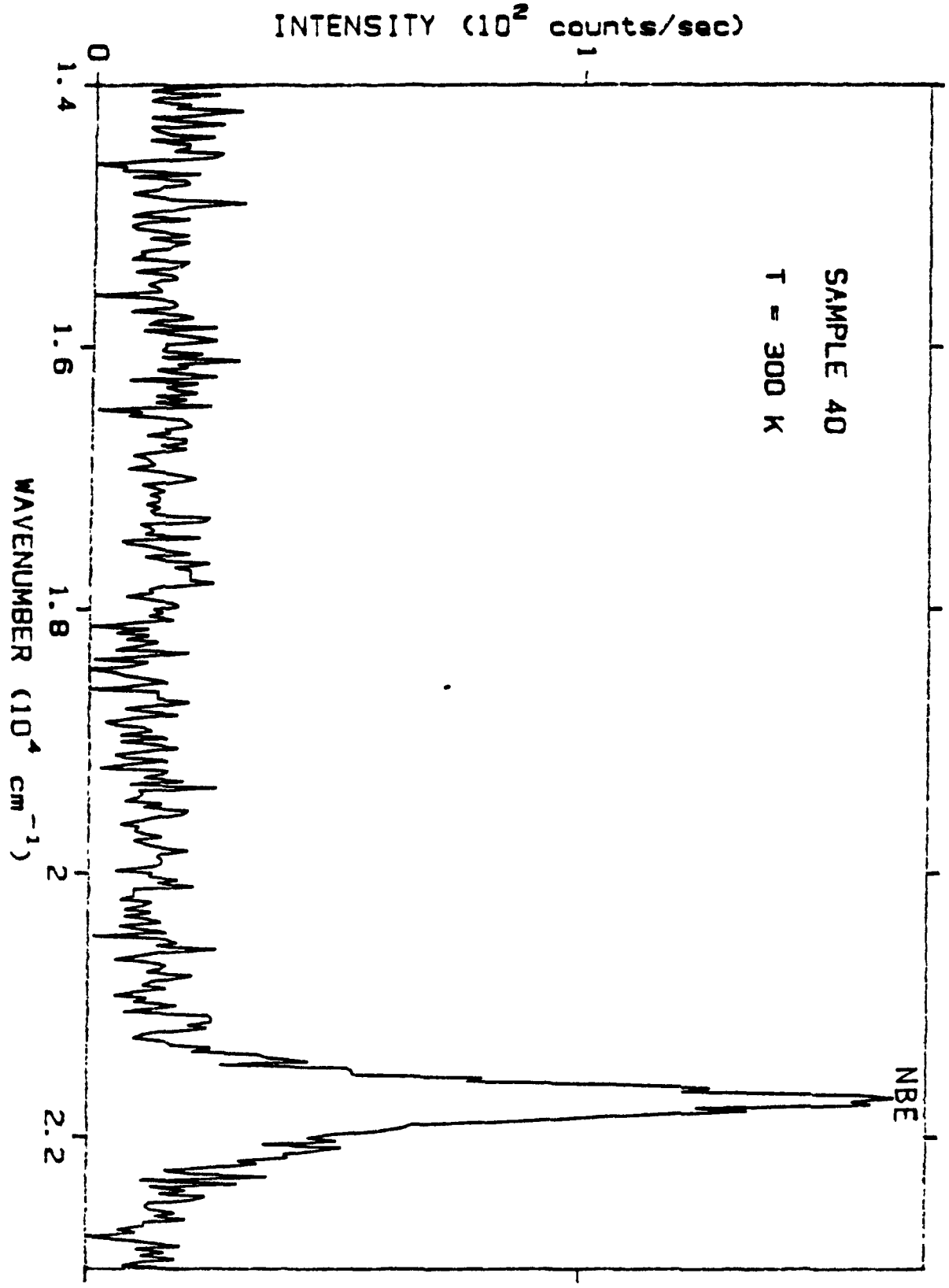
INTENSITY (10^2 counts/sec)
0
1
1.4
1.6
1.8
2
2.2
WAVENUMBER (10^4 cm^{-1})
SAMPLE 40
T = 300 K
NBE

Figure 4.6

figure 4.6a :

incident power - 40 mW

power density - 8 W/cm^2

scan range - 23000-14000 cm^{-1}

energy sampling - 25 cm^{-1}

sample time - 3 sec

slit width - 200 microns

Emission Bands :

NBE — The near band edge emission peaks at an energy of 2.69 eV.

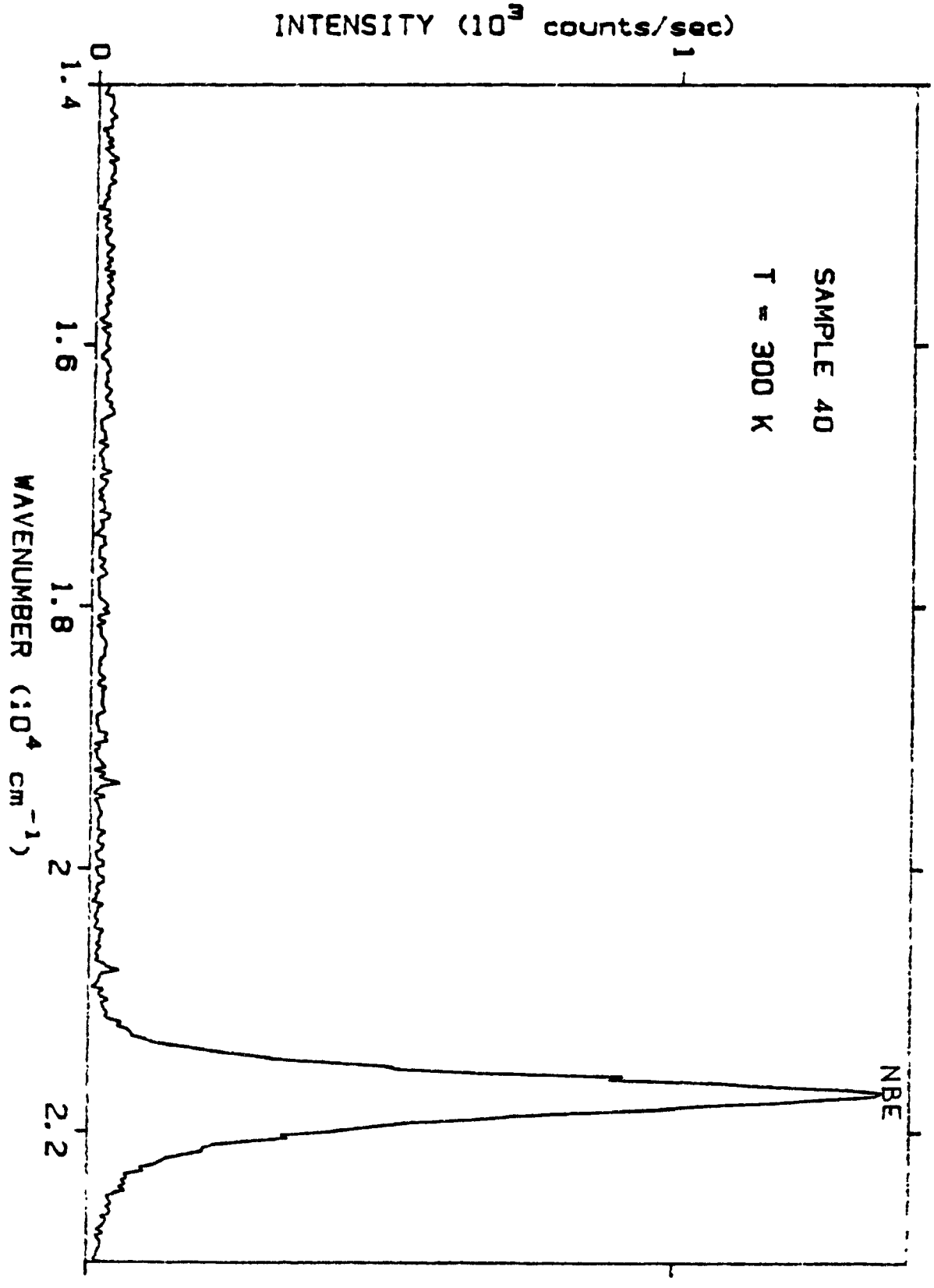
INTENSITY (10^3 counts/sec)
0
1
1.4
1.6
1.8
2
2.2
WAVENUMBER (10^4 cm^{-1})
SAMPLE 40
T = 300 K
NBE

Figure 4.6a

figure 4.7 :

incident power - 12.5 mW

power density - 2.5 W/cm^2

scan range - 23000-14000 cm^{-1}

energy sampling - 25 cm^{-1}

sample time - 3 sec

slit width - 200 microns

Emission Bands :

NBE -- The near band edge emission peaks at an energy of 2.69 eV.

A -- The emission band centered at 2.14 eV corresponds to a free to bound transition involving the A-center (deep acceptor).

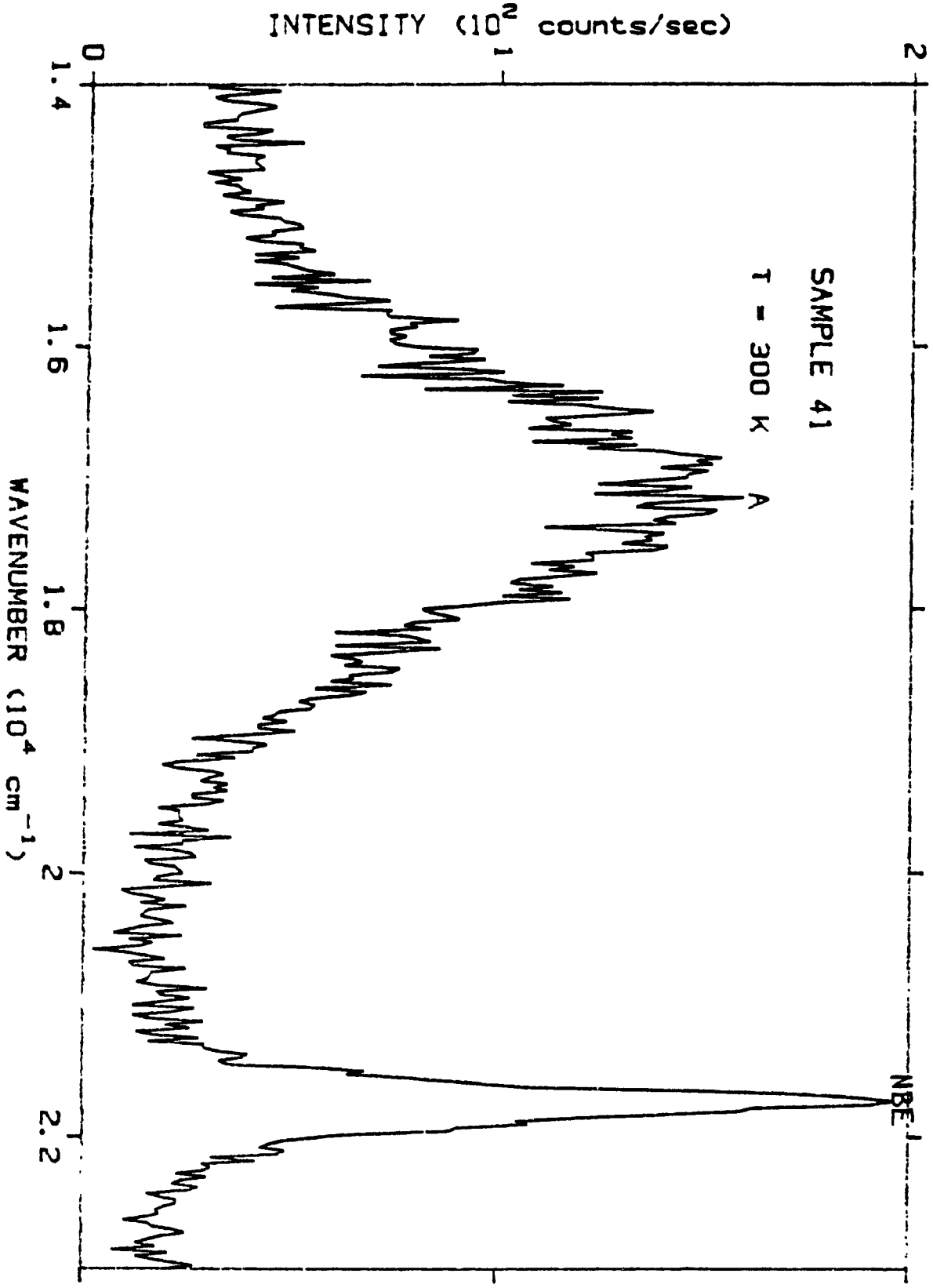
INTENSITY (10² counts/sec)
0
1
2
1.4
1.6
1.8
2
2.2
WAVENUMBER (10⁴ cm⁻¹)
SAMPLE 41
T = 300 K
A
NBE

Figure 4.7

figure 4.8 :

incident power - 12.5 mW

power density - 2.5 W/cm^2

scan range - 23000-14000 cm^{-1}

energy sampling - 25 cm^{-1}

sample time - 2 sec

slit width - 200 microns

Emission Bands :

NBE -- The near band edge emission peaks at an energy of 2.79 eV.

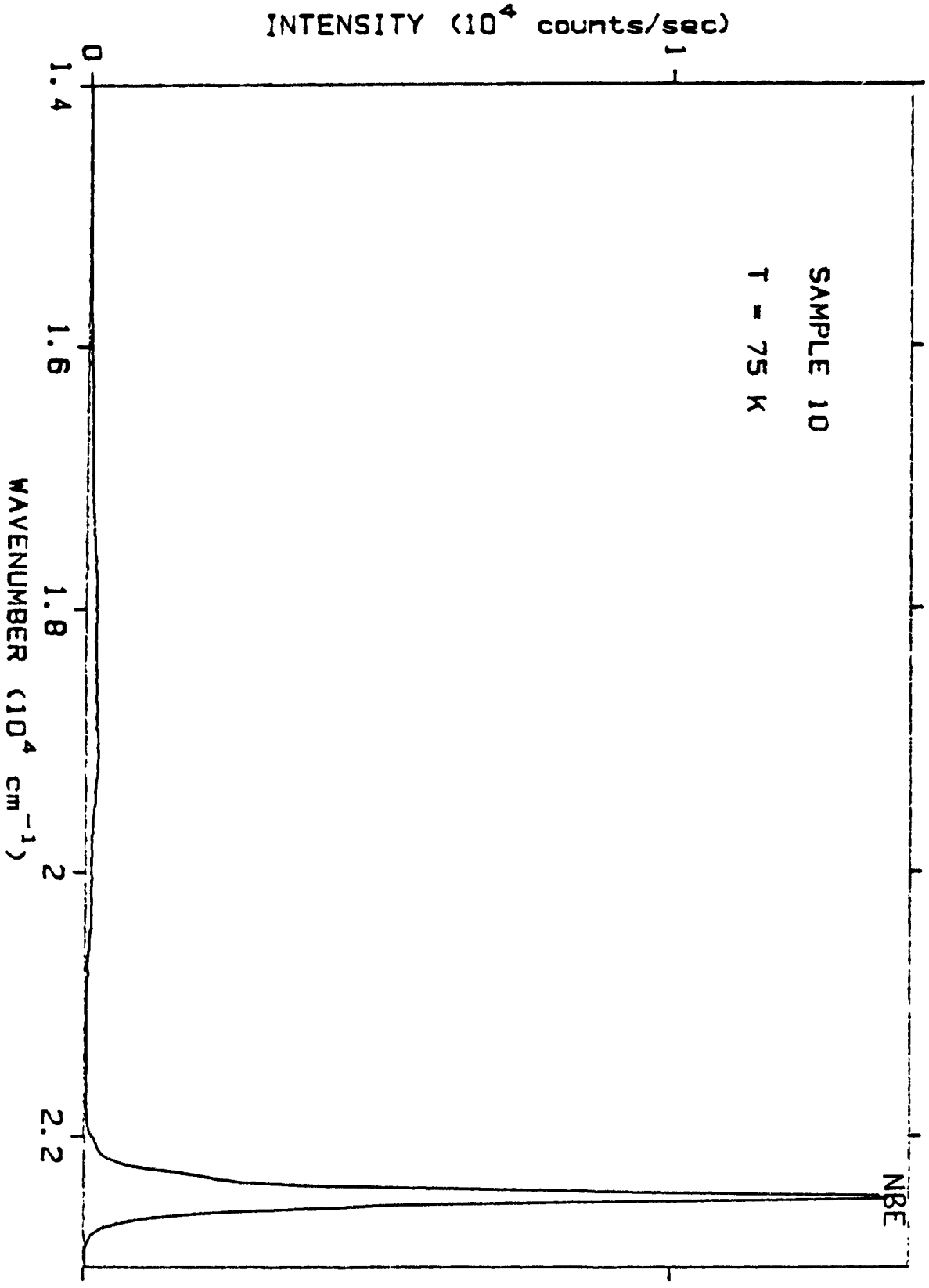
INTENSITY (10^4 counts/sec)
0
1
1.4
1.6
1.8
2
2.2
WAVENUMBER (10^4 cm^{-1})
SAMPLE 10
T = 75 K
NBE

figure 4.8

figure 4.9 :

incident power - 1.25 mW

power density - 250 mW/cm^2

scan range - 23000-14000 cm^{-1}

energy sampling - 25 cm^{-1}

sample time - 2 sec

slit width - 200 microns

Emission Bands :

NBE -- The near band edge emission peaks at an energy of 2.79 eV.

SA -- The self-activated (SA) emission peaks at an energy of 2.13 eV. The emission is due to (e,A°) and DAP transitions involving the A-center (deep acceptor).

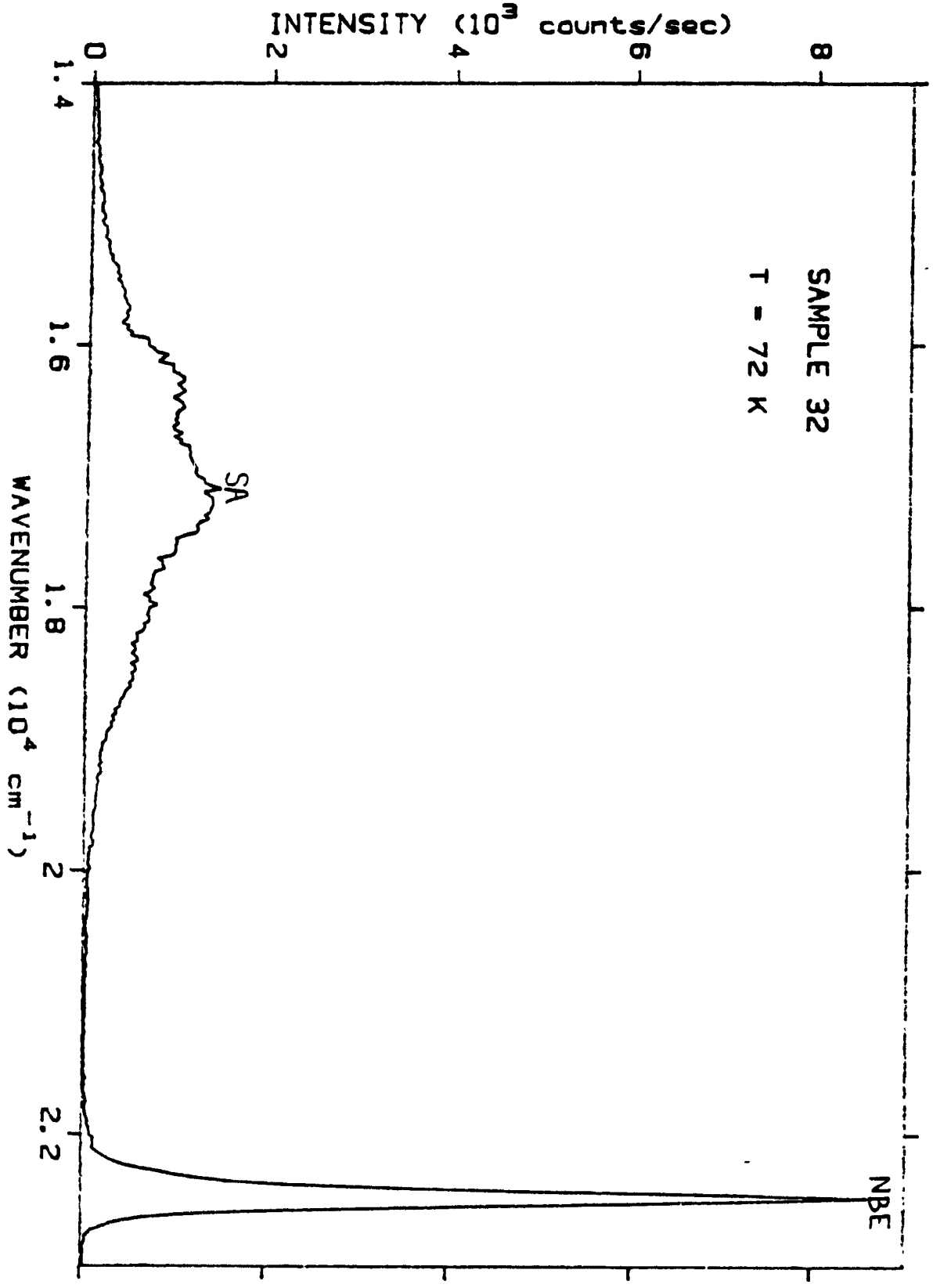
INTENSITY (10^3 counts/sec)
0
2
4
6
8
1.4
1.6
1.8
2
2.2
WAVENUMBER (10^4 cm^{-1})
SAMPLE 32
T = 72 K
SA
NBE

figure 4.9

figure 4.10 :

incident power - 1.25 mW

power density - 250 mW/cm^2

scan range - 23000-14000 cm^{-1}

energy sampling - 25 cm^{-1}

sample time - 2 sec

slit width - 200 microns

Emission Bands :

NBE -- The near band edge emission peaks at an energy of 2.79 eV.

Cu-GREEN -- The copper-green (Cu-GREEN) emission peaks at an energy of 2.31 eV. The emission is due to (e,A^o) and DAP transitions involving a Cu-complex acceptor.

SA -- The self-activated (SA) emission peaks at an energy of 2.18 eV. The emission is due to (e,A^o) and DAP transitions involving the A-center (deep acceptor).

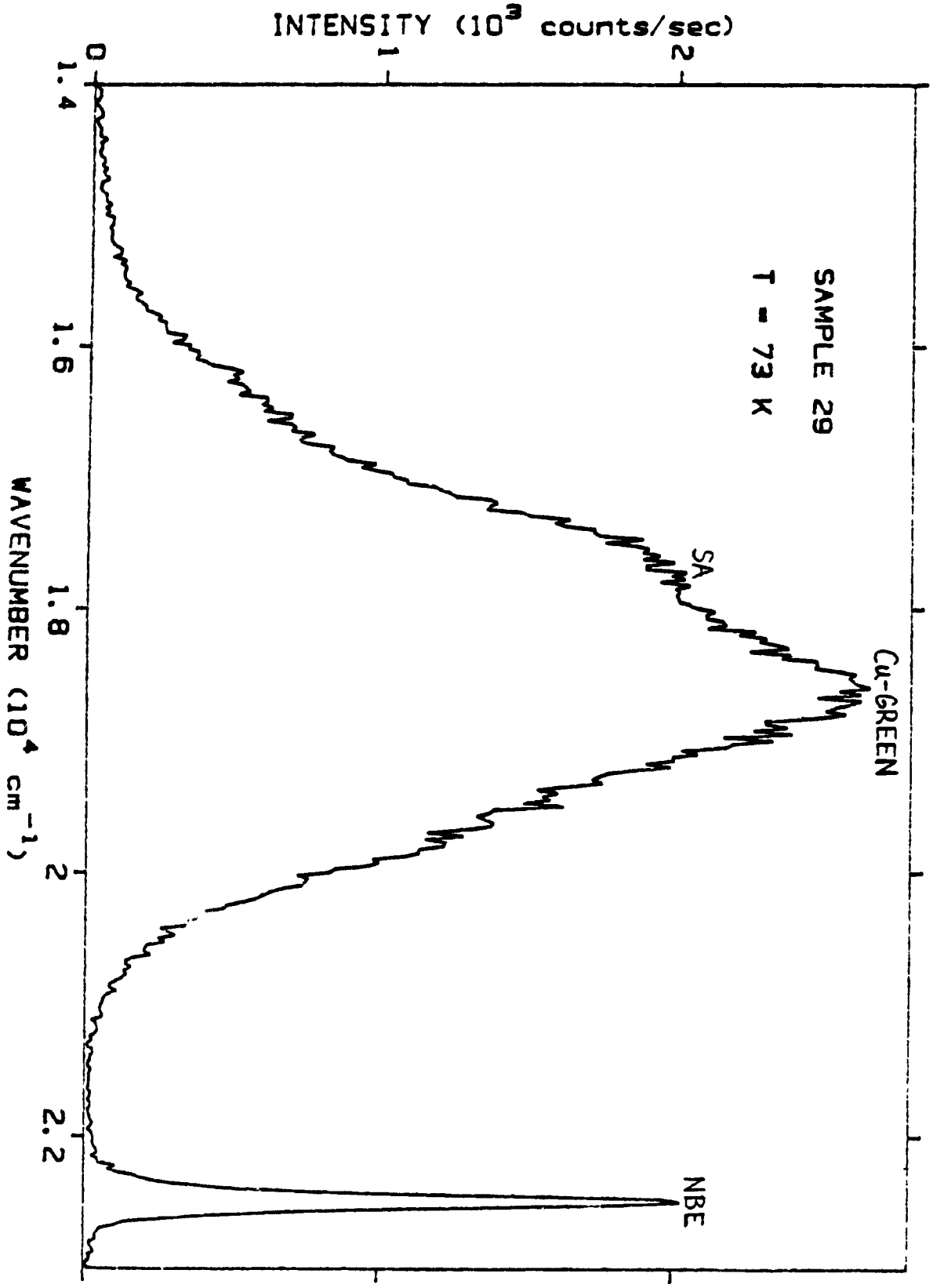
INTENSITY (10^3 counts/sec)
0
1
2
1.4
1.6
1.8
2
2.2
WAVENUMBER (10^4 cm^{-1})
SAMPLE 29
T = 73 K
SA
Cu-GREEN
NBE

figure 4.10

figure 4.11 :

incident power - 1.25 mW

power density - 250 mW/cm^2

scan range - 23000-14000 cm^{-1}

energy sampling - 25 cm^{-1}

sample time - 2 sec

slit width - 200 microns

Emission bands :

NBE -- The near band edge emission peaks at an energy of 2.79 eV.

Cu-GREEN -- The copper-green emission peaks at an energy of 2.26 eV. The emission is due to (e,A°) and DAP transitions involving a Cu-complex acceptor.

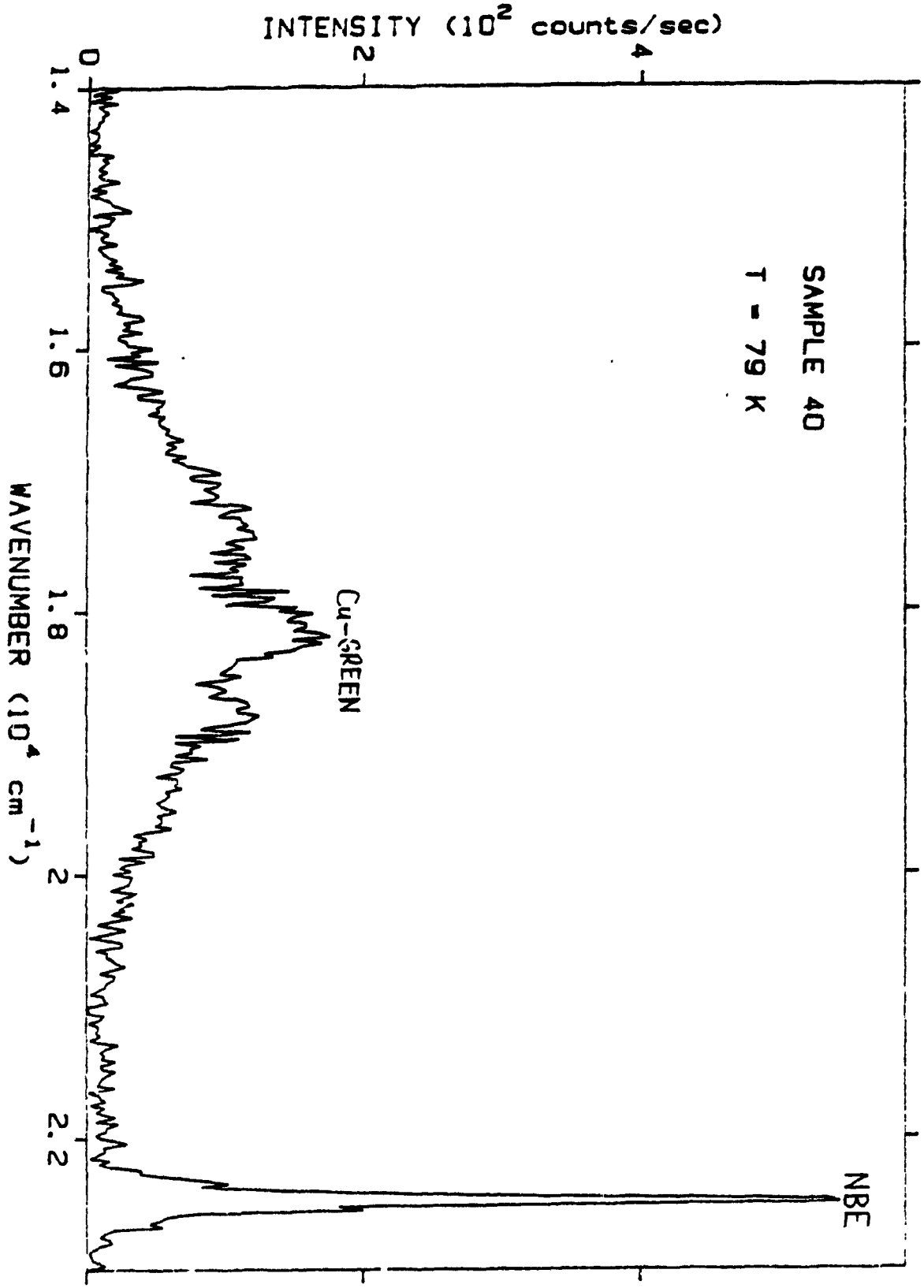
INTENSITY (10^2 counts/sec)
0
2
4
1.4
1.6
1.8
2
2.2
WAVENUMBER (10^4 cm^{-1})
SAMPLE 40
T = 79 K
Cu-GREEN
NBE

figure 4.11

figure 4.12 :

incident power - 1.25 mW

power density - 250 mW/cm^2

scan range - 23000-14000 cm^{-1}

energy sampling - 25 cm^{-1}

sample time - 2 sec

slit width - 200 microns

Emission Bands :

NBE — The near band edge emission peaks at an energy of 2.79 eV.

SA — The self-activated emission peaks at an energy of 2.09 eV. The emission is due to (e,A°) and DAP transitions involving the A-center.

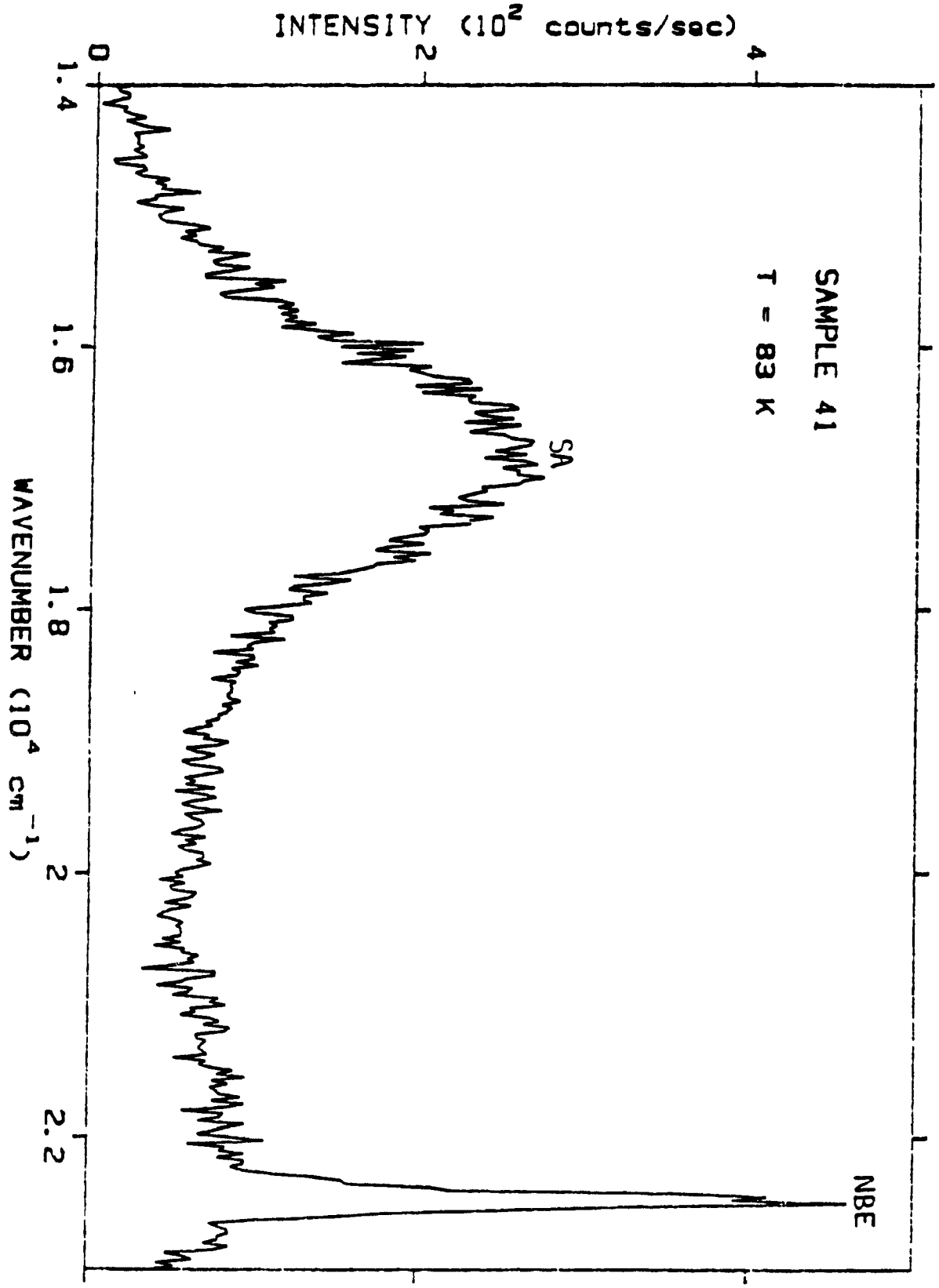
INTENSITY (10² counts/sec)
0
2
4
1.4
1.6
1.8
2
2.2
WAVENUMBER (10⁴ cm⁻¹)
SAMPLE 41
T = 83 K
SA
NBE

figure 4.12

figure 4.13 :

incident power - 12.5 mW

power density - 1.25 W/cm^2

scan range - 23000-14000 cm^{-1}

energy sampling - 25 cm^{-1}

sample time - 2 sec

slit width - 200 microns

Emission Bands :

NBE -- The near band edge emission peaks at an energy of 2.79 eV.

Y -- The origin of the Y band, centered at 2.59 eV, is uncertain. It may be due to the recombination of excitons at an extended defect.

S -- The S band, positioned at an energy of 2.49 eV, is due to (e,A$^\circ$) and DAP transitions involving an unknown acceptor.

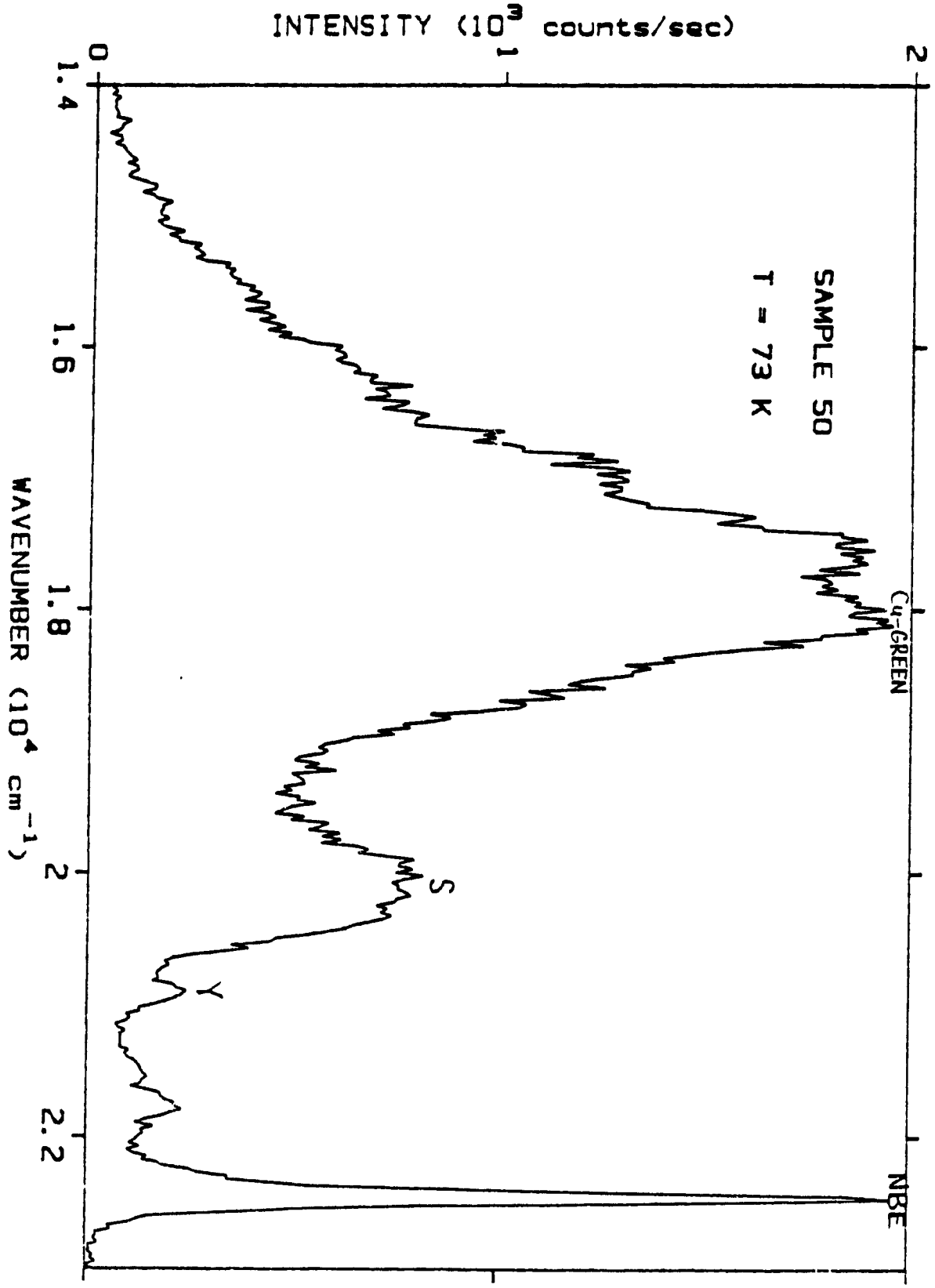
INTENSITY (10^3 counts/sec)
0
1
2
1.4
1.6
1.8
2
2.2
WAVENUMBER (10^4 cm^{-1})
SAMPLE 50
T = 73 K
C_4-GREEN
S
Y
NBE

figure 4.13

figure 4.14 :

incident power - 1.25 mW

power density - 250 mW/cm^2

scan range - 22700–22200 cm^{-1}

energy sampling - 2 cm^{-1}

sample time - 2 sec

slit width - 200 microns

Emission Bands :

I_1 — The luminescence peak positioned at an energy of 2.7980 eV is the I_1, or (D°,X), transition.

LPB - The peak at 2.8027 eV is the lower polariton branch (LPB) emission and occurs at the transverse free exciton energy (E_{ex}^T).

UPB - The shoulder at 2.8040 eV is the upper polariton branch (UPB) emission.

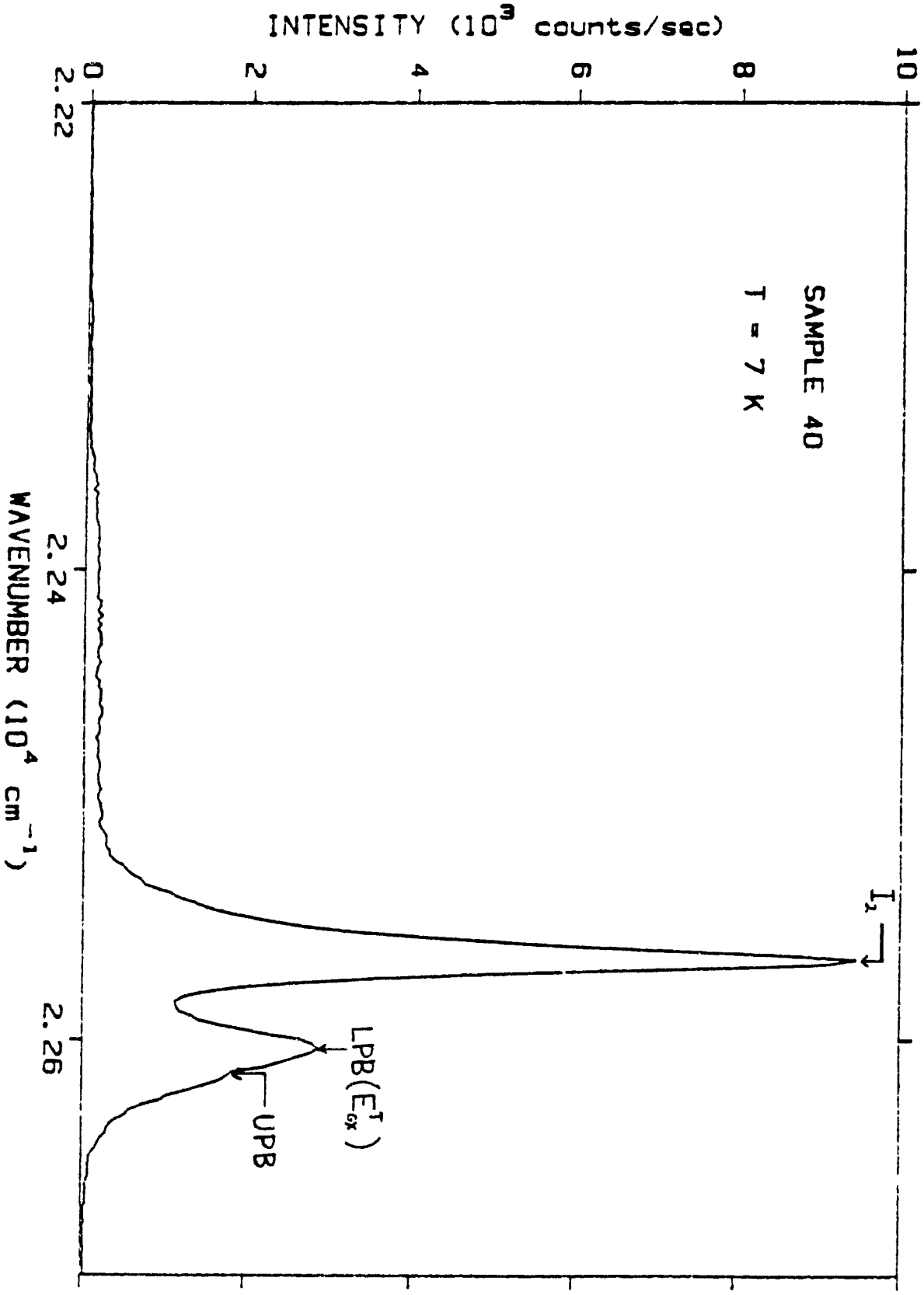
INTENSITY (10^3 counts/sec)
0
2
4
6
8
10
2.22
2.24
2.26
WAVENUMBER (10^4 cm^{-1})
SAMPLE 40
T = 7 K
I_x
LPB(E_{ex}^T)
UPB

figure 4.14

figure 4.15 :

incident power - 40 mW

power density - 8 W/cm^2

scan range - 22000-21000 cm^{-1}

energy sampling - 5 cm^{-1}

sample time - 1 sec

slit width - 200 microns

Emission Bands :

No DAP emission associated with the presence of shallow acceptors is observed.

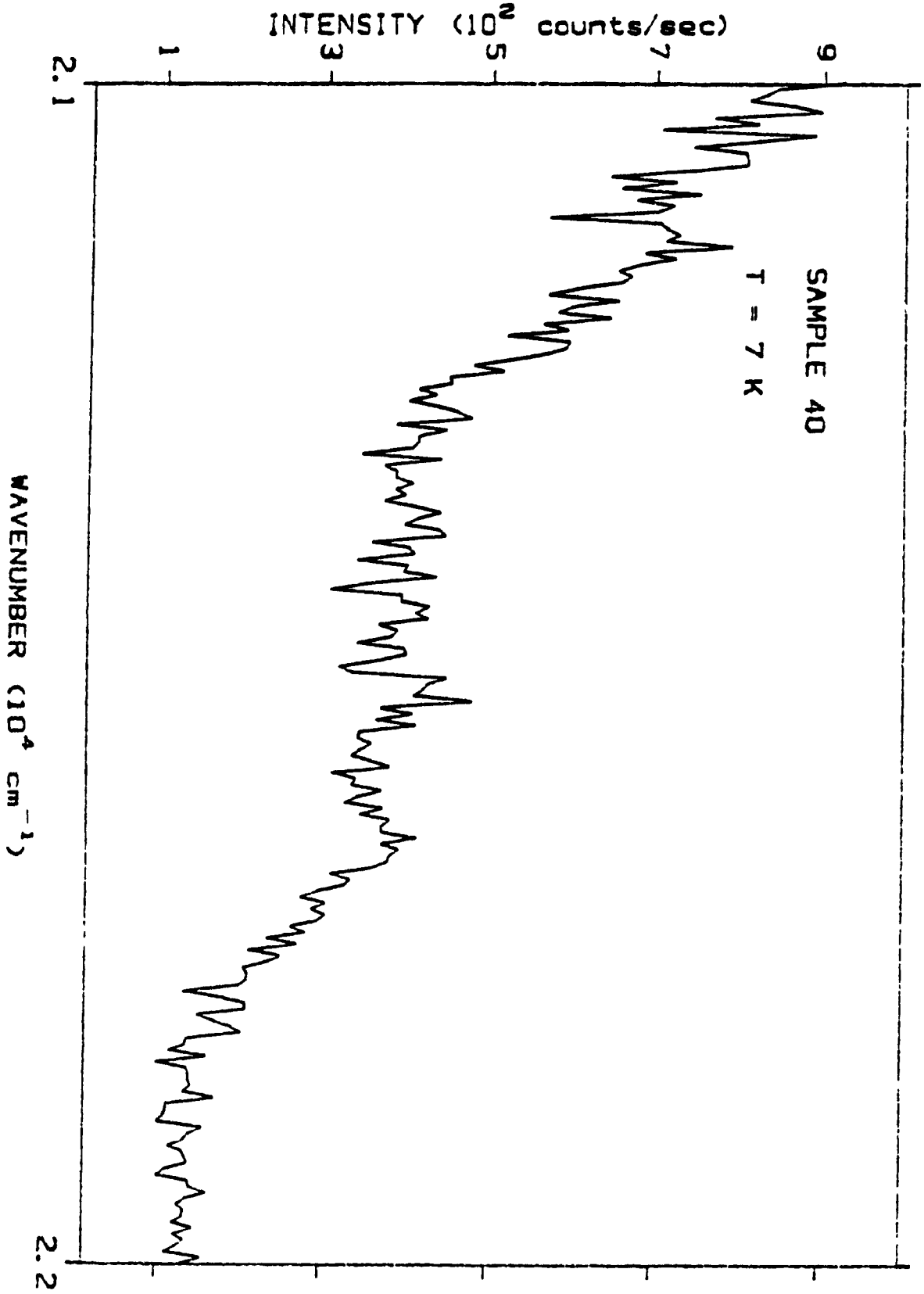
INTENSITY (10^2 counts/sec)
1
3
5
7
9
2.1
2.2
WAVENUMBER (10^4 cm^{-1})
SAMPLE 40
T = 7 K

Figure 4.15

figure 4.16 :

incident power - 12.5 mW

power density - 2.5 W/cm^2

scan range - 22700–21000 cm^{-1}

energy sampling - 5 cm^{-1}

sample time - 1 sec

slit width - 200 microns

Emission Bands :

I_1 -- The luminescence peak positioned at an energy of 2.7957 eV is the I_1^{lh}, or (D^0,X), transition.

No DAP emission associated with the presence of shallow acceptors is observed.

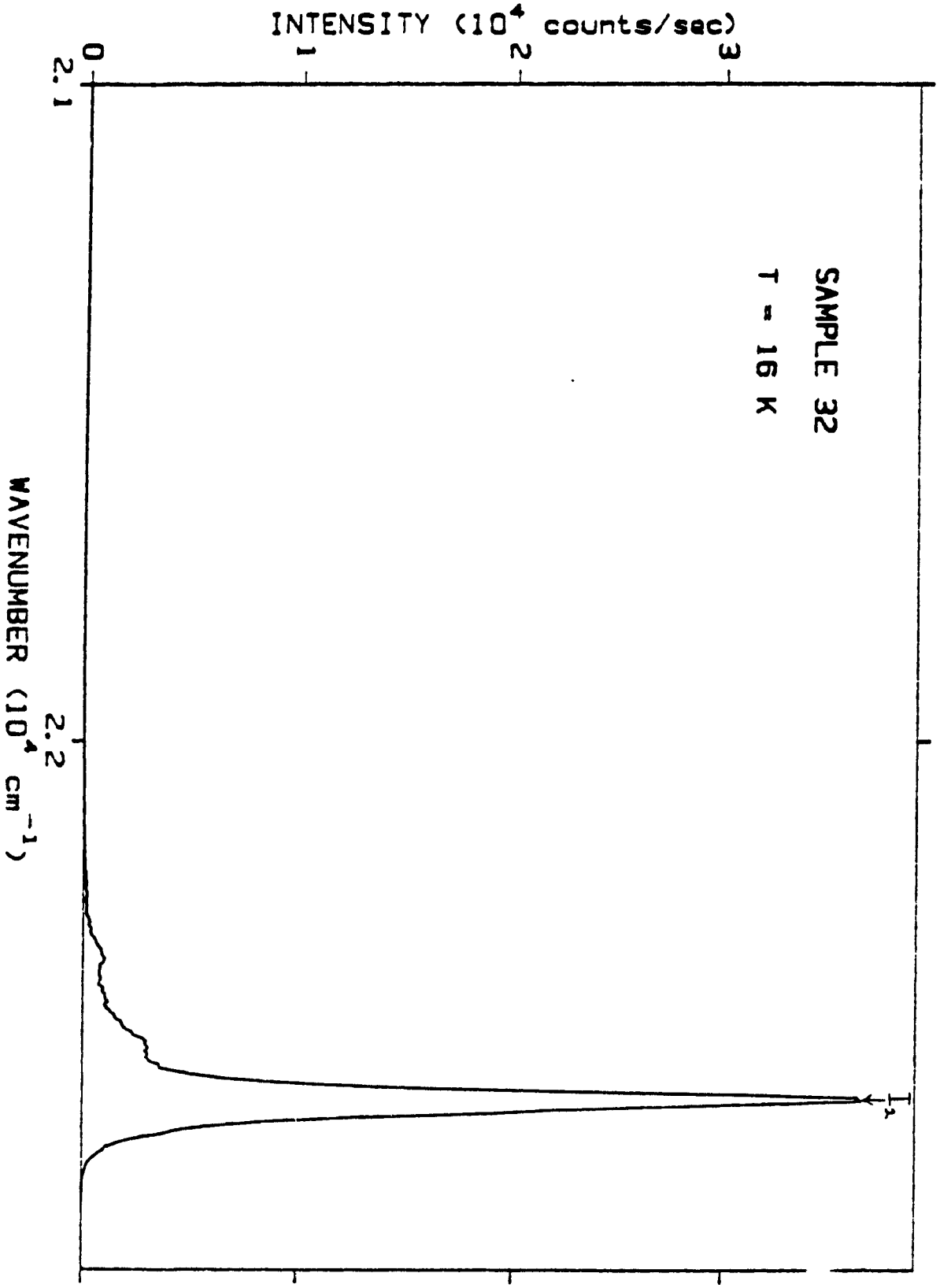
INTENSITY (10^4 counts/sec)
0
1
2
3
2.1
2.2
WAVENUMBER (10^4 cm^{-1})
SAMPLE 32
T = 16 K
I_x

figure 4.16

figure 4.17 :

incident power - 12.5 mW

power density - 2.5 W/cm^2

scan range - 22700-22200 cm^{-1}

energy sampling - 2 cm^{-1}

sample time - 2 sec

slit width - 200 microns

Emission Bands :

I_1 -- The luminescence peak positioned at an energy of 2.7957 eV is the I_1^{lh}, or (D^o,X), transition.

B -- Two transitions contribute to the B emission, observed as a shoulder on the high energy side of principal I_1 peak : 1) the radiative decay of free excitons and 2) the I_1^{hh} transition associated with heavy hole excitons.

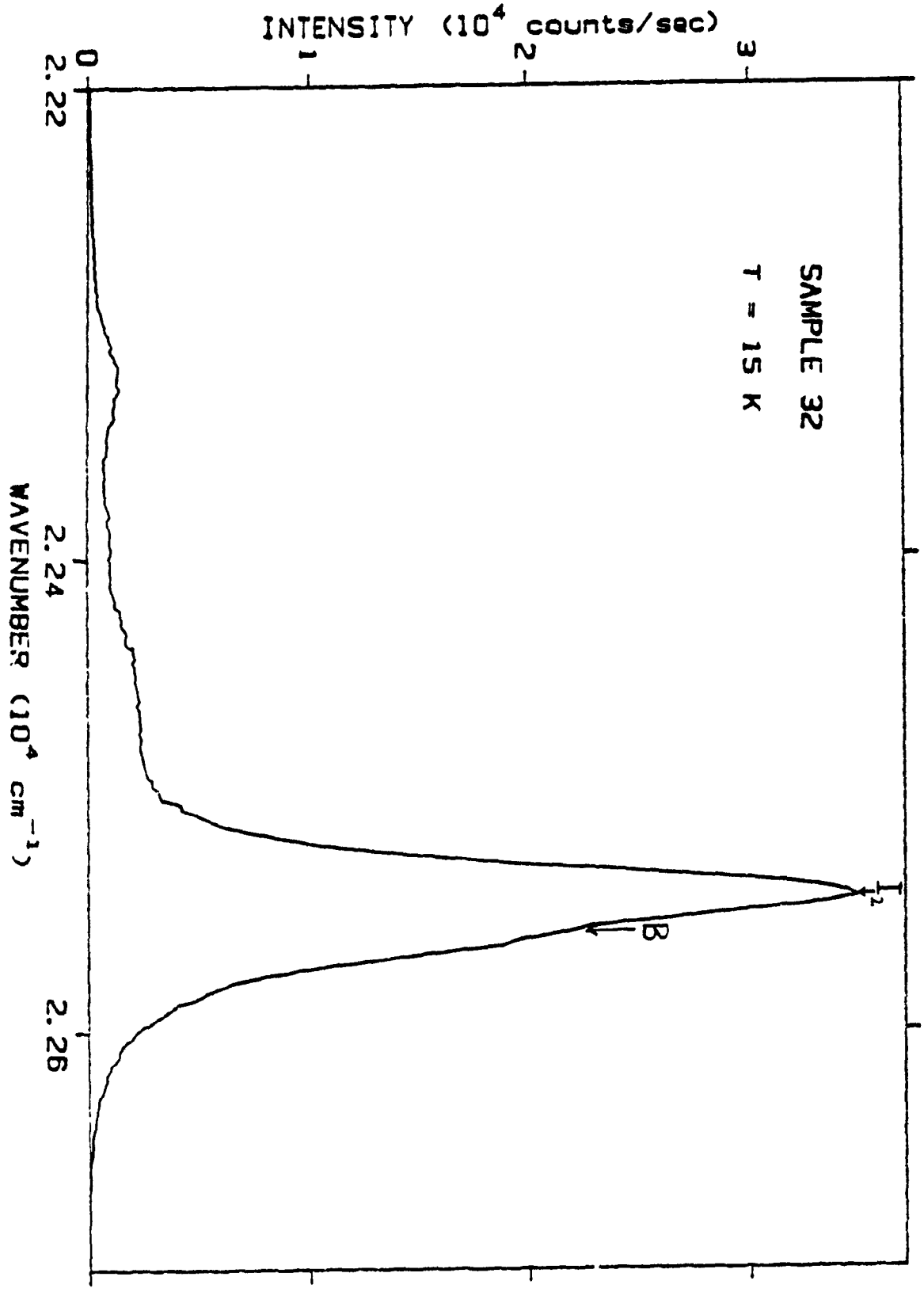
INTENSITY (10^4 counts/sec)
0
1
2
3
2.22
2.24
2.26
WAVENUMBER (10^4 cm^{-1})
SAMPLE 32
T = 15 K
I_2
B

Figure 4.17

figure 4.18 :

incident power - 12.5 mW

power density - 2.5 W/cm^2

scan range - 19000-16000 cm^{-1}

energy sampling - 10 cm^{-1}

sample time - 1 sec

slit width - 200 microns

Emission Bands :

SA -- The self-activated emission peaks at an energy of 2.06 eV. The emission is due to a DAP transition involving the A-center.

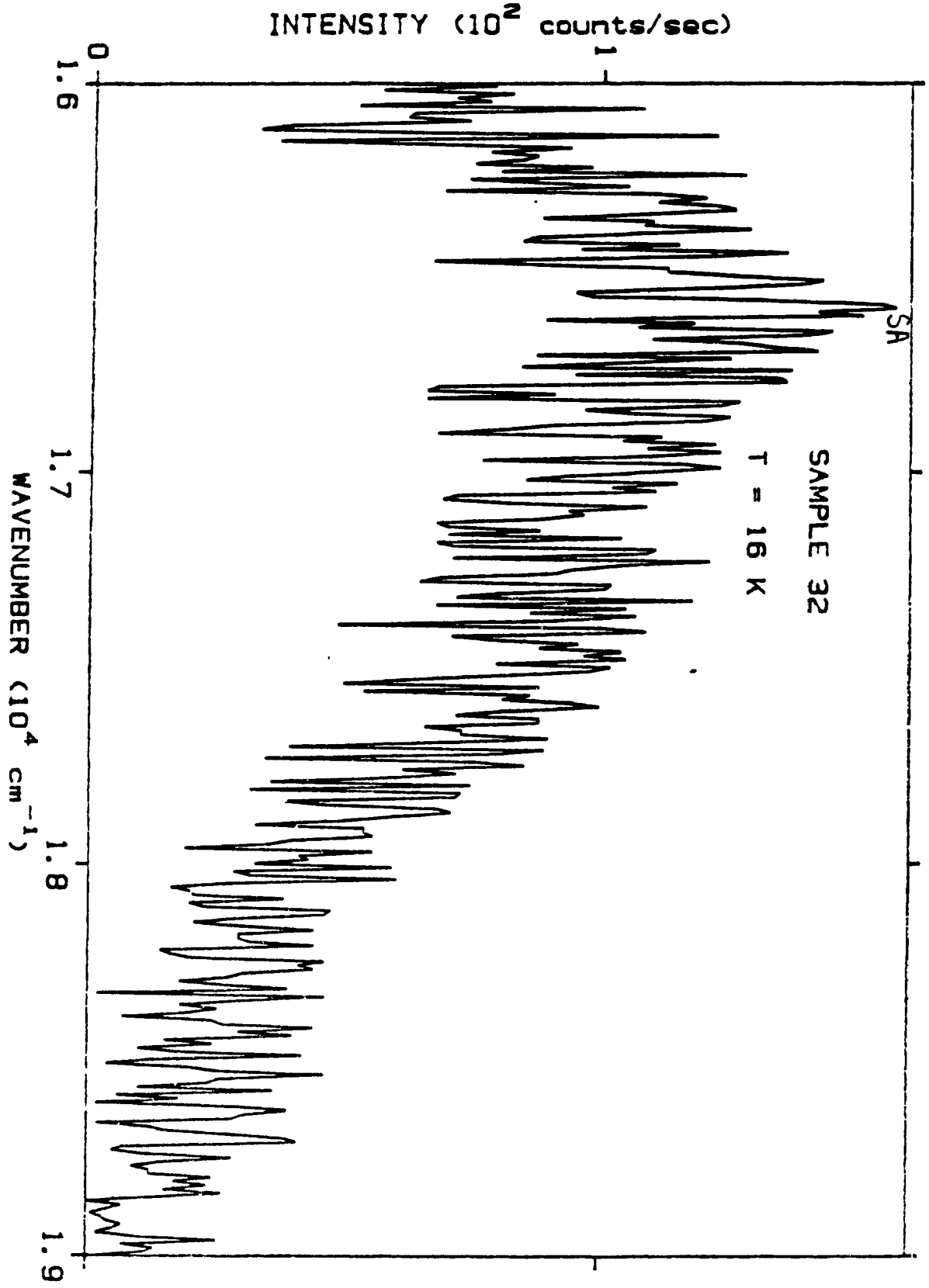
INTENSITY (10² counts/sec)
0
1
1.6
1.7
1.8
1.9
WAVENUMBER (10⁴ cm⁻¹)
SAMPLE 32
T = 16 K
SA

Figure 4.18

figure 4.19 :

incident power - 0.6 mW

power density - 120 mW/cm^2

scan range - 22700-22200 cm^{-1}

energy sampling - 2 cm^{-1}

sample time - 1 sec

slit width - 200 microns

Emission Bands :

I_1 -- The luminescence peak positioned at an energy of 2.7950 eV is the I_1^{lh}, or (D°,X), transition associated with light hole excitons.

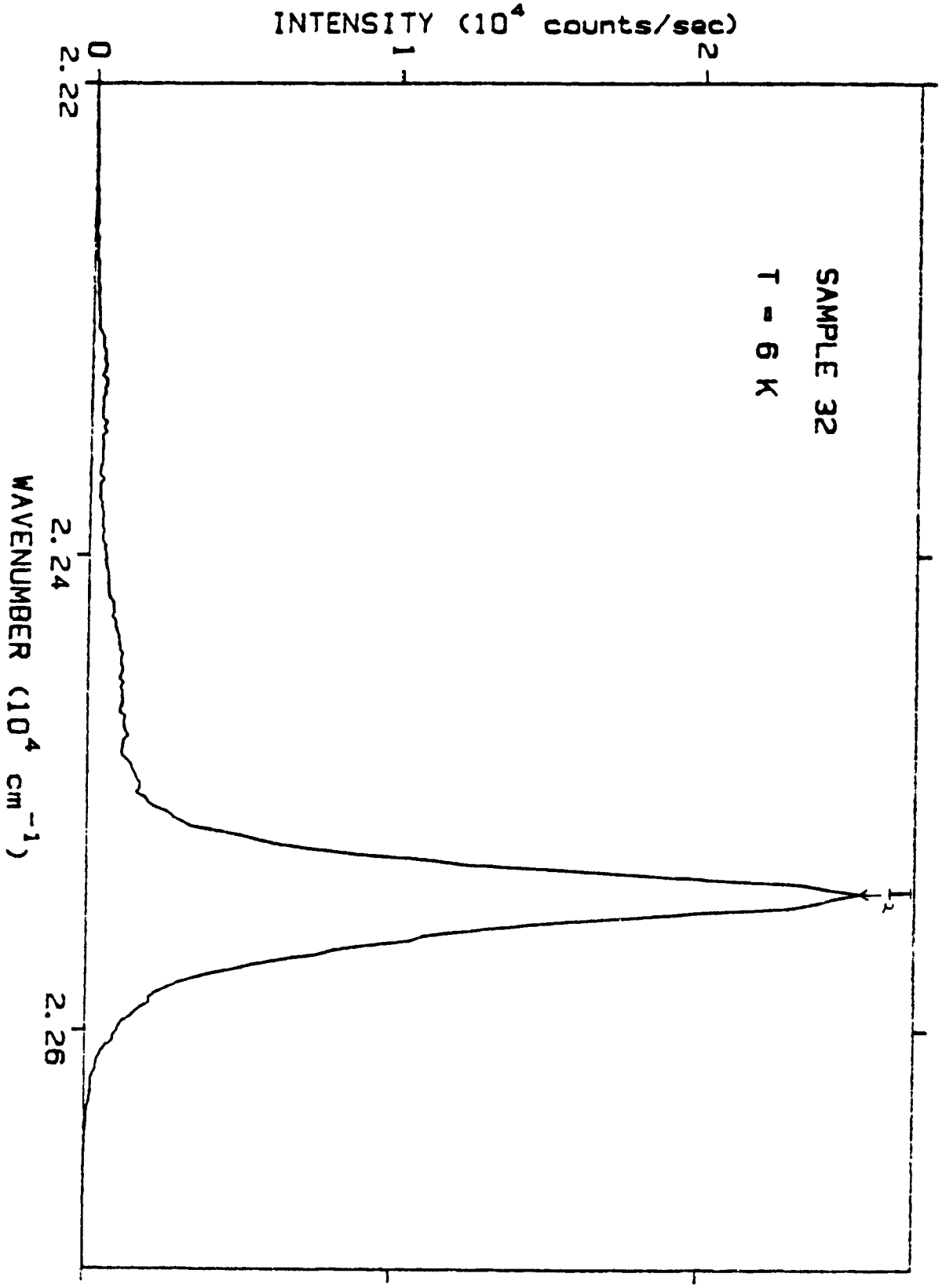
INTENSITY (10^4 counts/sec)
0
1
2
2.22
2.24
2.26
WAVENUMBER (10^4 cm^{-1})
SAMPLE 32
T = 6 K
I_2

figure 4.19

figure 4.20 :

scan range	- 22700-22500	22500-21750	cm^{-1}
incident power	- 0.6	19	mW
power density	- 120 $\xrightarrow{x32}$	3800	$\mu W/cm^2$
energy sampling	- 2	2	cm^{-1}
sample time	- 1	1	sec
slit width	- 200	200	microns

Emission Bands :

I_1 -- The luminescence peak positioned at an energy of 2.7950 eV is the I_1^{lh}, or (D^0,X), transition associated with light hole excitons.

C -- The origin of the C band, centered at 2.7836 eV, is uncertain. Three transitions contribute to the emission : 1) the I_1^{deep}, or (A^0,X) transition, 2) the radiative decay of free excitons which scatter inelastically at neutral donors, and 3) free exciton recombination following inelastic scattering at other free excitons.

TES - The two-electron satellite transitions associated with the principal I_1^{lh} luminescence result in the peak centered at 2.7759 eV.

FE_{1-LO} - The peak at 2.7688 eV is due to the radiative decay of free excitons with the simultaneous emission of an LO phonon.

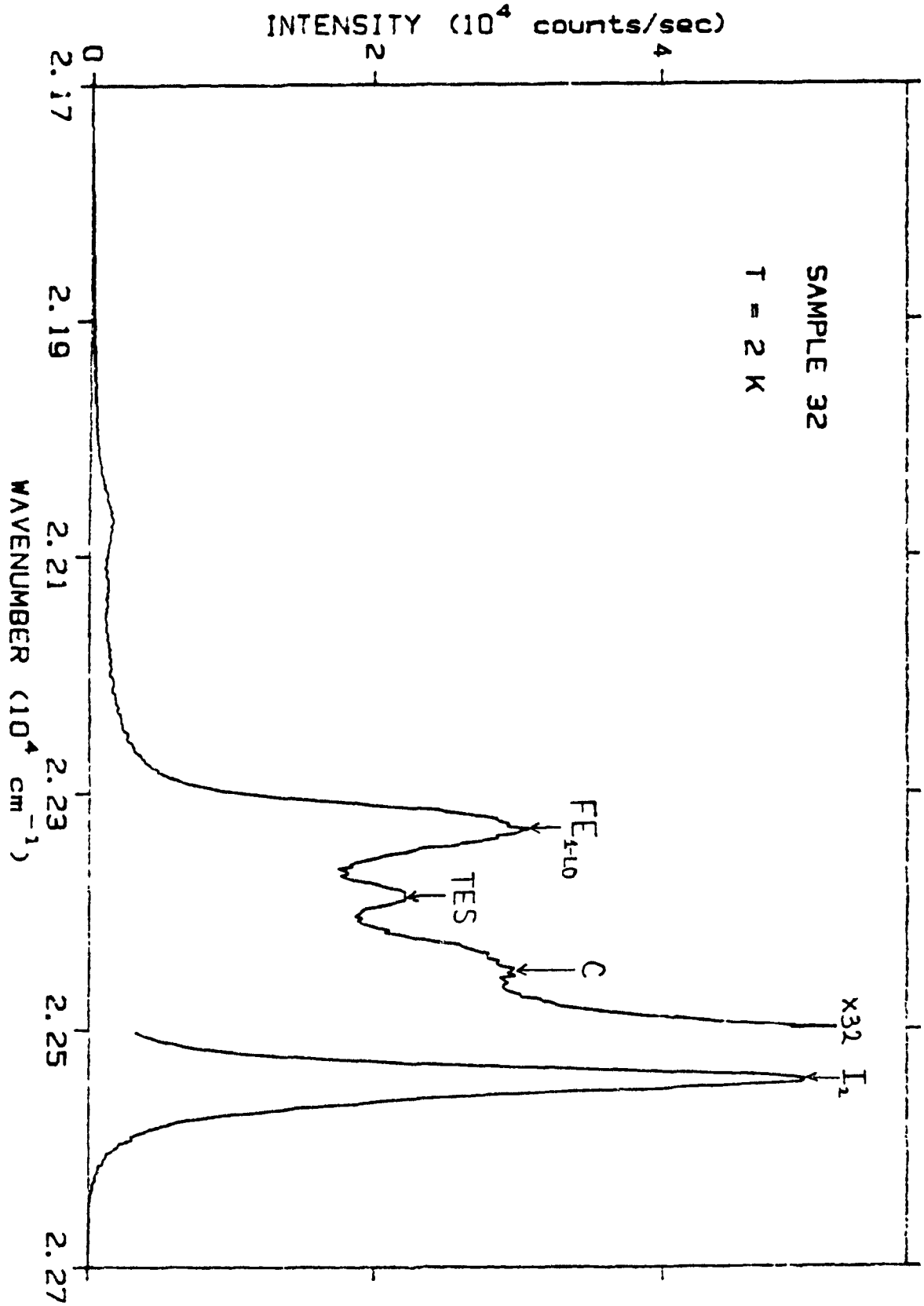
INTENSITY (10^4 counts/sec)
0
2
4
2.17
2.19
2.21
2.23
2.25
2.27
WAVENUMBER (10^4 cm^{-1})
SAMPLE 32
T = 2 K
FE_{1-LO}
TES
C
×32
I_1

figure 4.20

figure 4.21 :

scan range	- 22700-22500	22500-22300	22300-21750	cm^{-1}
incident power	- 0.8	25	80	mW
power density	- 80 $\xrightarrow{x31}$	2500 $\xrightarrow{x100}$	8000	mW/cm^2
energy sampling	- 2	2	2	cm^{-1}
sample time	- 2	2	2	sec
slit width	- 200	200	200	microns

Emission Bands :

I_1 — The luminescence peak positioned at an energy of 2.7950 eV is the I_1^{lh}, or (D^o,X), transition associated with light hole excitons.

C — See caption for figure 4.20.

TES - The two-electron satellite transitions associated with the principal I_1^{lh} luminescence result in the peak centered at 2.7759 eV.

FE_{1-LO} The peak at 2.7688 eV is due to the radiative decay of free excitons with the simultaneous emission of an LO phonon.

FE_{1-LO} The peak at 2.7365 eV is due to the radiative decay of free excitons with the simultaneous emission of two LO phonons.

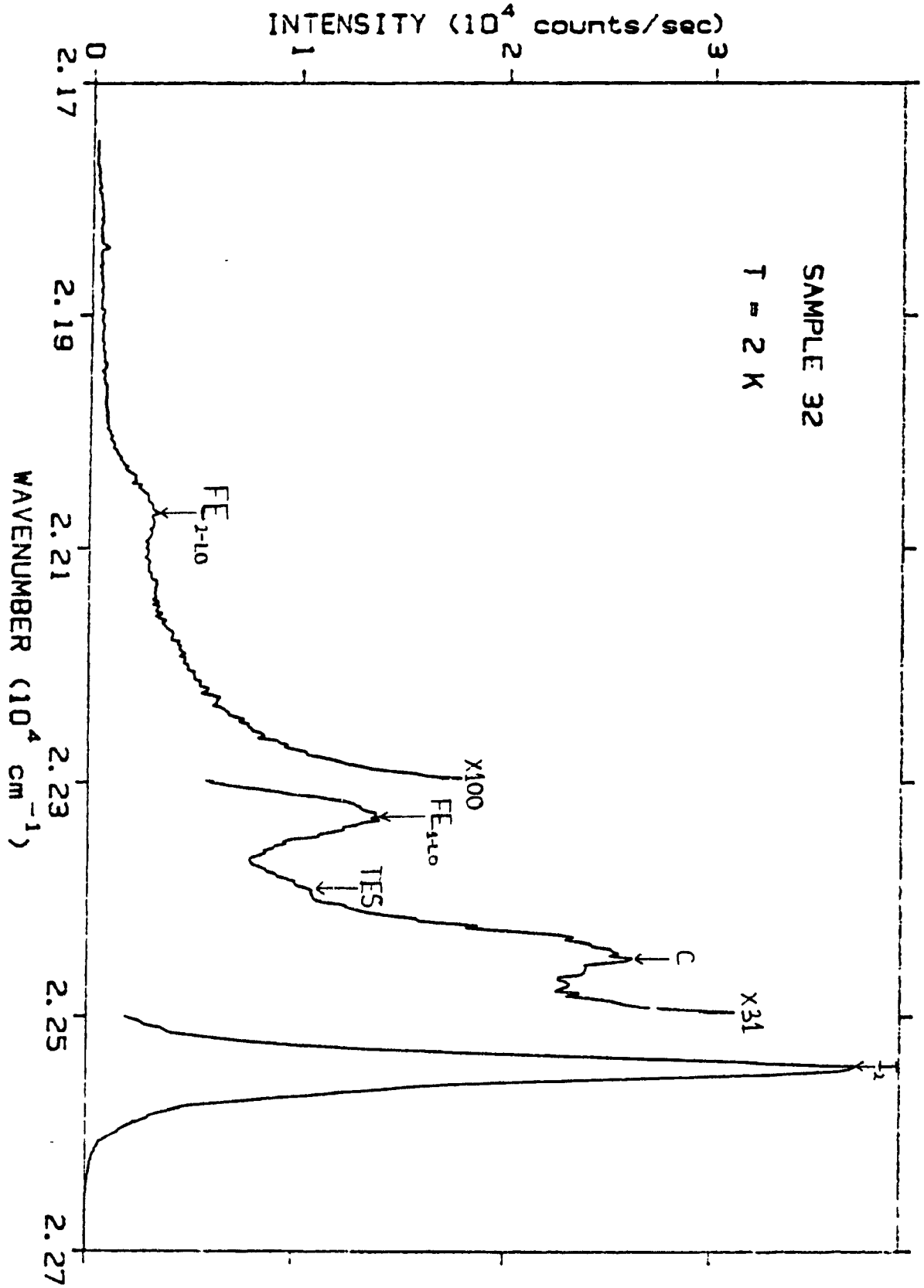
INTENSITY (10^4 counts/sec)
0
1
2
3
SAMPLE 32
T = 2 K
FE_{1-LO}
X100
FE_{1-LO}
TES
C
X31
I_2
2.17
2.19
2.21
2.23
2.25
2.27
WAVENUMBER (10^4 cm^{-1})

figure 4.21

figure 4.22 :

incident power - 80 mW

power density - 8 W/cm^2

scan range - 22200-21000 cm^{-1}

energy sampling - 5 cm^{-1}

sample time - 1 sec

slit width - 200 microns

Emission Bands :

FE_{1-LO} The peak at 2.7365 eV is due to the radiative decay of free excitons with the simultaneous emission of two LO phonons.

No DAP emission associated with the presence of shallow acceptors is observed.

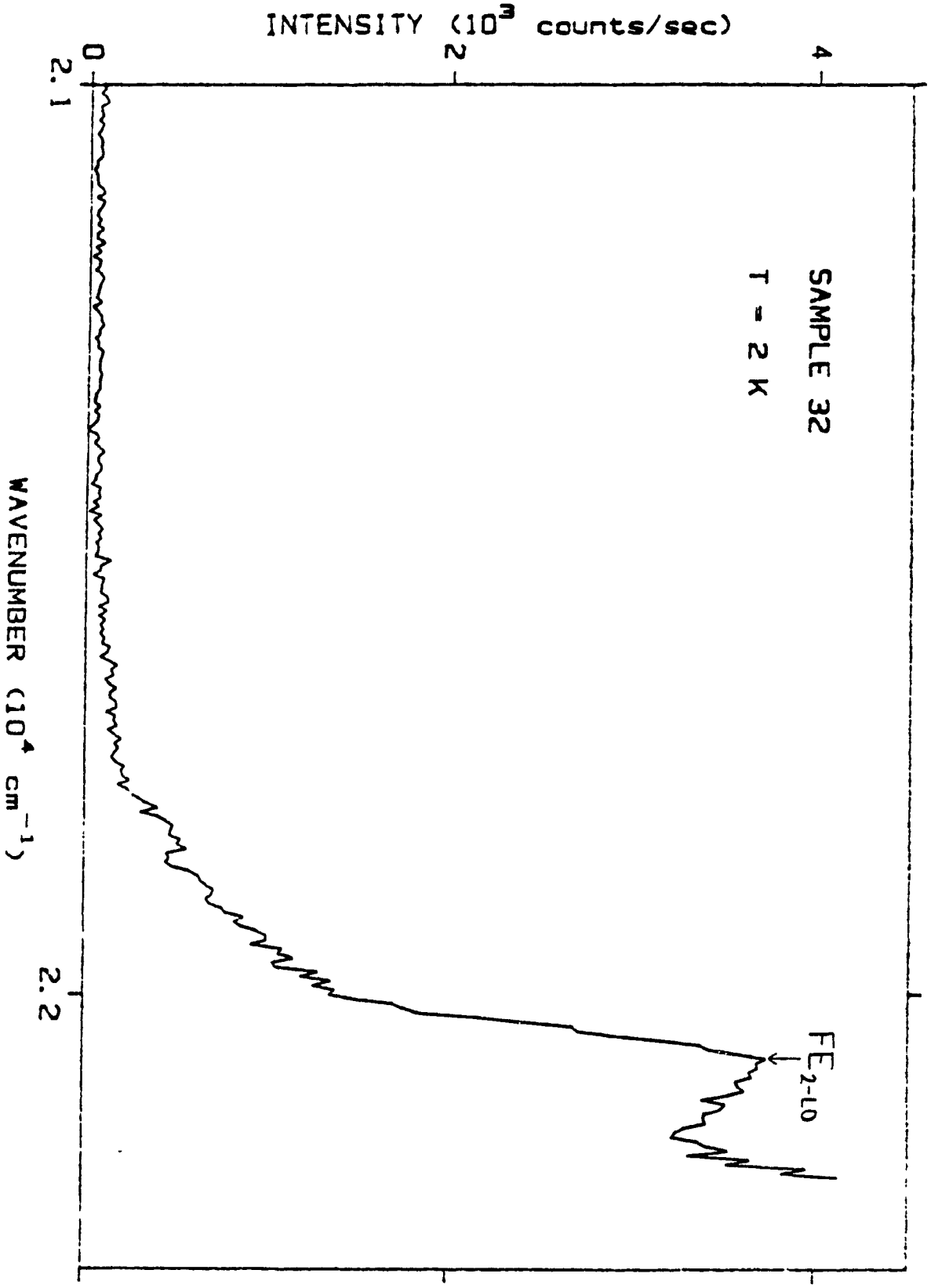
INTENSITY (10^3 counts/sec)
0
2
4
2.1
2.2
WAVENUMBER (10^4 cm^{-1})
SAMPLE 32
T = 2 K
FE_{2-LO}

figure 4.22

figure 4.23 :

incident power - 1.25 mW

power density - 250 mW/cm^2

scan range - 22700-22200 cm^{-1}

energy sampling - 3 cm^{-1}

sample time - 1 sec

slit width - 200 microns

Emission Bands :

I_1 — The luminescence peak situated at 2.7957 eV is the I_1^{lh}, or (D^0,X), transition associated with light hole excitons.

B — Two transitions contribute to the B emission, observed as a shoulder on the high energy side of the principal I_1^{lh} peak : 1) the radiative decay of free excitons and 2) the I_1^{hh} transition associated with heavy hole excitons.

TES - The peak centered at an energy of 2.777 eV is due to two-electron satellite transitions associated with the principal I_1^{lh} luminescence.

FE_{1-LO} - The peak at 2.770 eV is due to the radiative decay of free excitons with the simultaneous emission of an LO phonon.

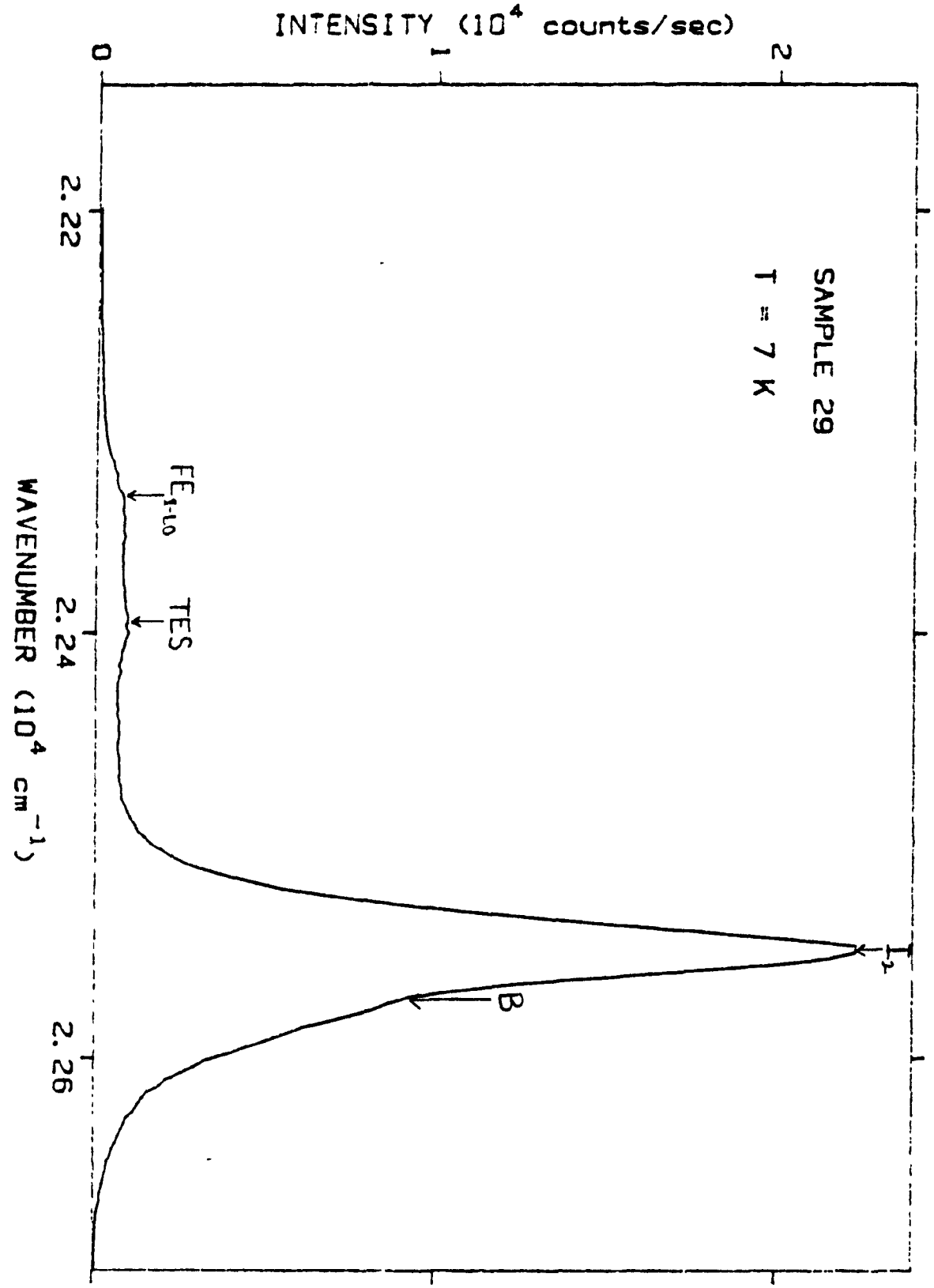
INTENSITY (10^4 counts/sec)
0
1
2
SAMPLE 29
T = 7 K
2.22
2.24
2.26
WAVENUMBER (10^4 cm^{-1})
FE_{1-LO}
TES
I_2
B

figure 4.23

figure 4.24 :

incident power - 1.25 mW

power density - 250 mW/cm^2

scan range - 22200-20000 cm^{-1}

energy sampling - 5 cm^{-1}

sample time - 1 sec

slit width - 200 microns

Emission Bands :

W_0 -- The W_0 band, centered at 2.741 eV, is the principal (zero phonons emitted) DAP transition associated with the shallow acceptor P.

W_1 -- The W_1 band, centered at 2.709 eV, is the DAP transition (P acceptor) with the simultaneous emission of an LO phonon.

P_0 -- The P_0 band, centered at 2.685 eV, is the principal DAP transition associated with the shallow acceptor Na.

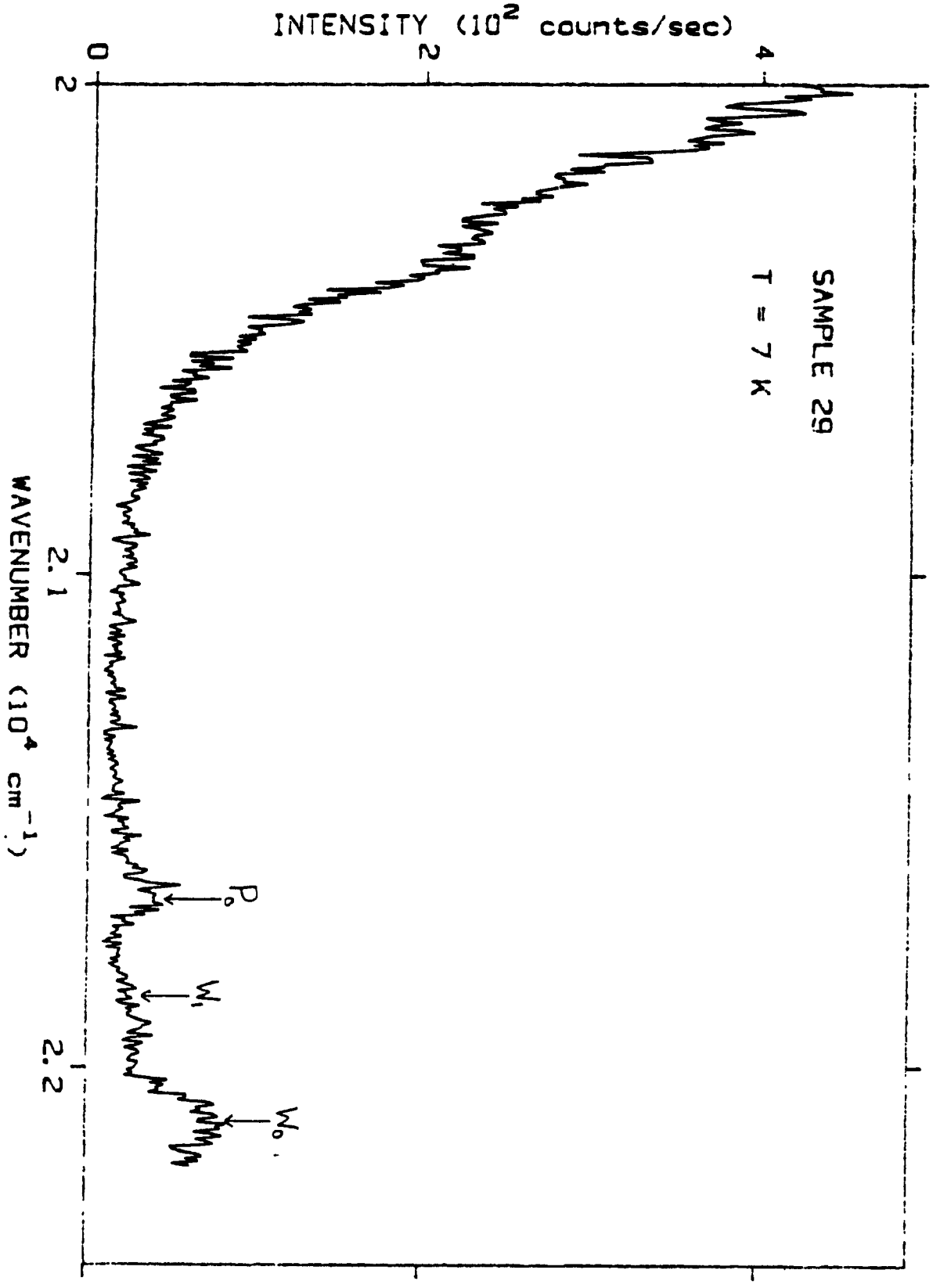
INTENSITY (10² counts/sec)
0
2
4
2
SAMPLE 29
T = 7 K
2.1
WAVENUMBER (10⁴ cm⁻¹)
2.2
P₀
W₁
W₀

figure 4.24

figure 4.25 :

incident power - 1.25 mW

power density - 250 mW/cm^2

scan range - 22700-22200 cm^{-1}

energy sampling - 2 cm^{-1}

sample time - 1 sec

slit width - 200 microns

Emission Bands :

FE -- The peak positioned at an energy of 2.8030 eV is due to the radiative decay of free excitons.

I_1 -- The luminescence peak positioned at an energy of 2.7983 eV is the I_1^{hh}, or (D^0,X), transition associated with heavy hole excitons.

I_1 -- The peak positioned at an energy of 2.7938 eV is the I_1, or (A^0,X), transition.

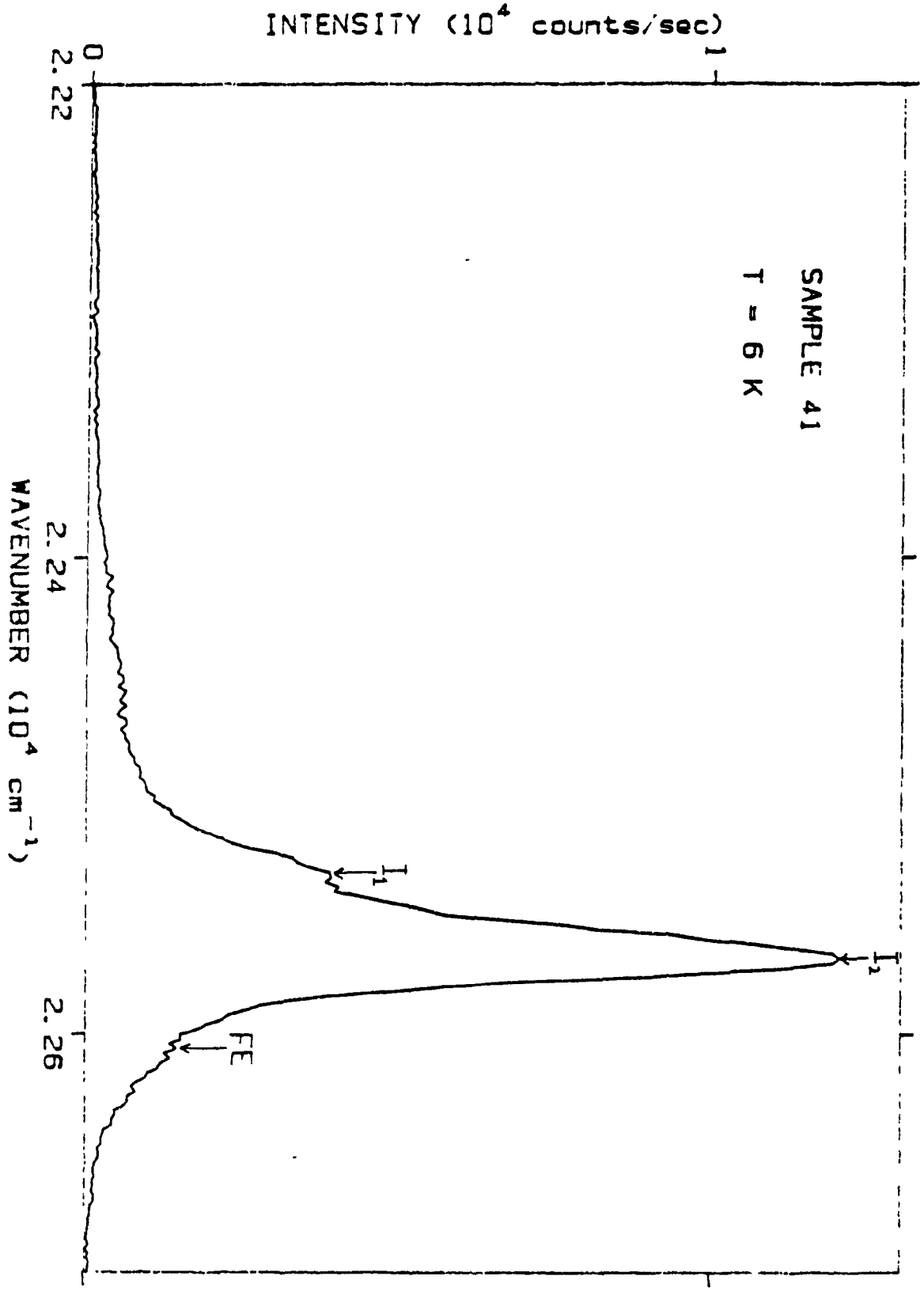
INTENSITY (10^4 counts/sec)
0
1
2.22
2.24
2.26
WAVENUMBER (10^4 cm^{-1})
SAMPLE 41
T = 6 K
I_1
I_2
FE

figure 4.25

figure 4.26 :

incident power - 40 mW

power density - 8 W/cm^2

scan range - 23000-22000 cm^{-1}

energy sampling - 2 cm^{-1}

sample time - 2 sec

slit width - 200 microns

Emission Bands :

FE -- The peak positioned at an energy of 2.7933 eV is due to the radiative decay of free excitons.

I_1 -- The luminescence peak situated at 2.7878 eV is due to the I_1, or (D°,X), transition.

(D°,h) - The peak positioned at an energy of 2.7859 eV corresponds to the radiative recombination of free holes with electrons bound to neutral donors.

D -- Several transitions contribute to the D emission band appearing on the low energy side of the free to bound transition : 1) TES transitions, 2) free exciton recombination with the simultaneous emission of an LO phonon, and 3) the I_1^{deep} transition.

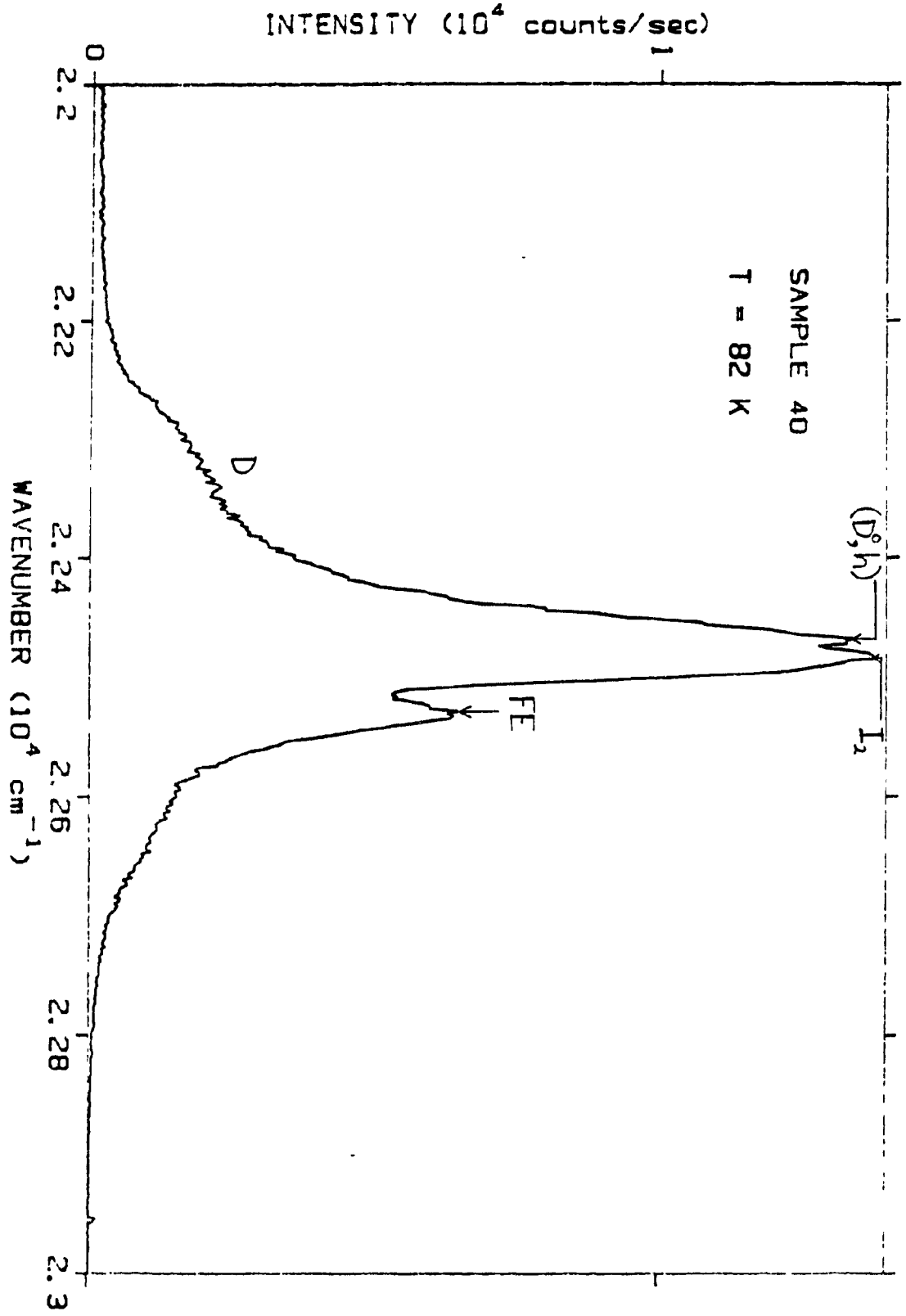
INTENSITY (10^4 counts/sec)
0
1
2.2
2.22
2.24
2.26
2.28
2.3
WAVENUMBER (10^4 cm^{-1})
SAMPLE 40
T = 82 K
D
(D^o,h)
FE
I_2

figure 4.26

figure 4.27 :

incident power - 12.5 mW

power density - 1.25 W/cm^2

scan range - 23000-21500 cm^{-1}

energy sampling - 5 cm^{-1}

sample time - 2 sec

slit width - 200 microns

Emission Bands :

FE -- The peak positioned at an energy of 2.7960 eV is due to the radiative decay of free excitons.

I_1 -- The luminescence peak situated at 2.7911 eV is the I_1, or (D°,X), transition.

(D°,h) - The peak positioned at an energy of 2.7892 eV corresponds to the radiative recombination of free holes with electrons bound to neutral donors.

D -- Several transitions contribute to the D emission band appearing on the low energy side of the free to bound transition : 1) TES transitions, 2) free exciton recombination with the simultaneous emission of an LO phonon, and 3) the I_1^{deep} transition.

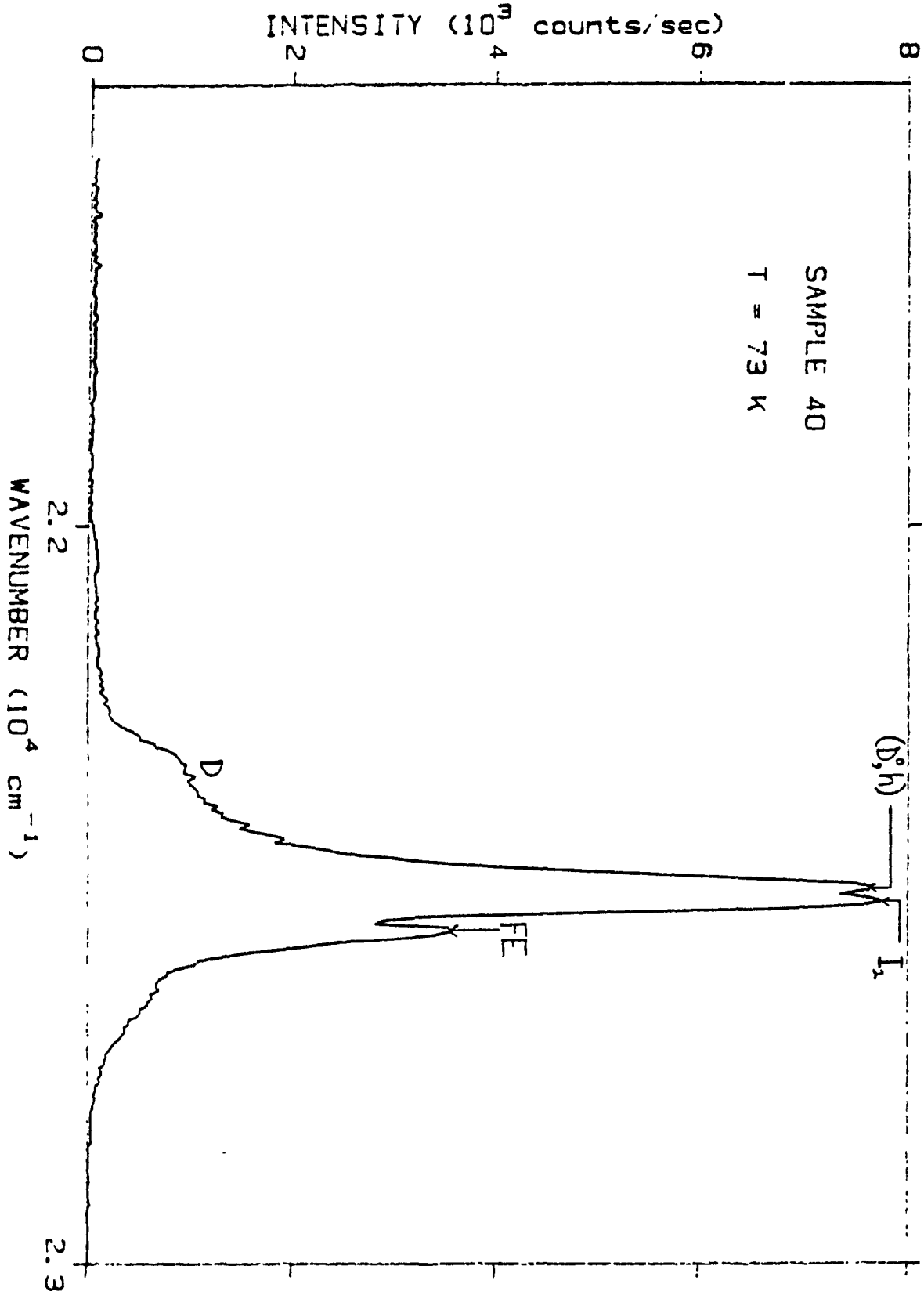
INTENSITY (10^3 counts/sec)
0
2
4
6
8
SAMPLE 40
T = 13 K
(D°,h)
I_1
FE
D
2.2
2.3
WAVENUMBER (10^4 cm^{-1})

figure 4.27

figure 4.28 :

incident power - 12.5 mW

power density - 2.5 W/cm^2

scan range - 23000-21500 cm^{-1}

energy sampling - 5 cm^{-1}

sample time - 2 sec

slit width - 200 microns

Emission Bands :

FE — The shoulder on the high energy side of the dominant I_1 peak is due to the radiative decay of free excitons.

I_1 and (D°,h) - The peak positioned at an energy of 2.786 eV is due to two transitions : 1) the I_1 transition and 2) the free to bound, or (D°,h), transition.

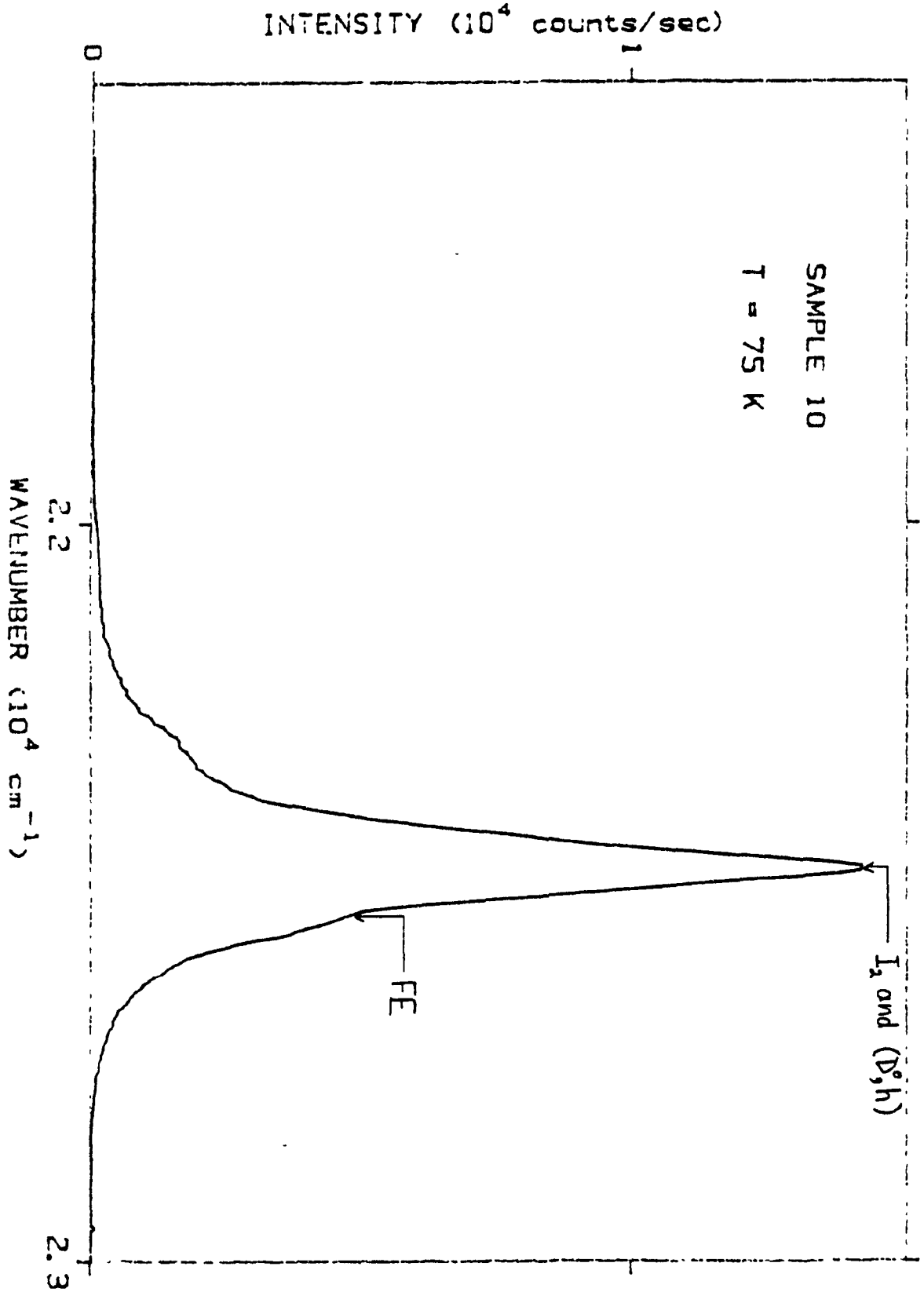
INTENSITY (10^4 counts/sec)
0
1
SAMPLE 10
T = 75 K
2.2
WAVENUMBER (10^4 cm^{-1})
2.3
I_2 and (D^0,h)
FE

figure 4.28

figure 4.29 :

incident power - 40 mW

power density - 4 W/cm^2

scan range - 23000-20500 cm^{-1}

energy sampling - 5 cm^{-1}

sample time - 2 sec

slit width - 200 microns

Emission Bands :

NBE — The near band edge emission peaks at an energy of 2.79 eV.

Q_o — The peak positioned at an energy of 2.7022 eV is a free to bound transition, (e,A^o), involving the acceptor Li.

Q_1 — The peak situated at 2.6696 eV is the 1 LO phonon replica of the Q_0 peak.

Q_2 — The peak situated at 2.6388 eV is the 2 LO phonon replica of the Q_0 peak.

Y — The origin of the Y band, centered at 2.5945 eV, is uncertain. It may be due to the recombination of excitons at an extended defect.

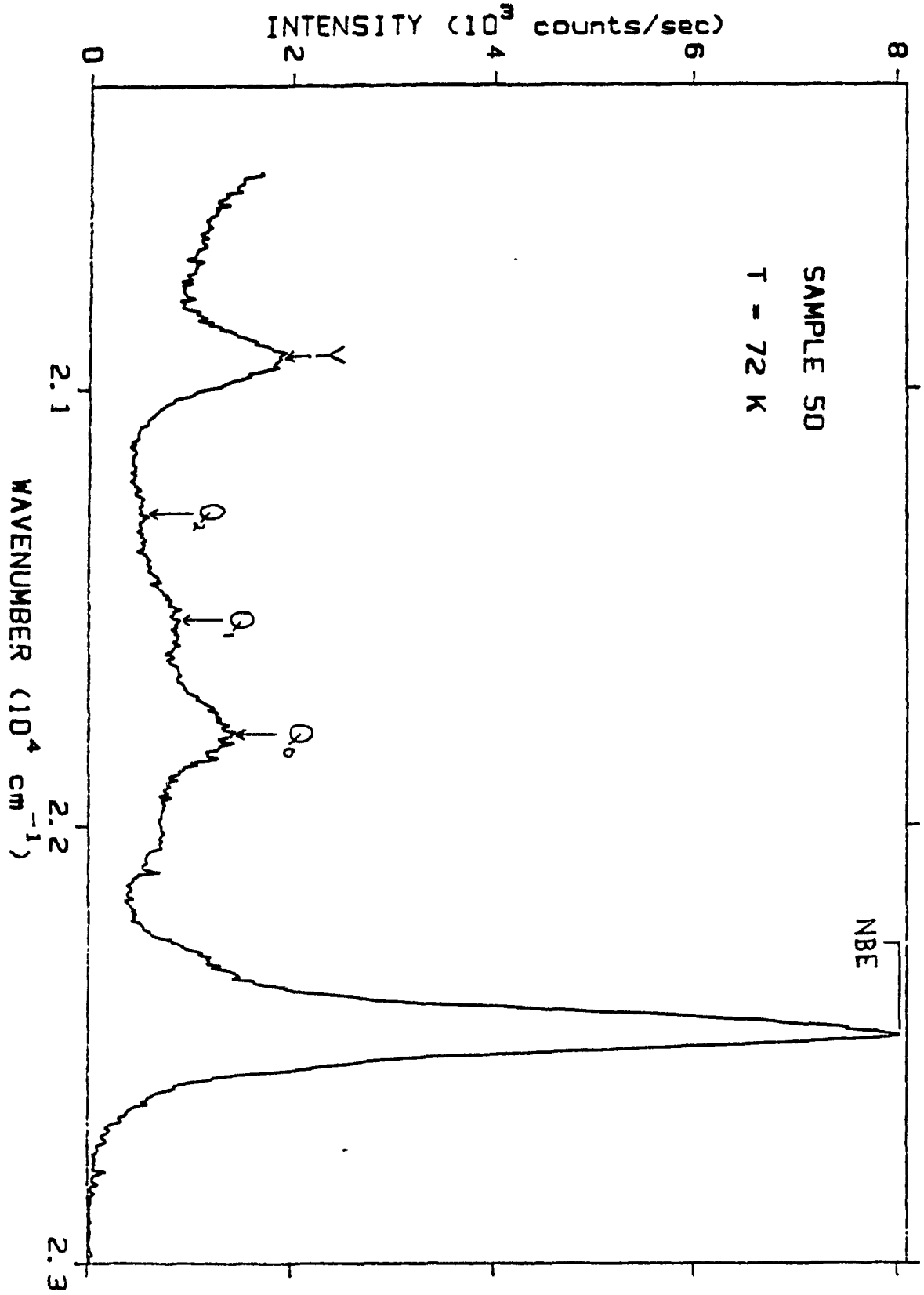
INTENSITY (10³ counts/sec)
0
2
4
6
8
SAMPLE 50
T = 72 K
Y
Q₂
Q₁
Q₀
NBE
2.1
2.2
2.3
WAVENUMBER (10⁴ cm⁻¹)

figure 4.29

CHAPTER 5

CONCLUSION

5.)CONCLUSION

ZnSe heteroepitaxial thin films were grown by conventional MOVPE and a novel pulsed technique developed here. Material was grown using the precursors DEZ, DMZ, H_2Se, and DEDSe. Films were deposited at temperatures ranging from 200 - 400 °C. The photoluminescence technique was utilized to characterize the epilayers.

A comparison of the 300 °K photoluminescence spectra of films grown at temperatures of 200 °C (sample 8), 250 °C (sample 9), and 300 °C (sample 10) by conventional MOVPE shows an improvement in optoelectronic quality with increasing T_G.

The 300 °K and 2-16 °K photoluminescence spectra of sample 32, which was grown by conventional MOVPE using DEZ and H_2Se, show that the material contains a high concentration of shallow donor impurities, as indicated by the intense near band edge (NBE) emission at room temperature and the large (D^0,X) linewidth at 2 °K. The downshift in the energy position of the I_2 peak is consistent with a decrease in the effective bandgap expected for a sample of this thickness. The decrease in the bandgap is a consequence of the fact that epilayers thicker than 1 micron are under a two-dimensional tensile stress as a result of differences in the thermal expansion coefficients of ZnSe and GaAs.

The 77 °K photoluminescence of sample 29, which was grown by conventional MOVPE using the precursors DMZ and H_2Se, reveals the presence of a Cu-complex center which acts as a compensating acceptor. The DMZ reactant is the source of the Cu impurity.

Sample 40 was grown by a novel pulsed technique. The reactants used were DMZ and H_2Se. Comparison of the 77 °K photoluminescence of samples 40 and 29 reveals a substantial reduction in the impurity concentration for the former. The (D^o,X) linewidth at 7 °K is comparable to that observed for material grown by MOVPE [25,59] and MBE [80,81]. The 7 °K photoluminescence of sample 40 shows evidence of polariton emission. The intense free exciton emission and narrow I_2 linewidth are characteristic of high purity material having a low density of dislocations. The improved optoelectronic quality is linked to the slow growth rates characteristic of the pulsed technique and a change in reaction mechanisms when using this technique.

77 °K and 6 °K photoluminescence spectra obtained for sample 41, which was grown by the pulsed technique using DMZ and H_2Se, reveal the presence of a high concentration of shallow donor impurities and compensating A-centers. Relaxation of strain arising from the inherent lattice mismatch occurs at the sample thickness of 0.4 microns. The relaxation process results in the generation of dislocations which, in turn, act as impurity sinks.

The 77 °K photoluminescence of sample 50, which was grown by conventional MOVPE using the reactants DMZ and DEDSe, indicates the presence of the shallow acceptor Li. The source of this impurity is the metal-organic DEDSe.

The 77 °K photoluminescence of sample 40 shows that three transitions contribute to the NBE emission at this temperature. The transitions include the (D^o,X) transition, the radiative decay of free excitons, and finally, the radiative recombination of free

holes with electrons bound to donors, or (D^o,h). These features of the 77 °K NBE emission have not been reported in the literature on the ZnSe/GaAs system.

It is planned, in the near future, to grow thin (less than 0.15 microns) coherently strained ZnSe epilayers using the pulsed technique. Electrical and optical measurements show evidence for electron accumulation on the ZnSe side of the interface [86]. Photoluminescence measurements of the thin films will provide additional information about the band offset at the interface.

REFERENCES

[1] T. Yodo, T. Koyama and K. Yamashita, J. Cryst. Growth, **86**, 273 (1988)

[2] B.J. Skromme, M.C. Tamargo, J.L. de Miguel and R.E. Nahory, Appl. Phys. Lett., **53**, 2217 (1988)

[3] P. Blanconnier, M. Cerclet, P. Henoc and A.M. Jean-Louis, Thin Solid Films, **55**, 375 (1978)

[4] J.E. Butler, N. Bottka, R.S. Sillmon and D.K. Gaskill, J. Cryst. Growth, **77**, 163 (1986)

[5] Y. Monteil, M.P. Berthet, R. Favre, A. Hariss, J. Bouix, M. Vaille and P. Gibart J. Cryst. Growth, **77**, 172 (1986)

[6] S.P. DenBaars, B.Y. Maa, P.D. Dapkus, A.D. Danner and H.C. Lee, J. Cryst. Growth, **77**, 188 (1986)

[7] G.B. Stringfellow, Rep. Prog. Phys., **45**, 469 (1982)

[8] T.F. Kuech, Materials Science Reports, **2**, 1 (1987)

[9] R.H. Moss and J.S. Evans, J. Cryst. Growth, **55**, 129 (1981)

[10] G.B. Stringfellow, J. Cryst. Growth, **68**, 111 (1984)

[11] W. Stutius, J. Appl. Phys., **53**, 284 (1982)

[12] H. Mitsuhashi, I. Mitsuishi and H. Kukimoto, J. Cryst. Growth, **77**, 219 (1986)

[13] P.J. Wright, P.J.M. Griffiths and B. Cockayne, J. Cryst. Growth, **66**, 26 (1984)

[14] W. Stutius, J. Cryst. Growth, **59**, 1 (1982)

[15] J.B. Mullin, S.J.C. Irvine and D.J. Ashen, J. Cryst. Growth, **55**, 92 (1981)

[16] P.J. Wright and B. Cockayne, J. Cryst. Growth, **59**, 148 (1982)

[17] W. Stutius, J. Electron. Mater., **10**, 95 (1981)

[18] S. Sritharan, K.A. Jones and K.M. Motyl, J. Cryst. Growth, **68**, 656 (1984)

[19] S. Fujita, A. Tanabe, T. Sakamoto, M. Isemura and S. Fujita, Jpn. J. Appl. Phys., **26**, L2000 (1987)

[20] A. Yoshikawa, A. Sirai, S. Yamaga and H. Kasai, Jpn. J. Appl. Phys., **25**, 673 (1986)

[21] W. Stutius, Appl. Phys. Lett., **33**, 656 (1978)

[22] N. Shibata, A. Ohki and S. Zembutsu, Jpn. J. Appl. Phys., **26**, 1305 (1987)

[23] T. Yodo, H. Oka, T. Koyama and K. Yamashita, Jpn. J. Appl. Phys., **26**, L561 (1987)

[24] S. Fujita, Y. Matsuda and A. Sasaki, J. Cryst. Growth, **68**, 231 (1984)

[25] G. Fan, J. Davies, N. Maung, M.J. Parrott and J.O. Williams, J. Electron. Mater., **15**, 251 (1986)

[26] G. Fan and J.O. Williams, J. Chem. Soc., Faraday Trans. 1, **83**, 323 (1987)

[27] A. Yoshikawa, K. Tanaka, S. Yamaga and H. Kasai, Jpn. J. Appl. Phys., **23**, L773 (1984)

[28] Y. Shirikawa and H. Kukimoto, J. Appl. Phys., **51**, 5859 (1980)

[29] N. Shibata, A. Ohki, H. Nakanishi and S. Zembutsu, J. Cryst. Growth, **86**, 268 (1988)

[30] P.J. Dean, A.D. Pitt, M.S. Skolnick, P.J. Wright and B. Cockayne, J. Cryst. Growth, **59**, 301 (1982)

[31] J.I. Pankove, Optical Processes in Semiconductors, (Prentice-Hall, Englewood Cliffs, New Jersey, 1971)

[32] O. Madelung, Introduction to Solid State Theory, (Springer-Verlag, Berlin, New York, 1978)

[33] P.J. Dean, D.C. Herbert, C.J. Werkhoven, B.J. Fitzpatrick and R.N. Bhargava, Phys. Rev. B, **23**, 4888 (1981)

[34] M. Aven, D.T.F. Marple and B. Segall, J. Appl. Phys., **32**(supplement), 2261 (1961)

[35] R.J. Elliot, Introduction to the Theory of Excitons in Polarons and Excitons in Polar Semiconductors and Ionic Crystals, edited by J.T. Devreese and F. Peeters, NATO ASI Series, Series B: physics, **108**, Antwerp (1982)

[36] G.E. Hite, D.T.F. Marple, M. Aven and B. Segall, Phys. Rev., **156**, 850 (1967)

[37] H. Venghaus and R. Lambrich, Solid State Commun., **25**, 109 (1978)

[38] P.J. Dean and J.L. Merz, Phys. Rev., **178**, 1310 (1969)

[39] J.L. Merz, H. Kukimoto, K. Nassau and J.W. Shiever, Phys. Rev. B, **6**, 545 (1972)

[40] B. Sermage and M. Voos, Phys. Rev. B, **15**, 3935 (1977)

[41] Y. Shirakawa and H. Kukimoto, J. Appl. Phys., **51**, 2014 (1980)

[42] M. Isshiki, T. Kyotani, K. Masumoto, W. Uchida and S. Suto, Phys. Rev. B, **36**, 2568 (1987)

[43] K. Yoneda, Y. Hishida, T. Toda, H. Ishii and T. Niina, Appl. Phys. Lett., **45**, 1300 (1984)

[44] R.M. Park, H.A. Mar and N.M. Salansky, J. Vac. Sci. Technol. B, **3**, 676 (1985)

[45] T. Yao, Y. Okada, S. Matsui, K. Ishida and I. Fujimoto, J. Cryst. Growth, **81**, 518 (1987)

[46] K. Ohkawa, T. Mitsuyu and O. Yamazaki, J. Appl. Phys., **62**, 3216 (1987)

[47] P.J. Dean, P.J. Wright and B. Cockayne, J. Phys. C:Solid State Phys., **16**, 3493 (1983)

[48] A. Kamata, T. Uemoto, M. Okajima, K. Hirahara, M. Kawachi and T. Beppu, J. Cryst. Growth, **86**, 285 (1988)

[49] D.D. Sell, S.E. Stokowski, R. Dingle and J.V. DiLorenzo, Phys. Rev. B, **7**, 4568 (1973)

[50] P.J. Dean, A.D. Pitt, P.J. Wright, M.L. Young and B. Cockayne, Physica, **116B**, 508 (1983)

[51] J.L. Merz, K. Nassau and J.W. Shiever, Phys. Rev. B, **8**, 1444 (1973)

[52] W. Stutius, Appl. Phys. Lett., **40**, 246 (1982)

[53] H. Tews, H. Venghaus and P.J. Dean, Phys. Rev. B, **19**, 5178 (1979)

[54] P.N. Bhargava, R.J. Seymour, B.J. Fitzpatrick and S.P. Herko, Phys. Rev. B, **20**, 2407 (1979)

[55] P.J. Dean, W. Stutius, G.F. Neumark, B.J. Fitzpatrick and R.N. Bhargava, Phys. Rev. B, **27**, 2419 (1983)

[56] T. Yao and Y. Okada, Jpn. J. Appl. Phys., **25**, 821 (1986)

[57] P.J. Dean, Czech. J. Phys. B, **30**, 272 (1980)

[58] R.N. Bhargava, J. Cryst. Growth, **59**, 15 (1982)

[59] P.J. Dean, Phys. Stat. Solidi (a), **81**, 625 (1984)

[60] F. Williams, Phys. Stat. Solidi, **25**, 493 (1968)

[61] D.G. Thomas, M. Gershenzon and F.A. Trumbore, Phys. Rev., **133**, A269 (1964)

[62] J.J. Hopfield, D.G. Thomas and M. Gershenzon, Phys. Rev. Lett., **10**, 162 (1963)

[63] G.F.J. Garlick, Rep. Prog. Phys., **30** part II, 491 (1967)

[64] B.J. Fitzpatrick, C.J. Werkhoven, T.F. McGee III, P.M. Harnack, S.P. Herko, R.N. Bhargava and P.J. Dean, IEEE Transactions on Electron Devices, **ED-28**, 440 (1981)

[65] K. Kosai, B.J. Fitzpatrick, H.G. Grimmeiss, R.N. Bhargava and G.F. Neumark, Appl. Phys. Lett., **35**, 194 (1979)

[66] D. Walsh, K. Mazurul and M. Benzaquen, Phys. Rev. B, **36**, 2883 (1987)

[67] J.E. Nicholls and J.J. Davies, J. Phys. C:Solid State Phys., **12**, 1917 (1979)

[68] R.K. Watts, W.C. Holton and M. de Wit, Phys. Rev. B, **3**, 404 (1971)

[69] A.R. Reinberg, W.C. Holton, M. de Wit and R.K. Watts, Phys. Rev. B, **3**, 410 (1971)

[70] J.L. Patel, J.J. Davies and J.E. Nicholls, J. Phys. C:Solid State Phys., **14**, 5545 (1981)

[71] S. Iida, Journal of the Physical Society of Japan, **25**, 177 (1968)

[72] K.M. Lee, L.S. Dang and G.D. Watkins, Solid State Commun., **35**, 527 (1980)

[73] W.P. Dumke, Phys. Rev., **132**, 1998 (1963)

[74] X.W. Fan and J. Woods, IEEE Transactions on Electron Devices, **ED-28**, 428 (1981)

[75] T. Yao, M. Ogura, S. Matsuoka and T. Morishita, Appl. Phys. Lett., **43**, 499 (1983)

[76] H. Mitsuhashi, I. Mitsuishi, M. Mizuta and H. Kukimoto, Jpn. J. Appl. Phys., **24**, L578 (1985)

[77] T. Yao, Jpn. J. Appl. Phys., **25**, L544 (1986)

[78] D.V. Shenai-Khatkhate, E.D. Orrell, J.B. Mullin, D.C. Cupertino and D.J. Cole-Hamilton, J. Cryst. Growth, **77**, 27 (1986)

[79] T. Yao, M. ogura, S. Matsuoka and T. Morishita, Jpn. J. Appl. Phys., **22**, L144 (1983)

[80] H.A. Mar and R.M. Park, J. Appl. Phys., **60**, 1229 (1986)

[81] J.E. Potts, H. Cheng, S. Mohapatra and T.L. Smith, J. Appl. Phys., 61, 333 (1987)

[82] S. Fujita, T. Yodo and A. Sasaki, J. Cryst. Growth, **72**, 27 (1985)

[83] K. Shahzad, Phys. Rev. B, **38**, 8309 (1988)

[84] J. Petruzzello, B.L. Greenberg, D.A. Cammack and R. Dalby, J. Appl. Phys., **63**, 2299 (1988)

[85] W. Taylor, Phys. Lett., **24A**, 556 (1967)

[86] D. Walsh, K. Mazuruk, M. Benzaquen and P. Weissfloch, Semicond. Sci. Technol., 3, 116 (1988)